Geological and Petrologic Evolution of Seamounts Near the EPR Based on Submersible and Camera Study

RODEY BATIZA,[1] TERRI L. SMITH[2] and YAOLING NIU[1]

[1]*Department of Geological Sciences, Northwestern University, Evanston, IL 60208**

[2]*2427 Cherokee Dr. NW, Calgary, Alberta, Canada 72L 0X6*

(Received 4 October, 1988; revised 25 April, 1989)

Key words: seamounts, East Pacific Rise, submersible studies, basalt geochemistry.

Abstract. Observations from 17 ALVIN dives and 14 ANGUS runs plus laboratory study of basalt samples collected with ALVIN help to constrain the morphologic, volcanic and petrologic evolution of four seamounts near the East Pacific Rise (EPR). Comparison among the four volcanoes provides evidence for a general pattern of near-EPR seamount evolution and shows the importance of sedimentation, mass wasting, hydrothermal activity and other geologic processes that occur on submerged oceanic volcanoes. Seamount 5, closest to the EPR (1.0 Ma) is the youngest seamount and may still be active. Its summit is covered by fresh lavas, recent faults and hydrothermal deposits. Seamount D is on crust 1.55 Ma and is inactive; like seamount 5, it has a breached caldera and is composed exclusively of N-MORB. Seamounts 5 and D represent the last stages of growth of typical N-MORB-only seamounts near the EPR axis. Seamounts 6 and 7 have bumpy, flattish summits composed of transitional and alkalic lavas. These lavas probably represent caldera fillings and caps overlying an edifice composed of N-MORB. Evolution from N-MORB-only cratered edifices to the alkalic stage does not occur on all near-EPR seamounts and may be favored by location on structures with relative-motion-parallel orientation.

1. Introduction

Oceanic central volcanoes, or seamounts, are ubiquitous in the vicinity of active mid-ocean ridges. Batiza and Vanko (1983, 1984) summarized the petrology of seamounts near the East Pacific Rise (EPR). Since then, new studies of near-EPR seamounts (Allan *et al.*, 1987; Fornari *et al.*, 1984, 1987a, b; Hekinian *et al.*, 1988) have provided additional data for other seamount groups. Previous studies indicate that near-EPR seamounts (within 2–3 Ma of the axis) are composed mainly of depleted mid-ocean ridge basalt (MORB). Compared to MORB from the adjacent EPR, seamount basalts are systematically more primitive, more heterogeneous, and in some cases more depleted (Fornari *et al.*, 1988a, b). At greater distances from the EPR axis (greater than 2–3 Ma) seamounts may also contain transitional and alkalic basalts which document the extent of mantle heterogeneity of the mantle source of MORB (Zindler *et al.*, 1984; Graham *et al.*, 1988; Fornari *et al.*, 1988b). In general, seamounts appear to be fed by relatively small, diverse batches of melt which rise rapidly from the mantle without extensive modification.

The primitive (high MgO, high temperature) nature of near-EPR seamounts makes them useful mantle probes to elucidate conditions of melting, the nature of the mantle source and the thermomechanical conditions of the lithosphere near the EPR. The utility of seamounts is enhanced because they occur near a variety of EPR offsets as well as near along-axis bathymetric highs (Macdonald *et al.*, 1988; Lonsdale, 1985; 1989a, b; Fornari *et al.*, 1987a, 1988b). Near-EPR seamounts occur individually and also as short linear chains which may be oriented parallel to relative plate motion (Barr, 1974; Batiza and Vanko, 1983), absolute plate motion (Davis and Karsten, 1986; Fornari *et al.*, 1984) or oblique to these directions (Vogt, 1971; Allan *et al.*, 1987 Schouten *et al.*, 1987). It is not yet known whether there are systematic chemical/isotopic differences among seamounts forming in these various tectonic settings. Such a comparison is hampered not only by lack of sufficient data, but also because individual seamounts evolve petrologically and comparisons must be made among volcanoes at similar stages of evolution.

* Present address: Hawaii Institute of Geophysics, 2525 Correa Rd, University of Hawaii, Honolulu, HI 96822

Marine Geophysical Researches **11**: 169–236, 1989.

TABLE I

ALVIN dives and ANGUS camera runs

Volcano	ALVIN/ANGUS	Transponders	Time on bottom (h)	Remarks
D	ALVIN 1402	3	5.5	south across gently sloping floor of breached caldera, near pit crater, up north-facing caldera wall to arcuate summit bench
D	ALVIN 1403	3	5.5	eastward across the caldera floor, up the west-facing caldera wall to the top of the summit bench
D	ALVIN 232	3	9.5	south across pit crater, up north-facing caldera wall across summit bench to outer flanks of the seamount. Along the top of the summit bench, down the northernmost part of the west-facing caldera wall and across caldera floor on a S-SE course
5	ALVIN 1396	3	7	northwest, then westward across gently sloping summit west of breached caldera
5	ALVIN 1397	3	6.5	westward across flat summit, up steep wall of summit bench to top; northward across summit bench, down north-facing caldera wall to caldera floor
5	ALVIN 1398	3	6.8	northern part of summit bench, down west-facing caldera wall to caldera floor, then eastward back up caldera wall
5	ALVIN 1399	3	7.5	eastward up stepped west-facing caldera wall and across southern part of summit bench
5	ALVIN 1400	3	6.8	caldera floor eastward across west-facing stepped caldera wall then westward back to caldera floor
5	ALVIN 1401	3	5.5	southeast, then north loop across the gently-sloping summit west of the southern summit bench
5	ANGUS 227	3	10.3	SE across western part of summit, looping northward down south-facing caldera wall across breached caldera floor then south up caldera wall and across the southern part of the summit bench
5	ANGUS 228	3	10.3	southward up the northern part of the summit bench then westward across summit bench, down caldera wall across caldera floor out to the flat summit area west of the caldera then northeast skirting the southern part of the summit bench, obliquely up caldera wall across central part of summit bench then westward across southern part of summit bench
5	ANGUS 229	3	8.0	caldera floor northeast to the outer flanks of volcano, southward up outer flanks to northern summit bench, westward down caldera wall, southeastward loop back up wall, across central summit bench with a west loop across the southern slopes of the south summit bench and out to the gently-sloping summit area west of the caldera
5	ANGUS 230	3	1.5	obliquely up the northeast outer flank of the volcano
5	ANGUS 231	3	6	southward across northern summit bench then southeast on the eastern slopes of the summit bench; at the southern end of summit bench, turning north across the flat 3 summit area, down the north-facing caldera wall to the floor of the breached caldera

TABLE I (continued).

Volcano	ALVIN/ANGUS	Transponders	Time on bottom (h)	Remarks
	ALVIN 1392	3	6.8	northward then eastward up outer flanks and summit region to the summit of volcano
7	ALVIN 1393	3	3.0	northward up gently-sloping summit area
7	ALVIN 1394	2	3.7	northward across small cone in cone and lava field on the gentle southern outer slopes of the volcano
7	ALVIN 1395	none	3.0	southward up fault scarp on the northernmost outer flanks of the volcano
7	ANGUS 224	3	9.6	starting on the gently-sloping summit southward and down the southwest flanks, turning north and then east, unslope and ending at the summit of the volcano
7	ANGUS 225	2	2.0	from south to north on the cone and lava field as the gentle southern flanks of the seamount
7	ANGUS 226	2	7.2	eastward traverse in the southern cone/lava field, as ANGUS 225
6	ALVIN 1387	3	5.8	across lip of caldera breach on 6E, down NE-facing caldera wall, across caldera floor northward, up south-facing caldera wall
6	ALVIN 1388	3	5.8	southward across caldera floor, up north-facing caldera wall, turning northeast, then east along the flat summit of 6E
6	ALVIN 1389	3	5.7	northward from gentle summit area toward summit of 6C, passing on the east side of the summit and looping west then south to end at the summit
6	ALVIN 1390	3	5.1	NNE track in cone and lava field on the south flanks of 6C
6	ALVIN 1391	3	5.6	study of south caldera wall of 6E, across caldera floor then east up west-facing caldera wall, across flat summit and up the arcuate summit bench, then north, northwest along the crest of the summit bench
6	ANGUS 219	3	7	southeast flank of 6C northeast to saddle with 6E, across breach in 6E caldera northward and eastward to summit bench
6	ANGUS 220	3	8	northward from flattish summit area to summit then turning east down northeast flank and looping south to cross the east flanks of 6C obliquely then east and northeast flanks of 6E, up and along the summit bench then down (westward) the northwest flanks of 6E
6	ANGUS 222	3	5.0	northward on the lower flanks of 6C across the southern cone and lava field
6	ANGUS 223	3	9.5	west across the lower flanks of 6C toward the saddle with 6W then northeast up the flanks of 6C to the summit terrace across the terrace eastward then south-east down the southeast slopes of 6C.

The purpose of this paper is to provide new data and interpretation bearing on the volcanic and petrologic evolution of near-EPR seamounts. We present the results of detailed submersible (DSV ALVIN) and photographic (ANGUS) study of four seamounts near the EPR (Table I). The four representative seamounts chosen (D, 5, 6 and 7) span a range of ages (1.0–3.0 Ma crust), sizes ($\sim$40–680 km^3), morphologic types and inferred stage of evolution. The geologic and petrologic results of this study provide detailed evidence for the roles of volcanism, tectonic activity, hydrothermal activity, sedimentation, mass wasting and other geologic processes during the evolution of individual seamounts. These results allow us to document various stages of seamount evolution and to speculate on the volcanological and petrologic processes that control the evolution of near-EPR seamounts.

Results

In this section, we summarize the ALVIN and ANGUS observations made on the four, seamounts (Figure 1). We start with seamount D, which is the smallest and geologically simplest and progress to the larger, generally older and more complex volcanoes: seamount 5, seamount 6 and seamount 7. For each volcano, we also present and summarize the petrologic and geochemical results from laboratory study of the volcanic rocks collected using ALVIN.

Seamount D

Figure 2 is a new map of seamount D showing the locations of one ANGUS camera run (232) and two ALVIN dives (1402 and 1403) on seamount D. Figure 3 shows the geology and sample locations along the ALVIN tracks and Figure 2 shows the

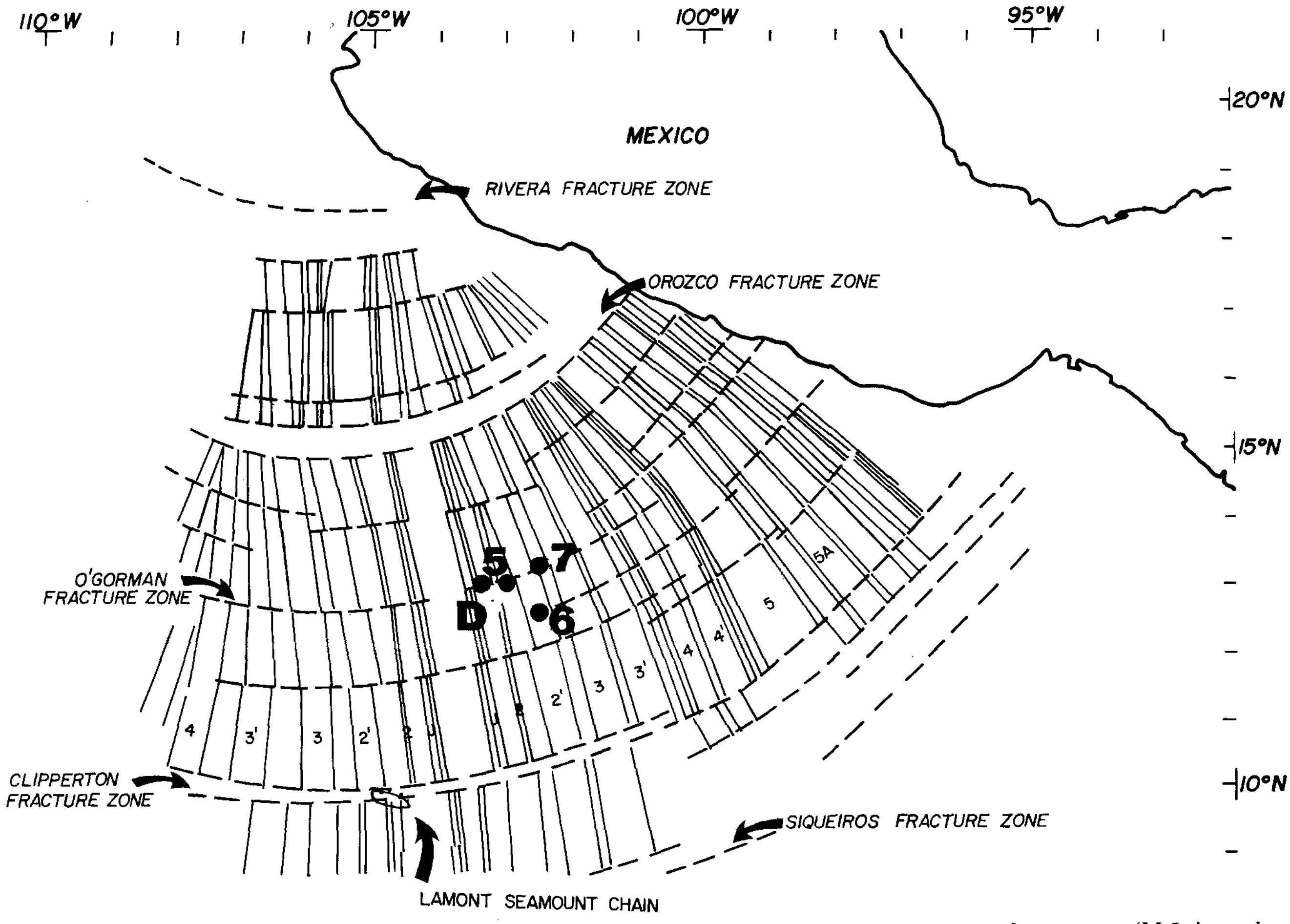

Fig. 1. Locations of seamounts 5, 6, 7 and D. Seamounts 5, D and 7 are located along the East O'Gorman fracture zone (McLain *et al.*, 1988). Seamount 6 is located south of this feature. Magnetic lineations after Klitgord and Mammerickx (1982).

geology in profiles. Seamount D has a volume of 38.6 km^3 and is located along the East O'Gorman fracture zone about 30 km east of seamount 5 on crust 1.55 Ma. It is roughly circular in plan, 1100 m high, has steep sides, a flat summit and a summit caldera which is open to the northwest. Most of the volcano is sedimented, giving an average of only about 20% rock outcrops in the areas examined. The volcanic rocks are coated with Fe-Mn oxides and hydroxides (hereafter called manganese) and are slightly to moderately weathered. Manganese thickness varies from only 1–2 mm to up to 2 cm, but is mostly 0.5 to 1.5 cm). There does not appear to be a systematic spatial distribution in the thickness of manganese coats, through, many of the samples collected deeper than 2250 m have thin (<0.5 cm) coats. These observations indicate that volcanic activity on seamount D ceased some time ago. Unfortunately, better age constraints on the youngest volcanic activity are unavailable.

A pit crater about 20 m deep is present between 2300 m and 2200 m depth within the broad arcuate depression of the breached caldera (Figures 2 and 3). The pit crater floor is completely covered with sediment whereas its surroundings are only partly buried. The flows in this area are mostly submarine pahoehoe cut by arcuate normal faults associated with caldera collapse. Some of these fault scarps are partly covered with younger pillow tubes.

The steep west and north-facing caldera walls are composed mostly of pillow basalt talus aprons alternating with 2–5 m high vertical walls and horizontal benches. The north facing wall (ALVIN 1402) is mostly talus with lobate pillows at the lip of the summit. The west facing wall also has abundant basalt talus mixed with sediment (ALVIN 1403), but along ANGUS 232, the wall mostly consists of a constructional pillow basalt slope. Above 2200 meters, the west facing slope consists of horizontal benches, between imbricate normal faults. Each bench is capped by submarine pahoehoe flows like those in the general vicinity of the pit crater.

The freshest looking flows, consisting of equant pillows, pahoehoe, hyaloclastite and lobate pillows in about equal amounts, are found at the summit above 2200 m. Outcrops appear fresh because they generally lack sediment cover; however, individual outcrops are separated by up to 20–10 m wide expanses of white, rippled pelagic sand. On level surfaces, ripple orientations indicate that currents are moving mainly NW or SE. However, on sloping surfaces, streaks and ripples indicate downslope sediment movement. Volcanic outcrops at the summit are locally cut by circumferential faults. The steep outer flanks on the south side of seamount D are composed of loose rubble mixed with sediment.

On the basis of these observations we conclude that formation of the breached caldera on Seamount D was preceded by outpourings of submarine pahoehoe and lobate pillows. Caldera collapse was followed by localized, less voluminous eruptions of pillow lava. Since most of the outcrops are apparently close in age, these events may all have occurred within a fairly short period of time (10^2–10^3 yr?). Thereafter, mass wasting on steep slopes, sedimentation and sediment redeposition have been the dominant processes on seamount D.

Figures 2 and 3 show ALVIN sample sites. The rocks include in-place pillow and pahoehoe fragments as well as basalt talus. Hyaloclastite specimens recovered from seamount D and the other volcanoes of this study are described fully in Smith (1987) and Smith and Batiza (1988). With the exception of samples 1403–1801A and 1403–1801B, which are coarsely Pl-Ol porphyritic, the rocks are aphyric to sparsely phyric with phenocrysts and microphenocrysts of olivine and plagioclase. Megacrysts of these phases also occur in most of the samples but are abundant only in 1403–1801A and B, collected in the vicinity of the pit crater.

Table II gives chemical analyses of samples from seamount D. All the samples are relatively primitive, incompatible element-depleted N-MORB with a narrow range of MgO (7.65 to 8.81 wt%). Figure 4 shows variation of TiO_2 with MgO abundance. With decreasing MgO, the abundances of TiO_2 and K_2O increase and Ni and Cr decrease, indicating that fractional crystallization may have played a role in the origin of the relatively evolved lavas. Least squares mixing calculations for major oxides show that this fractionation could be accomplished by subtracting 4.6 wt% Ol, 13.1 wt% Plag and 0.3 wt% Cpx from the most primitive sample to yield the most evolved one (sum of $r^2 = 0.08$). In contrast, the incompatible trace elements Ta, Hf and Zr do not correlate with MgO, indicating that multiple parental melts, are required to explain the trace element data. This interpretation follows Batiza and

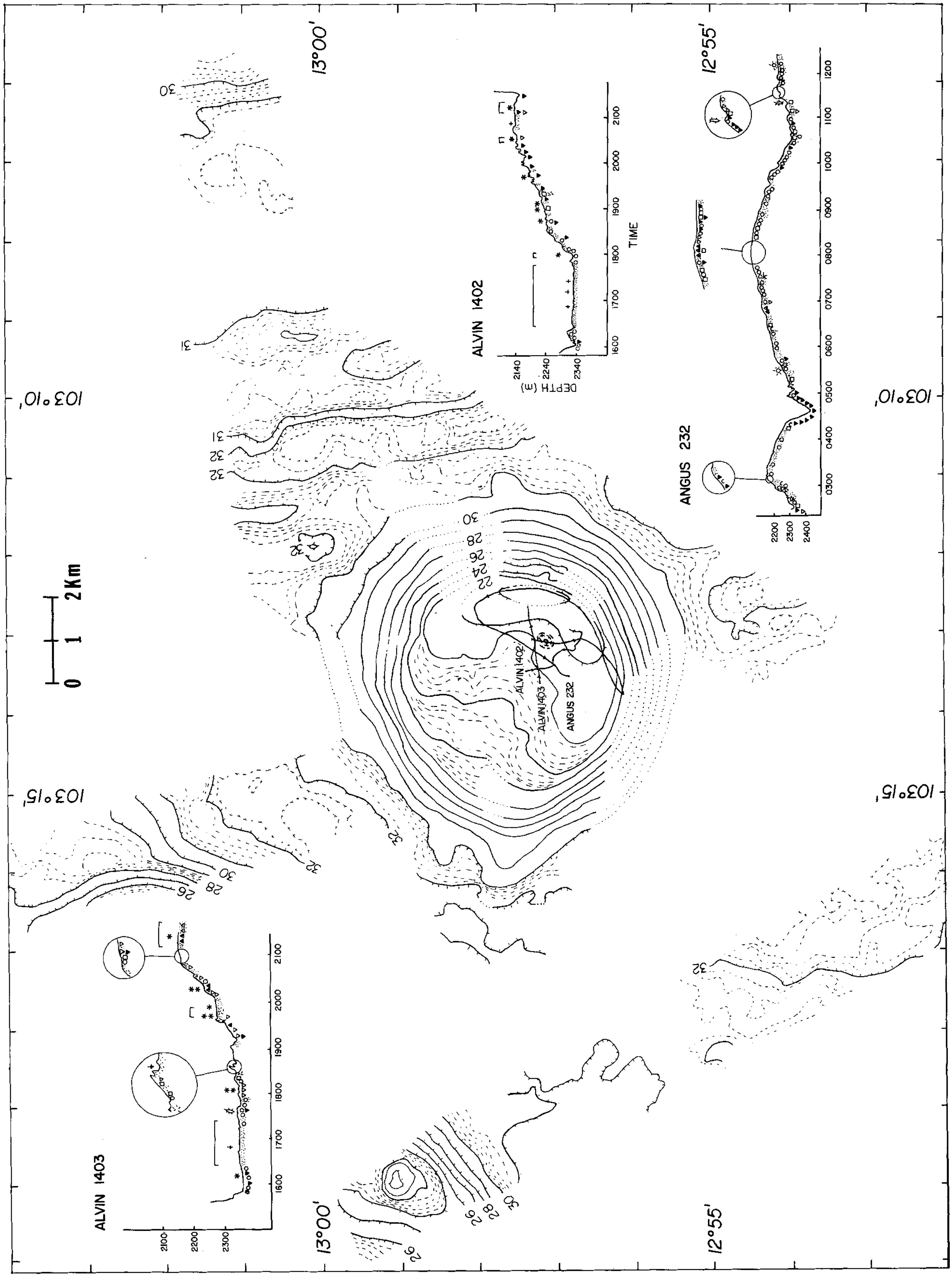

Fig. 2. Map of seamount D showing the locations of ALVIN dives and ANGUS camera runs. Also shown are profiles of geology (vertical exaggeration 4×) along the tracks (see legend of Figure 3).

Vanko (1984) and Allan *et al.* (1987) who showed this situation is common on near-EPR seamounts. Variation of the major elements, Ni and Cr are satisfactorily explained by fractional crystallization, but incompatible element abundances show that fractionation from a single parental liquid is not possible. We thus suggest that the lavas of seamount D represent a range of parental liquids with similar major element abudances but different trace element abundances. Such liquids could be related by variable extents of melting of a heterogeneous mantle source as shown by Batiza and Vanko (1984) and Allan *et al.* (1987). Support for this hypothesis is provided by Figure 5 which shows good correlation between $(La/Sm)_n$ and La/Hf. After segregation, these individual melt batches apparently undergo variable amounts of fractional crystallization before or during eruption.

On seamount D, there is a tendency for the most primitive (highest MgO) samples to occur at the shallowest depths. Table II shows that samples with Mg# > 67 are found shallower than 2200 m depth. These samples are all located on the N-S trending crest of the summit bench and are also the freshest looking samples on the seamount. Later, we discuss possible interpretations of these systematic chemical-stratigraphic relationships.

Seamount 5

Figure 6 shows a Seabeam map of seamount 5. It is located along the East O'Gorman fracture zone west of seamount D on crust 1.0 Ma old (Figure 1). The volcanic edifice is large (~2000 m high, ~490 km^3 in volume), steep-sided and has a broad, gently sloping summit area. The north and northeast side of the summit area contains an arcuate summit bench surrounding a ~1500 m wide caldera which is open (breached) to the north-northwest.

Figure 7 is a more detailed map of the summit area where the six ALVIN dives (1396–1401) and five ANGUS runs (227–231) were concentrated. Figures 8 and 9 show the geology in cross sections along the ALVIN and ANGUS tracks and Figure 10 shows the geology and sample locations in map view. Some tracks are located on the gentle summit region west of the caldera and arcuate summit bench, but most are in the vicinity of the caldera where hydrothermal deposits are widely distributed. Seamount 5 is closer to the EPR than D and although 5 is much larger than seamount D, it is clearly much younger. The summit region has about 70% volcanic outcrop, the rocks generally have very thin (< 1–2 mm) manganese coating and are very fresh in appearance and in thin section. Much of the region near the caldera has active low-temperature hydrothermal venting.

The gently-sloping summit region west of the caldera is mainly covered with submarine pahoehoe and large, flat, lobate pillows with a light dusting of sediment (Plates 1–4).* Sediment has accumulated locally in small (1–2 m) sediment ponds but measurements with a meter-stick using ALVIN showed that the ponds are only a few centimeters thick. The volcanic deposits are cut by widely spaced (100's of meters) faults with circumferential orientations. The pahoehoe and lobate pillows are locally overlain by pillow lava flows and covered by hydrothermal deposits of several types.

LEGEND

UNITS:

PILLOW LAVA		PAHOEHOE/SHEET FLOW	□	PILLOW ELONGATION DIRECTION	→
Bulbous	○	PAHOEHOE/SHEET FLOW TALUS	▽	PAHOEHOR FLOW STREAK	
Tubes	●	MASSIVE ROCK		CONTACT	—
Mixed	◑	HYALOCLASTITE	△	FAULT	∿
Pillow Talus	▼	SEDIMENT	∴	HAYSTACK	
LOBATE FLOW	⌒	CRUST	×	HYALOCLASTITE VENT	(1,2,3)
				ROCK SAMPLE	*
				SEDIMENT SAMPLE	+

Note: This legend also applies to Figures 3, 15, 16, 17 and 19.

*For Plates 1–15, see pp. 229–236.

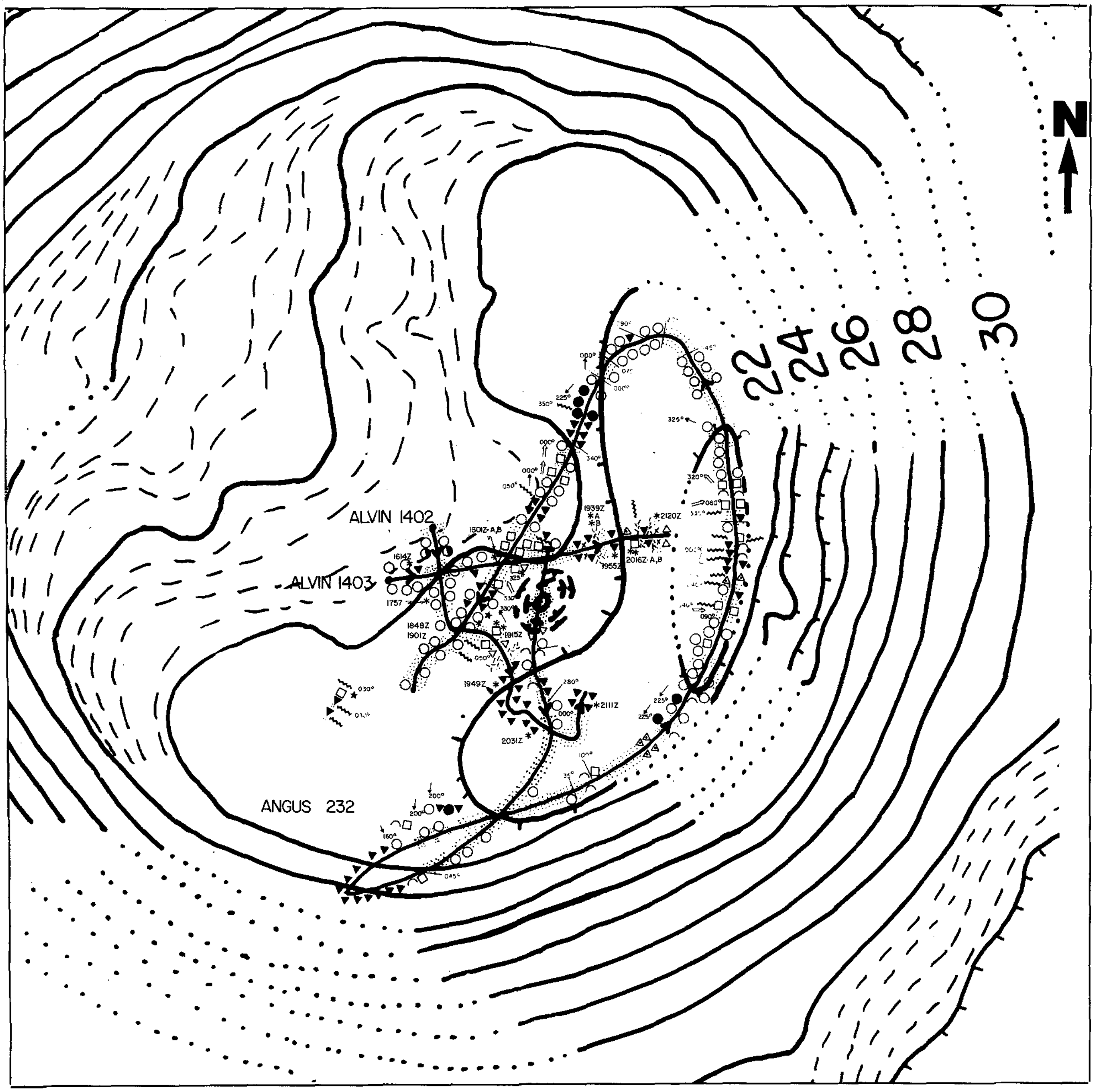

Fig. 3. Geology of Seamount D along ALVIN and ANGUS tracks.

The arcuate summit bench consists of several 50–100 m topographic highs which define the margin of the breached collapse caldera. The highs, as well as the arcuate platform from which they rise, are intensely faulted and mainly consist of pillow lava (Plates 5–7). The prominent west and north facing fault scarps which bound the arcuate summit bench are up to 200 m high. These Scarps, as well as many smaller ones that cut the area of the summit bench and the caldera itself, are locally characterized by aprons of sediment-free basalt talus but in many cases are vertical walls. Some scarps are covered with steeply dipping tubular pillows erupted during or shortly after faulting occurred (Plate 5). In some cases, these pillow flows are themselves cut by faults implying several episodes of faulting and eruption.

The breached caldera does not have a well defined, flat floor. Instead, it is characterized by stepped benches between major fault scarps, with stepwise deepening to the north-northwest. Where studied, these flat areas are covered with hydrothermal mineral deposits. These soft, friable deposits are greyish, reddish or dark brown but locally may be covered by large (100's of meters) patchy networks of bright yellow and white bacterial mats (Plate 8). The areas with bacterial mats also contain very delicate thin (1–5 mm) tubes of hydrothermal material which we interpret as vents for warm hydrothermal fluids (Alt *et al.*, 1987; Alt, 1988) localized along circumferential faults associated with the caldera (Figure 11). As with seamount D, the steep outer flanks of seamount 5 are composed mostly of loose rubble.

Though clearly younger than seamount D, seamount 5 has had a very similar geologic history. Caldera collapse was preceded by outpourings of submarine pahoehoe and lobate pillows and followed by local eruptions of pillow lava. Low temperature hydrothermal venting along with mass wasting and sedimentation have followed.

The mineralogy and petrology of seamount 5 based on dredged samples was discussed by Batiza (1980), Batiza and O'Hearn (1982) and Batiza and Vanko (1984). Table III and Figures 12 and 13 show that samples recovered during the ALVIN program are chemically very similar to those analyzed previously, with the exception of some new, high-MgO samples collected with ALVIN. The samples from seamount 5 are all depleted N-MORB ranging from primitive ($Mg/Mg + Fe^{2+} \times 100 = Mg\#$ of 67) to somewhat fractionated ($MgO = 6.31$ wt%, $Mg\# = 55$). Most of the samples with $Mg\# > 65$ are found on the summit bench at depths shallower than 1050 m, in a similar setting to those recovered from seamount D. Fractionation of 9 wt% Ol, 25 wt% Plag and 6 wt% Cpx from the most primitive lava is capable of producing the most fractionated basalt (stepwise calculations in 7 steps, mean sum of $r^2 = 0.34$).

Fractional crystallization of observed phenocryst phases can also explain the increases of Ta, Th, U, Zr, Ba and Hf with decreasing MgO (Figure 12) but the observed scatter calls for either differences in the extent of melting for parental melts or mantle heterogeneity or both. Based on correlations such as shown in Figure 13, we propose that primitive melts are produced by variable extents of melting of heterogeneous mantle sources which are mixed prior to melting. The interpretations follow those of Batiza and Vanko (1984) and Allan *et al.* (1987) and are supported by isotopic and volatile abundance data (Graham *et al.*, 1988; Aggrey *et al.*, 1988).

Seamount 6

Seamount 6 consists of three coalesced edifices aligned parallel to the relative motion of the Cocos plate (Batiza and Vanko, 1983; Figure 14). The linear seamount group is located about 75 km south of the East O'Gorman fracture zone almost directly south of Seamount 7 (Figure 1) on crust ~3.0 Ma old. The middle edifice of the group (6C) is the largest (52 km^3, ~1300 m high) whereas the east and west edifices (6E and 6W) are smaller (21 km^3, 750 m high and ~22 km^3, 420 m high, respectively). Volcano 6E has an arcuate summit bench and a 750 m wide summit crater open to the west whereas 6C has a gently sloping, terraced summit interpreted to be a filled caldera. 6C has a prominent flank rift zone on its north side, (Figure 14) that trends 340°, subparallel to the trend of the East Pacific Rise. The lower flanks of 6C are gentle and contain numerous small (up to 100 m high) volcanic cones. These are similar to the cones and lava fields surrounding volcanoes of the Lamont Seamount chain (Fornari *et al.*, 1988a, b). The cone and lava fields south of 6C were studied during ALVIN 1390 and with ANGUS 222. The summit and flanks of 6C were studied during ALVIN 1389 and with ANGUS 219, 220 and 223. The summit and flanks of 6E were studied with ANGUS 221 and during three ALVIN dives (1387, 1388 and 1391). Figures 15, 16, 17, 18 and 19 show the geology of these traverses in map view and cross section.

The cone and lava field (Figure 19) is composed almost exclusively of pillow lava forming haystacks and outcrops of bulbous and tubular pillows. Most outcrops, even on steep slopes, are evenly covered with dark fine-grained sediment. The rocks themselves have thick (up to 2 cm) coatings of manganese and are weathered. In addition to in situ tubular pillows, very steep slopes (probably fault-controlled) may also have aprons of pillow talus. Similar deposits, though almost completely covered with sediment and with more abundant talus, characterize the deeper (below 2500 m) flanks elsewhere on 6C and

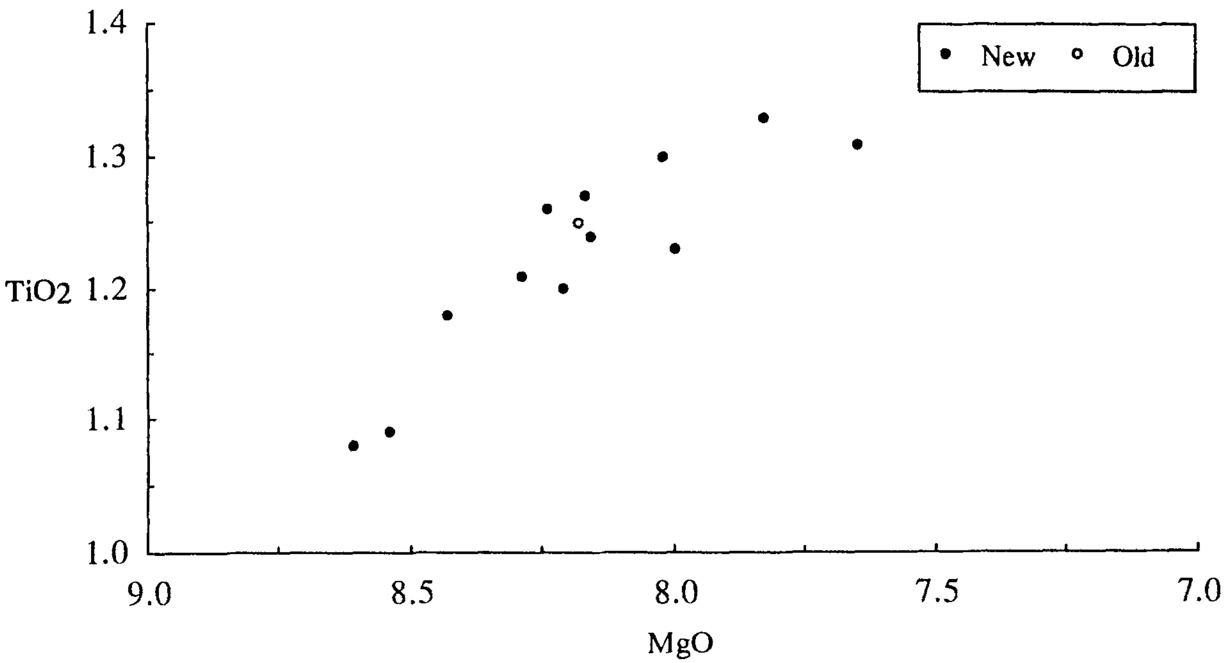

Fig. 4. TiO_2 vs. MgO for seamount D lavas showing their generally primitive nature and narrow range of chemical variation.

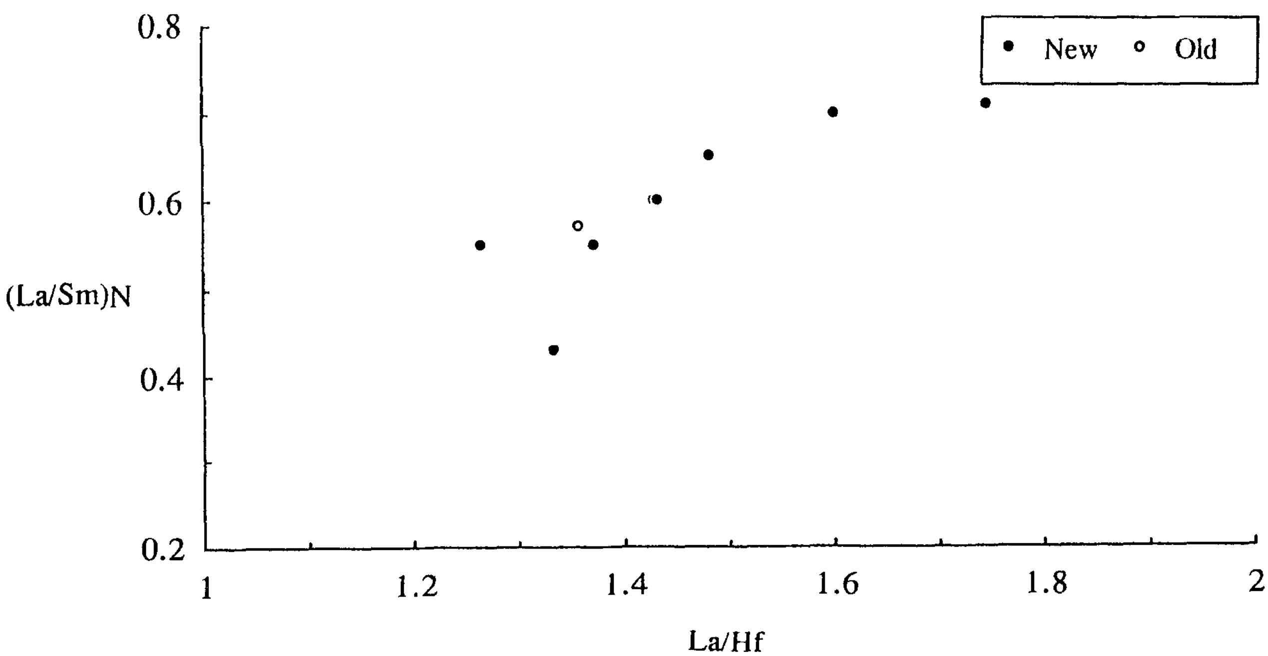

Fig. 5. $(La/Sm)_n$ vs. La/Hf showing the good correlation of incompatible trace element ratios.

TABLE II

Major and trace element data for Seamount D

Sample	1402/1757	1402/1848	1402/1901	1402/2031	1402/2111	1402/2111R	1403/1614	1403/1801A
Depth (m)	2341	2259	2255	2162	2154	2154	2318	2308
Sample type	PT	Pa	M	PT	PaT	PaT	Pa	Pa
SiO_2	50.52	49.97	49.90	49.83	50.23	50.41	50.35	51.02
TiO_2	1.31	1.21	1.30	1.27	1.24	1.26	1.33	1.23
Al_2O_3	14.97	16.34	15.90	16.30	16.40	16.59	15.62	16.01
FeO*	9.75	8.86	8.82	8.53	8.39	8.49	9.13	8.75
MgO	7.65	8.29	8.02	8.17	8.16	8.24	7.83	8.00
CaO	12.77	12.23	12.35	12.29	12.19	12.22	12.49	12.39
Na_2O	2.53	2.64	2.73	2.66	2.65	2.65	2.60	2.56
K_2O	0.11	0.09	0.11	0.13	0.13	0.12	0.11	0.10
P_2O_5	0.15	0.11	0.14	0.13	0.13	0.18	0.15	0.13
Total	99.76	99.74	99.27	99.31	99.52	100.16	99.61	100.19
INNA-FeO*	8.78	8.32	8.62	8.36	8.11		8.45	8.51
INNA-Na_2O	2.47	2.6	2.74	2.65	2.59		2.52	2.63
La	2.70	2.78	2.96	3.60	3.56		2.77	3.00
Ce	8.16	8.87	9.04	10.61	10.58		8.41	8.79
Sm	2.57	2.74	3.73	2.86	2.74		2.75	2.74
Eu	1.016	1.097	1.082	1.089	1.057		1.134	1.043
Tb	0.61	0.61	0.62	0.63	0.59		0.70	0.59
Yb	2.55	2.45	2.49	2.34	2.34		2.48	2.37
Lu	0.36	0.36	0.41	0.35	0.35		0.36	0.35
Sc	41	37	37	38	38		39	39
Cr	355	333	337	338	331		342	381
Co	43	42	43	42	41		42	44
Ni	108	110	–	152	106		96	149
Rb	11	6	–	–	9			
Cs	0.05	0.06	0.08	0.12	0.08		0.08	–
Sr	78	127	138	143	154		162	113
Ba	49	66	25	67	50		46	53
Zr	77	71	–	–	83		71	–
Hf	1.99	2.2	2.22	2.25	2.04		2.02	2.1
Th	0.07	0.08	–	–	0.13		0.05	–
Ta	0.14	0.16	0.12	0.19	0.21		0.11	0.18
U	0.44	0.41	0.23	0.29	0.4		0.44	0.2
Mg#	62.6	66.7	66	67.2	67.5	67.5	64.7	66.1
$(La/Sm)_N$	0.57	0.55	0.43	0.7	0.71		0.55	0.6

TABLE II (continued)

Sample	1403/1801B	1403/2016A	1403/2120	1403/2120-R	7-1
Depth(m)	2308	2194	2100	2100	2400–2250
Sample type	Pa	Pa	PT	PT	–
SiO_2	50.38	50.10	49.94	50.27	50.17
TiO_2	1.20	1.18	1.09	1.08	1.25
Al_2O_3	15.99	16.44	16.44	16.32	15.97
FeO*	8.67	8.57	8.49	8.44	8.87
MgO	8.21	8.43	8.54	8.61	8.18
CaO	12.43	12.27	12.47	12.35	12.26
Na_2O	2.58	2.57	2.41	2.43	2.61
K_2O	0.11	0.09	0.08	0.09	0.10
P_2O_5	0.14	0.14	0.13	0.17	0.13
Total	99.71	99.79	99.59	99.76	99.54
INNA-FeO*	8.34		8.13		8.55
INNA-Na_2O	2.49		2.36		2.45
La	0.05		2.55		2.74
Ce	9.13		7.75		8.89
Sm	2.58		2.33		2.64
Eu	1.034		0.961		1.04
Tb	0.58		0.54		0.71
Yb	2.33		2.25		2.53
Lu	0.34		0.32		0.38
Sc	39		37		37
Cr	354		361		350
Co	42		43		42
Ni	108		146		139
Rb					5
Cs	0.07		0.05		–
Sr	167		118		151
Ba	53		40		17
Zr	98		66		92
Hf	2.06		1.78		2.02
Th	0.09		0.08		0.04
Ta	0.16		0.15		–
U	0.45		0.49		0.02
Mg#	66.9	67.8	68.2	68.5	65.9
$(La/Sm)_N$	0.65		0.6		0.57

Major elements by electron microprobe, Smithsonian Institution.
Trace elements by instrumental neutron activation at Washington University.
FeO* = total iron oxide
T = Talus
P = pillow, in place
Pa = pahoehoe, in place
M = massive flow
LP = lobate pillow

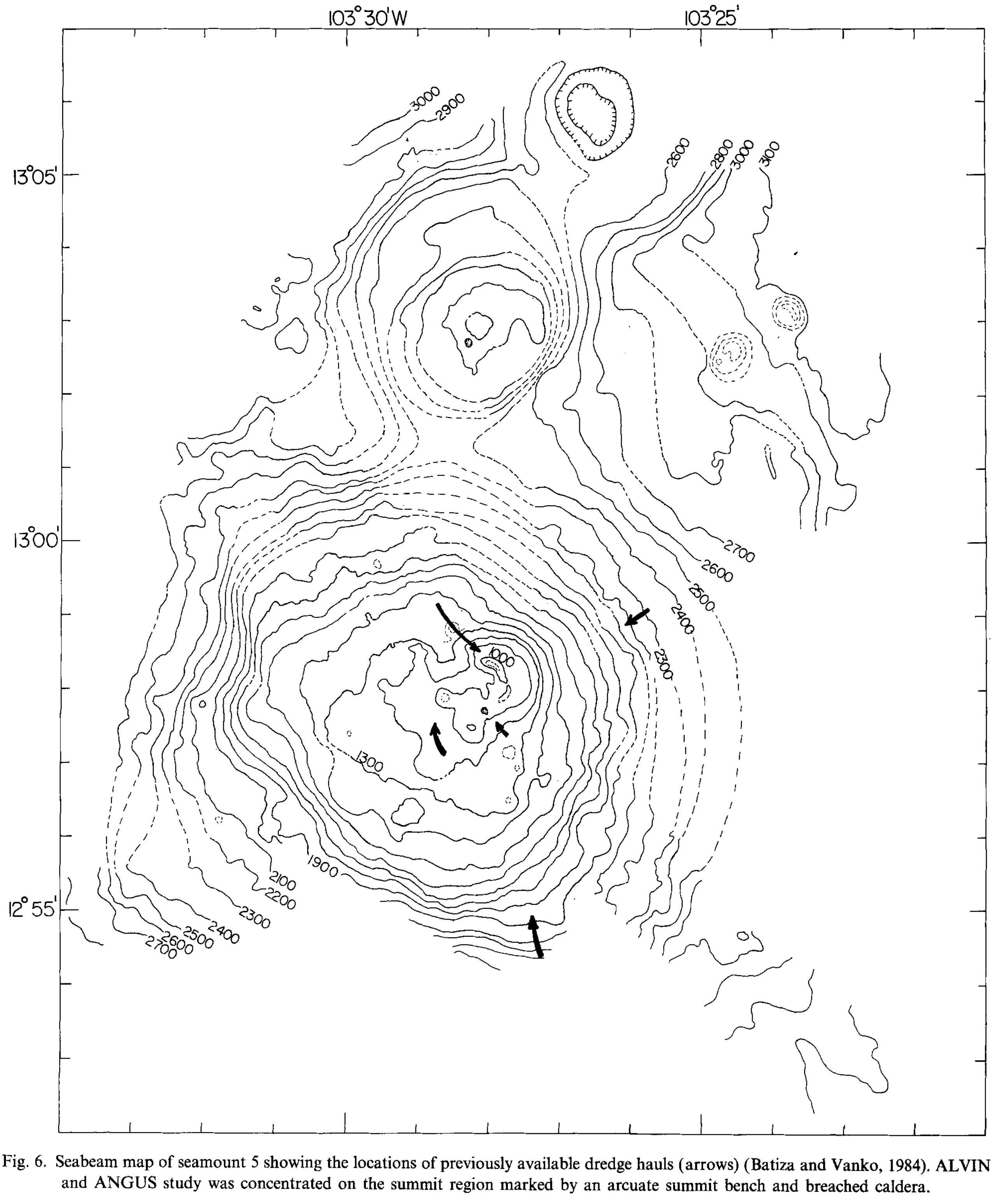

Fig. 6. Seabeam map of seamount 5 showing the locations of previously available dredge hauls (arrows) (Batiza and Vanko, 1984). ALVIN and ANGUS study was concentrated on the summit region marked by an arcuate summit bench and breached caldera.

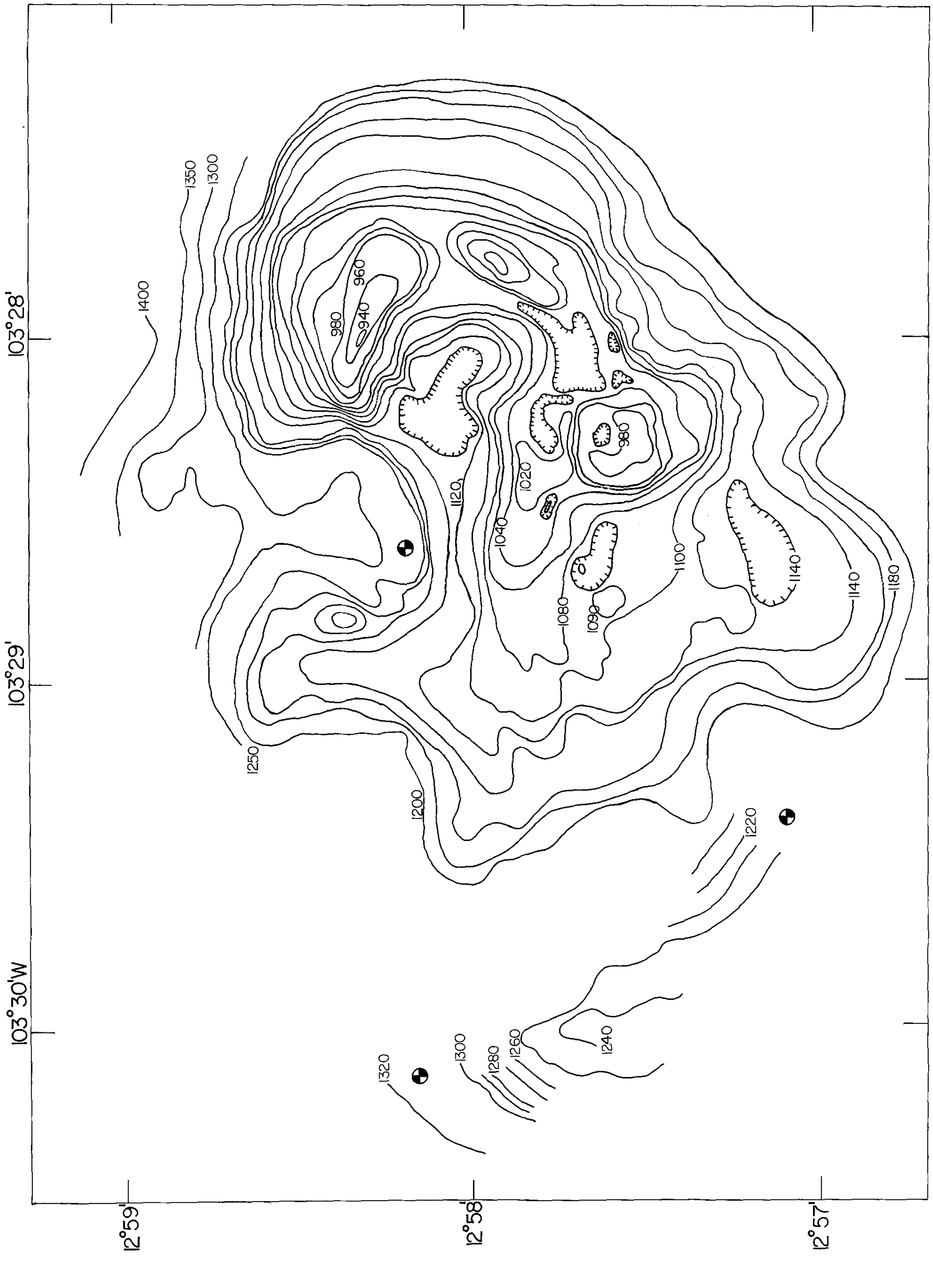

Fig. 7. Bathymetric map of the summit area of seamount 5. This map is based on Seabeam bathymetry supplemented by depths along ALVIN and ANGUS tracks.

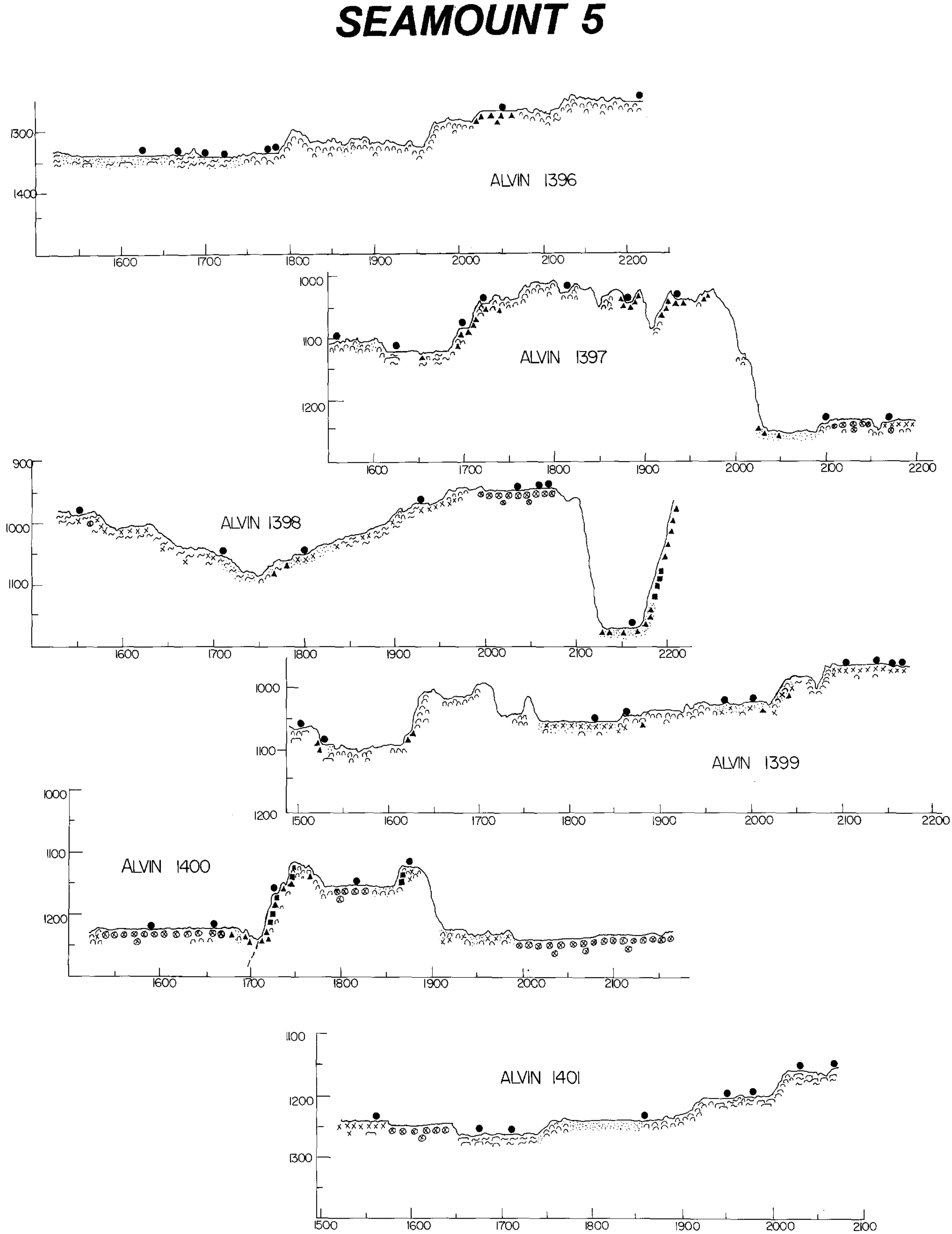

Fig. 8. Geologic profiles of seamount 5 (vertical exaggeration 4×) along ALVIN tracks. Same symbols as Figure 10.

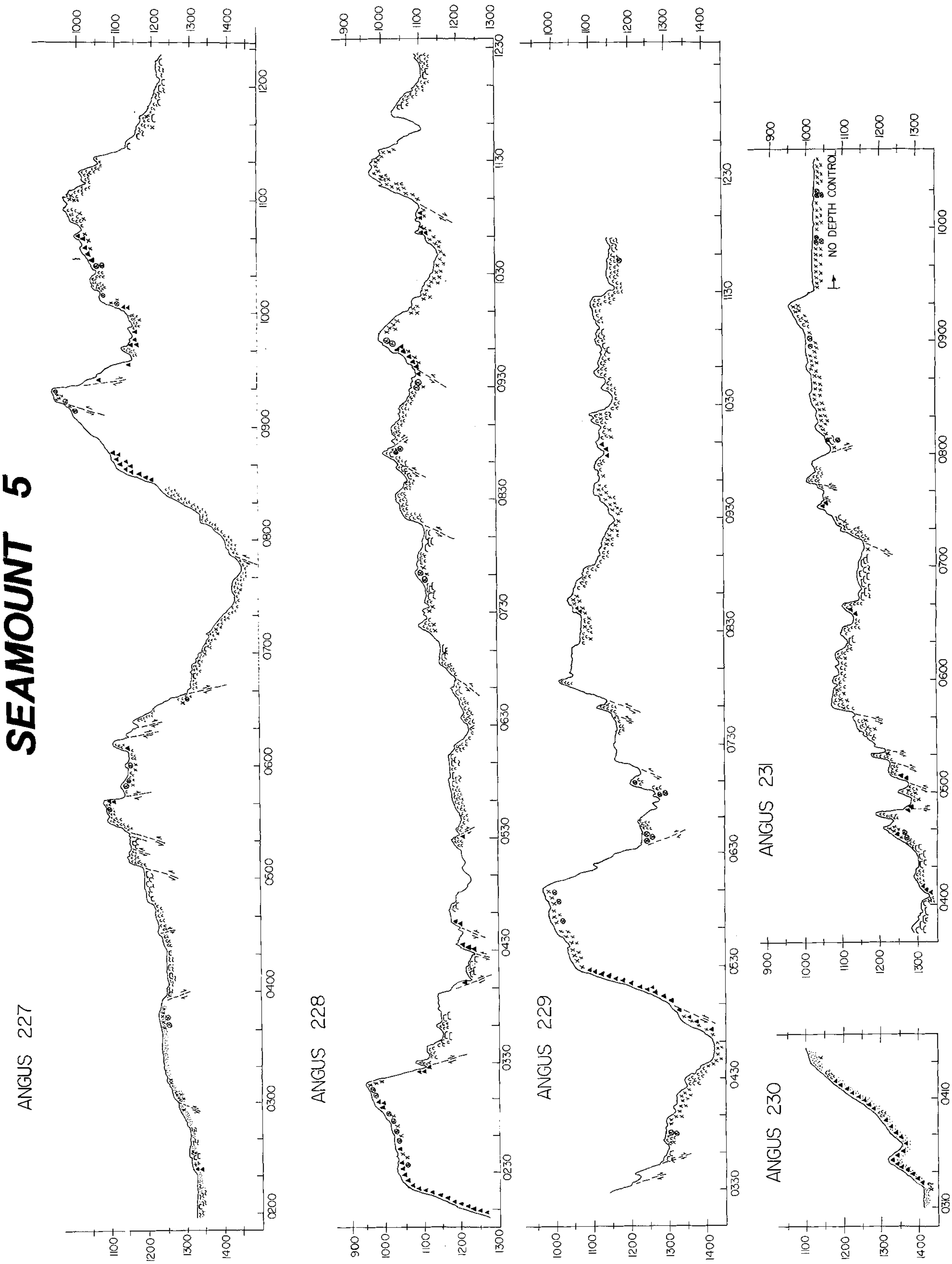

Fig. 9. Geologic profiles of seamount 5 (V.E. 4×) along ANGUS tracks. Same symbols of Figure 10.

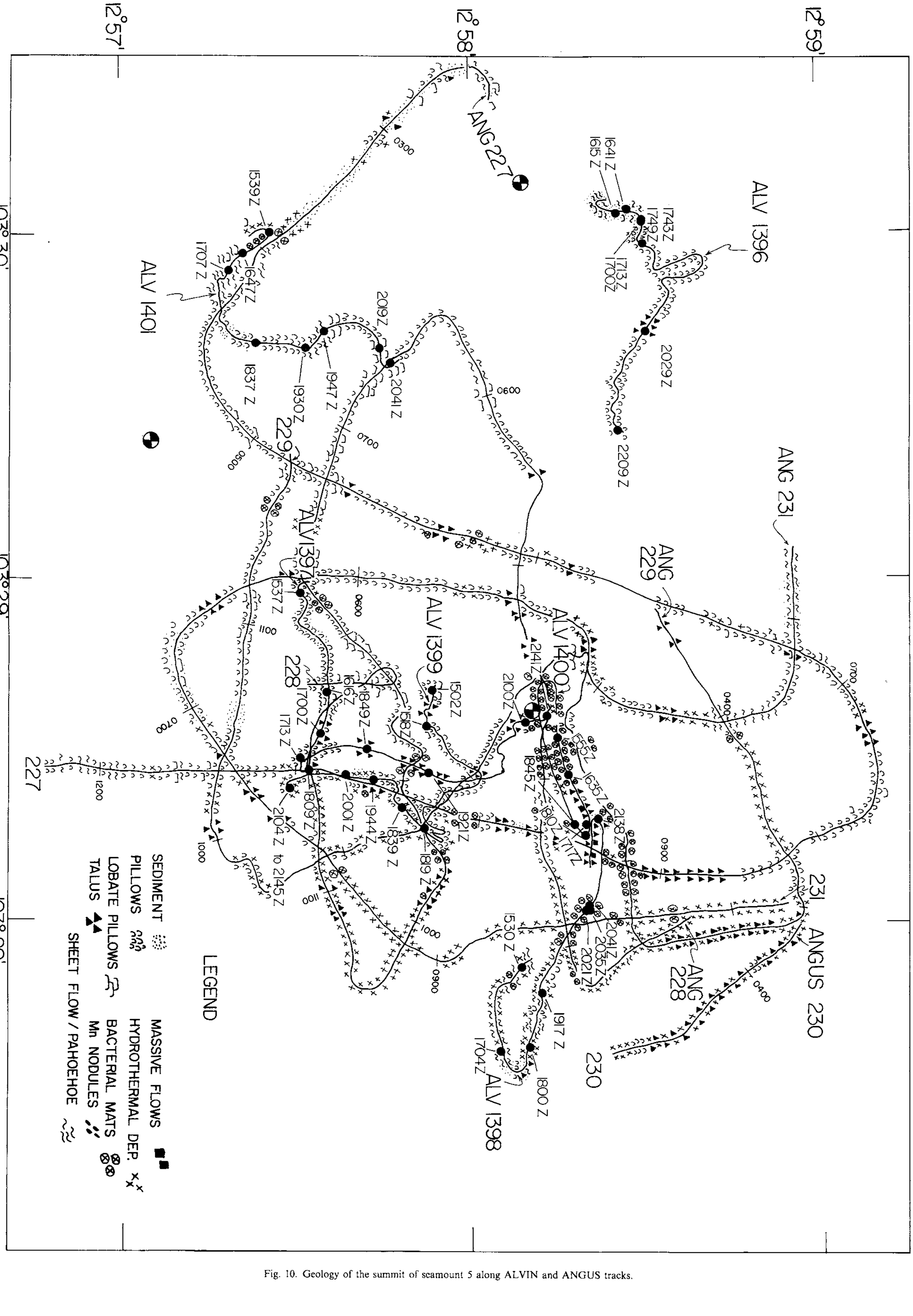

Fig. 10. Geology of the summit of seamount 5 along ALVIN and ANGUS tracks.

TABLE III

Major and trace element data for Seamount 5

Sample	1396/1615	1396/1641	1396/1711	1396/1713	1396/1743	1396/1749	1396/2209	1397/1537
Depth(m)	1345	1344	1348	1349	1340	1340	1241	1105
Sample type	P	Pa	Pa	P	P	P	P	Pa
SiO_2	50.31	50.28	50.74	50.96	50.83	51.00	50.71	50.68
TiO_2	1.59	1.58	1.85	1.90	1.66	1.74	1.64	1.67
Al_2O_3	15.11	16.91	15.08	15.02	15.40	14.80	15.36	15.20
FeO*	9.29	8.45	10.20	10.20	9.37	9.74	9.36	9.46
MgO	7.20	7.61	6.69	6.83	7.16	6.92	7.03	7.02
CaO	12.40	11.60	11.30	11.20	11.90	12.00	11.80	12.00
Na_2O	2.95	3.22	3.42	3.40	3.10	3.06	3.05	2.95
K_2O	0.20	0.22	0.18	0.26	0.18	0.18	0.16	0.20
P_2O_5	0.18	0.20	0.18	0.17	0.17	0.17	0.18	0.19
Total	99.18	100.11	99.58	99.9	99.77	99.56	99.33	99.34
INNA-FeO*		8.17		9.90		9.16	8.94	8.63
INNA-Na_2O		3.13		3.39		3.14	3.04	2.94
La		5.99		5.80		5.61	5.23	5.47
Ce		16.57		16.94		15.71	14.10	15.06
Sm		3.56		4.28		3.73	3.80	3.47
Eu		1.34		1.57		1.41	1.44	1.32
Tb		0.68		0.87		0.81	0.83	0.73
Yb		2.58		3.35		2.79	2.83	2.72
Lu		0.37		0.50		0.41	0.40	0.38
Sc		36		44		43	42	41
Cr		280		103		322	315	314
Co		39		41		40	40	40
Ni		138		40		–	66	102
Rb		7		8		–	11	5
Cs		<0.12		<0.13		<0.12	<0.13	<0.07
Sr		261		158		175	230	213
Ba		<0.84		<0.57		<0.55	<0.79	<0.56
Zr		103		125		–	129	143
Hf		2.98		3.46		3.05	3.07	2.87
Th		0.44		0.28		–	0.24	0.24
Ta		<0.4		<0.36		0.3	0.28	0.34
U		<0.24		<0.42		<0.24	<0.40	<0.31
Mg #	62.3	65.8	58.4	58.8	62.6	60.3	61.6	61.3
$(La/Sm)_N$		0.92		0.74		0.82	0.75	0.86

TABLE III (continued)

Sample	1397/1616	1397/1700	1397/1713	1397/1809	1397/1849	1397/1921	1397/2100	1397/2141Z
Depth(m)	1119	1080	1036	1025	1042	1033	1226	1229
Sample type	P	PT	Pa	P	P	PT	P	S
SiO_2	50.86	50.31	50.44	50.45	50.46	50.58	49.59	50.40
TiO_2	1.63	1.26	1.31	1.30	1.54	1.57	1.62	1.58
Al_2O_3	15.47	16.01	15.66	15.81	15.24	15.20	16.24	15.17
FeO*	9.23	8.71	8.98	8.88	9.20	9.48	9.10	9.30
MgO	7.14	7.94	7.80	7.81	7.42	7.27	7.55	7.28
CaO	11.80	12.23	12.22	12.22	12.29	12.17	11.56	12.28
Na_2O	3.04	2.82	2.86	2.87	2.91	2.97	3.08	2.97
K_2O	0.17	0.08	0.07	0.07	0.19	0.22	0.18	0.19
P_2O_5	0.17	0.11	0.14	0.11	0.17	0.18	0.20	0.18
Total	99.51	99.47	99.48	99.52	99.42	99.64	99.12	99.35
INNA-FeO*			8.56		8.56		8.65	
INNA-Na_2O			2.82		2.89		2.85	
La			2.38		4.74		5.42	
Ce			7.96		13.20		16.21	
Sm			2.72		3.40		3.59	
Eu			1.11		1.31		1.36	
Tb			0.64		0.74		0.73	
Yb			2.50		2.67		2.81	
Lu			0.36		0.39		0.41	
Sc			39		41		37	
Cr			356		331		247	
Co			44		41		40	
Ni			105		122		117	
Rb			<0.9		10		4	
Cs			<0.07		<0.11		<0.09	
Sr			115		34		174	
Ba			<0.33		<0.60		<0.58	
Zr			65		60		157	
Hf			2.13		2.65		3.12	
Th			0.04		0.38		0.17	
Ta			0.13		0.24		0.28	
U			<0.31		<0.36		<0.71	
Mg#	62.3	66.1	65	65.3	63.3	62.1	63.9	62.6
$(La/Sm)_N$			0.48		0.76		0.83	

TABLE III (continued)

Sample	1397/2100Z	1398/1704	1398/2021	1398/1800B	1398/2138	1399/1502	1399/1518	1399/1819
Depth(m)	1226	1044	953	1054	1190	1068	1096	1058
Sample type	S	Pa	S	Pa	Pa	P	PT	P
SiO_2	50.20	48.97	49.69	50.45	50.61	50.72	50.44	50.96
TiO_2	1.50	1.26	1.25	1.36	1.41	1.50	1.50	1.77
Al_2O_3	15.71	16.50	16.64	15.80	15.58	15.55	15.75	15.02
FeO*	9.03	8.80	8.63	8.97	9.11	9.08	9.03	10.05
MgO	7.49	7.98	8.17	7.56	7.48	7.42	7.51	6.77
CaO	12.15	11.92	11.94	12.02	12.09	12.11	11.98	11.68
Na_2O	2.92	2.87	2.85	3.02	3.00	2.91	2.96	3.10
K_2O	0.19	0.14	0.12	0.12	0.13	0.20	0.17	0.22
P_2O_5	0.19	0.14	0.17	0.15	0.16	0.19	0.20	0.21
Total	99.38	99.58	99.46	99.45	99.57	99.68	99.54	99.78
INNA-FeO*	8.92	8.5		8.45	8.80	8.47		9.29
INNA-Na_2O*	2.95	2.83		2.87	2.85	2.79		3.02
La	5.31	3.38		3.54	3.64	4.81		5.24
Ce	13.98	10.61		10.01	11.31	13.60		14.56
Sm	3.35	2.93		4.00	3.17	3.27		3.68
Eu	1.26	1.16		1.14	1.26	1.23		1.41
Tb	0.70	0.62		0.64	0.69	0.67		0.79
Yb	2.63	2.45		2.45	2.65	2.6		2.97
Lu	0.40	0.36		0.47	0.38	0.38		0.43
Sc	40	38		37	41	40		41
Cr	334	310		309	310	325		136
Co	41	42		42	41	40		41
Ni	–	102		128	66	86		62
Rb	–	5		–	6	4		5
Cs	<0.06	<0.09		<0.09	0.07	<0.06		<0.06
Sr	190	139		154	105	188		195
Ba	–	<0.44		<0.52	<0.52	<0.57		<0.58
Zr	–	11		–	75	132		130
Hf	2.70	2.29		2.33	2.52	2.69		3.04
Th	0.19	0.16		–	0.12	0.18		0.24
Ta	0.29	0.21		0.19	0.21	0.29		0.33
U	<0.35	<0.56		<0.16	<0.42	<0.35		<0.36
Mg#	63.9	66	66.9	64.3	63.7	63.6	64	59
$(La/Sm)_N$	0.87	0.63		0.48	0.63	0.81		0.78

TABLE III (continued)

Sample	1399/1839	1399/2117	1399/2124	1399/2145	1400/1635	1400/1717A	1400/1717B	1400/1810
Depth(m)	1048	961	972	971	1223	1166	1166	1153
Sample type	M	LP	LP	Pa	P	PT	PT	P
SiO_2	50.42	51.36	51.27	50.89	50.11	50.52	50.48	49.96
TiO_2	1.72	1.63	1.59	1.62	1.56	1.43	1.49	1.61
Al_2O_3	15.24	15.19	15.10	15.30	16.28	15.77	15.63	16.61
FeO*	9.81	9.53	9.56	9.64	9.06	9.00	8.98	8.88
MgO	7.02	7.21	7.18	7.01	7.56	7.45	7.43	7.61
CaO	11.52	11.60	11.72	11.71	11.40	12.11	12.08	11.50
Na_2O	3.14	3.04	3.03	3.09	3.06	2.88	2.84	3.06
K_2O	0.18	0.20	0.18	0.19	0.17	0.16	0.16	0.13
P_2O_5	0.20	0.18	0.18	0.22	0.18	0.18	0.16	0.19
Total	99.25	99.96	99.81	99.67	99.38	99.50	99.25	99.55
INNA-FeO*		9.25			8.86	8.57		8.48
INNA-Na_2O		2.99			3.19	2.83		3.03
La		5.14			5.75	4.72		5.80
Ce		14.77			16.30	13.28		16.80
Sm		3.61			3.85	3.35		3.65
Eu		1.37			1.46	1.33		1.37
Tb		0.82			0.80	0.68		0.77
Yb		2.88			2.83	2.73		2.74
Lu		0.40			0.42	0.39		0.41
Sc		42			37	40		36
Cr		187			245	328		344
Co		42			41	41		40
Ni		48			–	79		129
Rb		6			–	8		5
Cs		<0.1			<0.13	<0.14		<0.08
Sr		184			227	130		208
Ba		<0.76			<0.32	<0.60		<0.48
Zr		113			–	147		161
Hf		2.84			3.11	2.53		3.12
Th		0.23			0.18	0.4		0.17
Ta		0.31			0.28	0.13		0.29
U		<0.46			<0.10	<0.42		<0.43
Mg#	60.5	61.8	61.6	60.8	64.1	63.9	63.9	64.7
$(La/Sm)_N$		0.78			0.82	0.77		0.87

TABLE III (continued)

Sample Depth(m) Sample type	1401/1647 1264 P	1401/1707 1264 Pa	1401/1837 1259 LP	1401/1930 1200 Pa	1401/2019 1160 Pa	2041 1157 LP
SiO_2	50.99	51.14	50.58	50.06	50.88	50.67
TiO_2	1.68	1.74	1.34	1.32	1.69	1.63
Al_2O_3	14.74	14.76	16.25	16.08	15.21	15.43
FeO*	10.54	10.66	8.37	8.36	9.44	9.10
MgO	6.59	6.56	7.89	7.94	6.97	7.12
CaO	11.28	11.21	11.96	11.93	11.88	11.91
Na_2O	3.30	3.31	2.79	2.83	3.12	3.02
K_2O	0.14	0.16	0.16	0.17	0.20	0.21
P_2O_5	0.17	0.20	0.14	0.15	0.15	0.18
Total	99.43	99.63	99.48	98.84	99.54	99.27
INNA-FeO*	10.37	10.12	8.13	8.05		
INNA-Na_2O	3.37	3.2	2.71	2.82		
La	4.23	4.33	4.30	4.38		
Ce	12.81	12.85	12.05	12.00		
Sm	4.00	3.92	2.97	3.02		
Eu	1.48	1.50	1.15	1.21		
Tb	0.87	0.84	0.61	0.68		
Yb	3.28	3.33	2.39	2.44		
Lu	0.47	0.49	0.35	0.33		
Sc	42	42	38	38		
Cr	143	139	345	340		
Co	43	42	40	40		
Ni	–	34	147	95		
Rb	–	<11	6	9		
Cs	<0.09	<0.08	<0.07	<0.12		
Sr	174	126	173	152		
Ba	<0.72	<0.41	<0.57	<0.38		
Zr	–	124	76	70		
Hf	3.12	3.15	2.35	2.38		
Th	–	0.16	0.21	0.22		
Ta	0.27	0.27	0.26	0.24		
U	<0.20	<0.38	<0.36	<0.49		
Mg#	57.2	56.8	66.8	67	61.2	62.6
$(La/Sm)_N$	0.58	0.60	0.79	0.79		

FeO* = total iron oxide
S = glass in sediments
T = Talus
P = pillow, in place
Pa = pahoehoe, in place
M = massive flow
LP = lobate pillow.

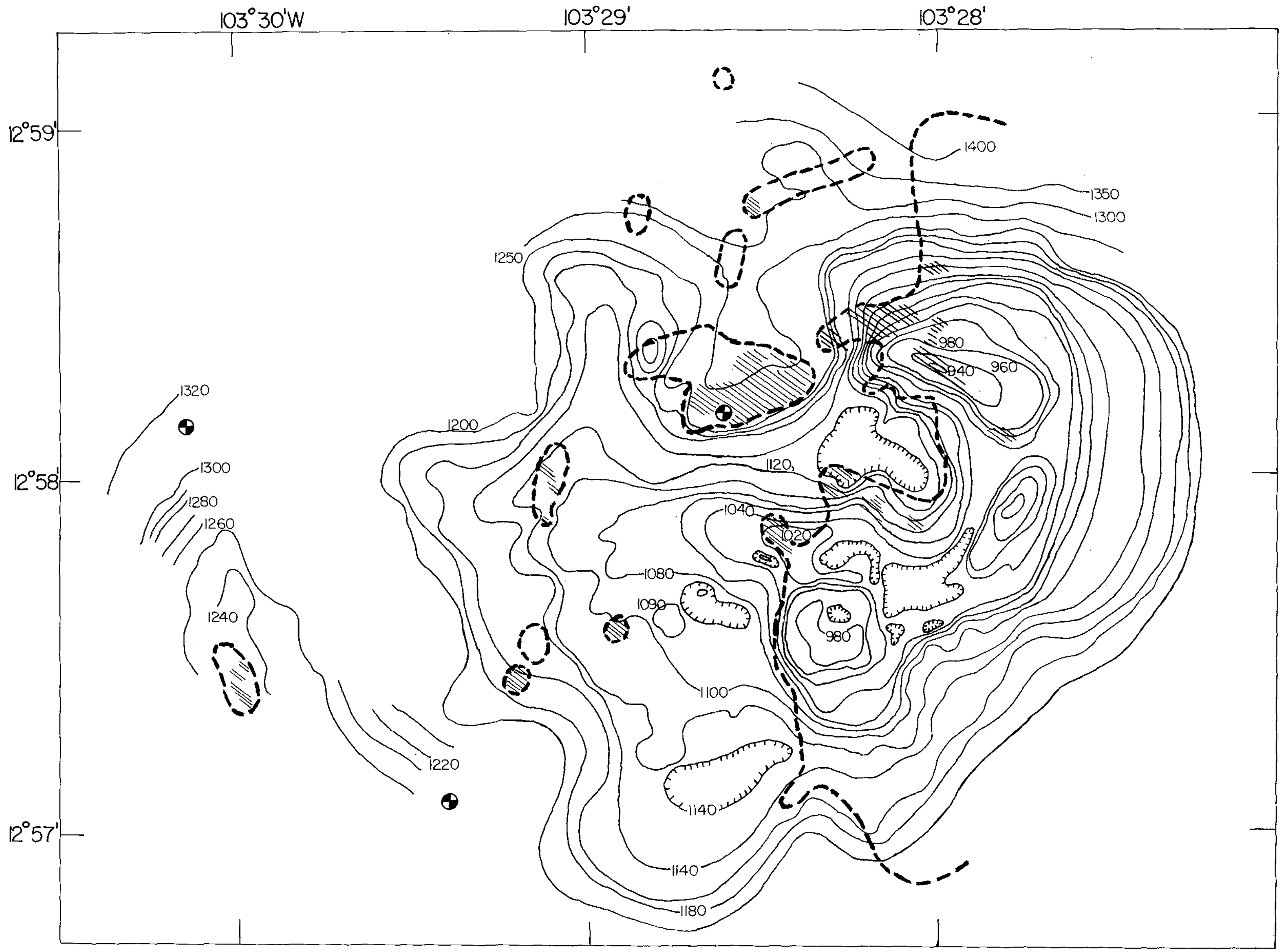

Fig. 11. Map of the summit of seamount 5 showing the location of hydrothermal precipitates. The areas enclosed by dashed lines are covered with hydrothermal precipitates whereas the diagonally ruled pattern represents areas of yellow and white bacterial mats which may be sites of active low-temperature hydrothermal venting.

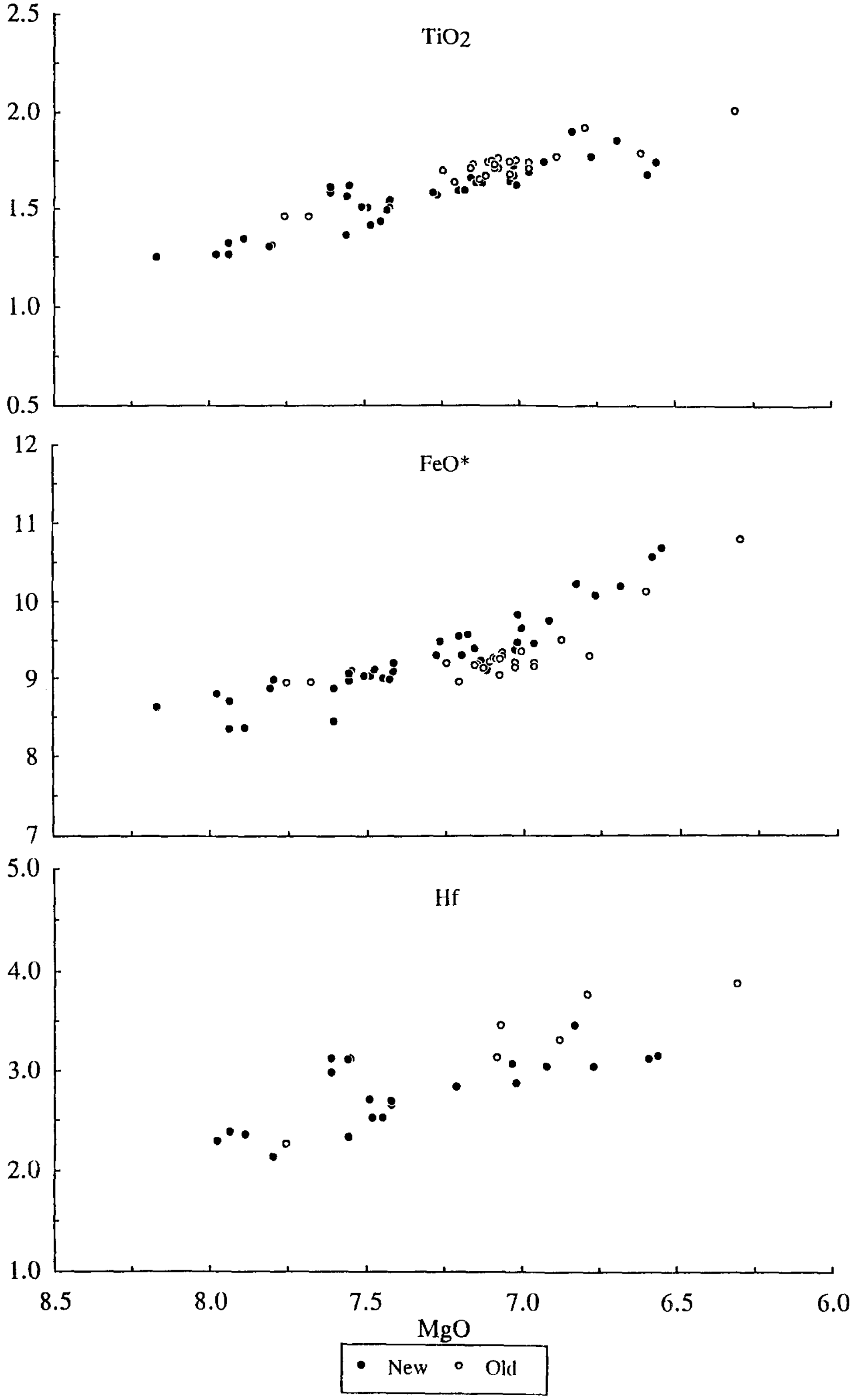

Fig. 12. TiO_2, FeO* and Hf vs. MgO for lava on seamount 5.

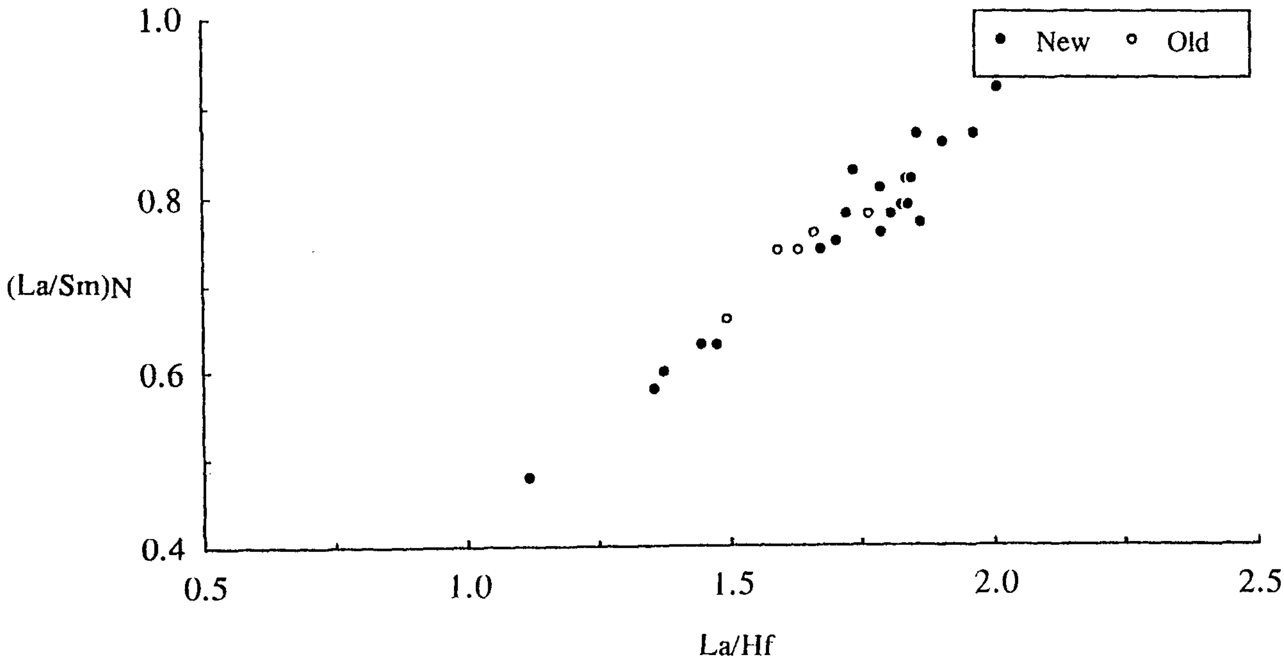

Fig. 13. $(La/Sm)_n$ vs. La/Hf for lavas of seamount 5.

on 6E. The steeper outer flanks of 6C and 6E (2500 m to 2300 m) are mostly sediment free and consist of pillow tubes elongated downslope. Scattered outcrops of bulbous pillows occur on gentler slopes (Plate 9) and minor talus deposits are common. The saddle between 6C and 6E is sedimented, with only about 50% or less rock outcrop. The slopes of 6C in the vicinity of the saddle consist almost entirely of lava haystacks and small pillow ridges. In contrast, the slopes of 6E near the saddle are mostly pahoehoe (Plate 10) and large lobate pillows with scattered outcrops of talus.

The gently-sloping summit of 6C from about 2200 m upward is mostly composed of hyaloclastite (described in detail by Smith and Batiza, 1989), sheet flows, submarine pahoehoe and lobate pillows (Plate 11). Above 2000 m elevation, these deposits appear very young and have only 2–3 mm of manganese coat. The summit area has greater than ~50% outcrop separated by sediment ponds which become rippled at elevations higher than ~2000 m (Plate 11). In contrast, the summit area of 6E consists mostly of pillow flows with only rare pahoehoe and lobate pillows. The summit of 6E is thickly covered with rippled sediment and directional indicators on 6C and 6E show the general sediment transport direction is to the east. In some cases, sediment ripples on 6E indicate transport up gentle slopes, whereas usually, elsewhere on 6C and 6E, sediment transport is locally downslope.

The caldera walls of 6E are mostly covered with pillow talus (Figure 18). In some cases, the wall is vertical but elsewhere on gentler slopes there may be scattered outcrops of bulbous pillows which appear in place. Toward the base of the caldera wall, the talus is covered and mixed wtih sediment. The caldera floor is almost entirely covered with sediment. Very rare and scattered outcrops consist of pahoehoe, lobate pillow and deposits of honeycomb-textured lava that resembles spatter. The rocks on the summit of 6E appear older than those on the summit of 6C. On 6E, rocks generally have thick (mostly 2–3 cm, up to 7 cm) coats of manganese and are weathered. Based on outcrop appearance, thickness of manganese coats and sediment thickness, we propose that the main edifices of 6W, 6E and 6C formed about the same time. Caldera collapse on 6E was preceded by pahoehoe and followed by pillow eruptions at the summit bench and elsewhere. At the time of formation of the 6E caldera, 6C may also have had a caldera. Its filling may have been contemporaneous with post caldera eruptions on 6E

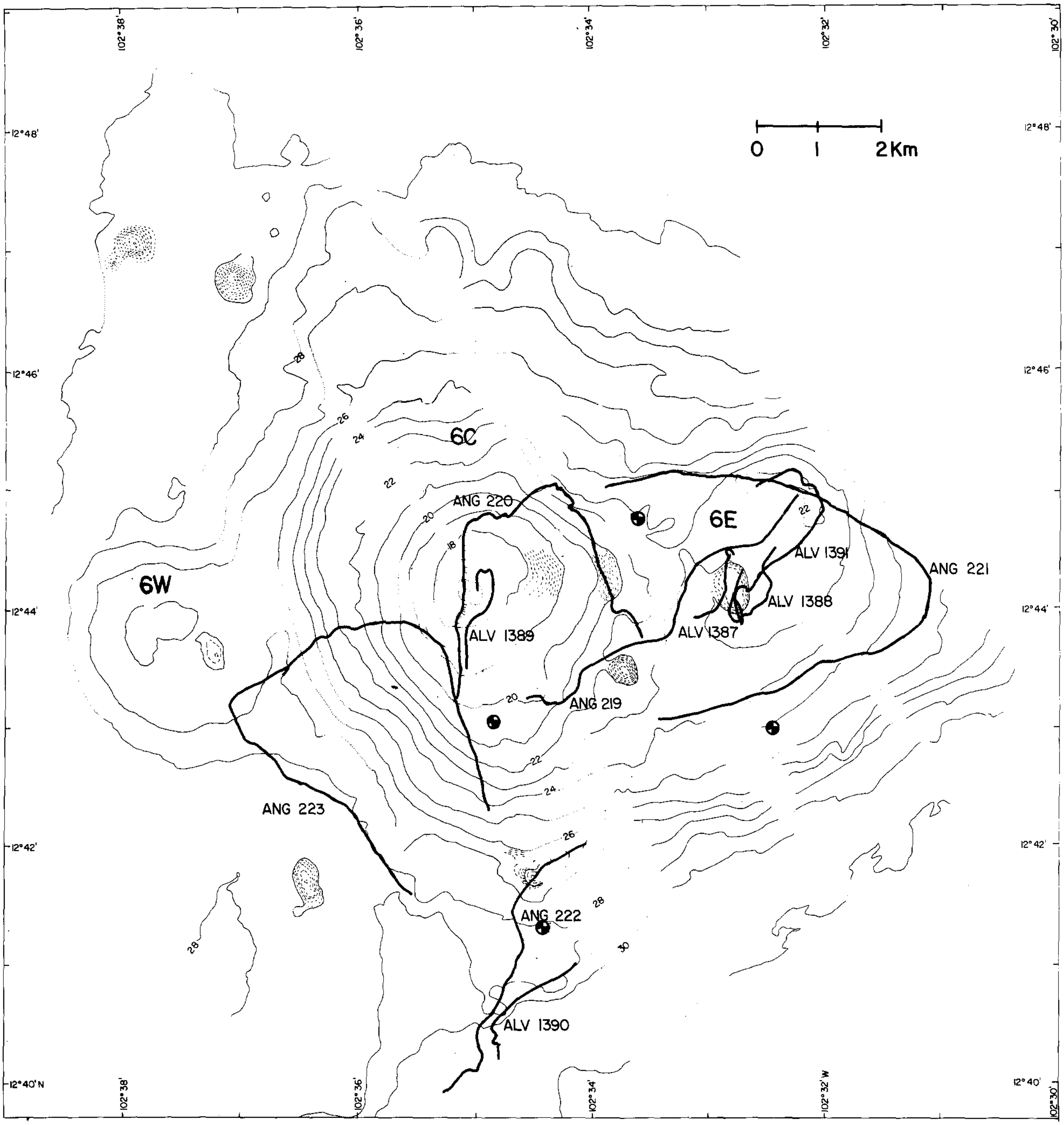

Fig. 14. Bathymetric map of seamount 6 showing the ALVIN and ANGUS tracks.

but apparently eruptions on the summit of 6C continued for some time after volcanic activity ceased on 6E. The youngest rocks on 6C appear to be somewhat older than those on either Seamount 5 or Seamount D.

The mineralogy, petrology and geochemistry of lavas from seamount 6 have been well studied (Batiza, 1980; Batiza and Vanko, 1984; Zindler *et al.*, 1984; Honda *et al.*, 1987; Graham *et al.*, 1987, 1988; Aggrey *et al.*, 1988). New samples recovered by ALVIN extend the previously known range of chemical composition of seamount 6 lavas (Batiza and Vanko, 1984), but do not dramatically alter the chemical variation patterns (Table IV, Figures 20 and 21). Mineral assemblages (Table V) and new mineral analyses of seamount 6 lavas (Tables VI,

TABLE IV

Major and trace element data for Seamount 6

Sample	1387/1712	1387/1910	1387/1920	1387/2042	1388/1629	1388/1724	1388/1752	1388/1859
Depth(m)	2302	2303	2298	2261	2328	2271	2200	2247
Sample type	PT	Pa	PT	PT	Pa	PT	P	Pa
SiO_2	50.37	50.20	48.26	50.63	50.20	48.80	50.04	50.71
TiO_2	1.31	1.29	1.86	1.28	1.38	1.87	1.28	1.14
Al_2O_3	14.89	15.03	17.38	15.04	14.83	17.36	15.85	15.05
FeO*	10.16	10.17	8.74	9.58	10.44	8.71	9.22	9.58
MgO	7.80	7.81	7.32	7.85	7.60	7.26	8.05	7.98
CaO	12.33	12.37	10.84	12.69	12.42	10.99	12.25	12.73
Na_2O	2.40	2.42	3.47	2.54	2.53	3.43	2.69	2.35
K_2O	0.06	0.07	0.47	0.08	0.06	0.49	0.06	0.06
P_2O_5	0.15	0.14	0.26	0.12	0.14	0.26	0.14	0.12
Total	99.47	99.50	98.60	99.81	99.60	99.17	99.58	99.72
INNA-FeO*		9.41	9	8.77		8.71	8.71	9.48
INNA-Na_2O		2.35	3.46	2.54		3.46	2.72	2.30
La		2.35	10.43	2.35		9.55	2.18	1.93
Ce		8.72	25.81	8.43		25.53	7.97	6.07
Sm		2.83	4.74	2.79		4.63	2.92	2.45
Eu		1.08	1.61	1.08		1.58	1.10	0.97
Tb		0.69	0.86	0.65		0.80	0.70	0.60
Yb		2.93	3.39	2.77		3.24	2.60	2.62
Lu		0.42	0.50	0.41		0.48	0.39	0.39
Sc		42	32	44		32	39	42
Cr		268	199	364		196	341	331
Co		44	32	43		38	42	45
Ni		106	112	89		130	90	–
Rb		11.4	–	5		8	7	–
Cs		0.08	–	0.08		0.12	0.12	0.1
Sr		101	261	98		233	54	61
Ba		43	50	40		41	62	42
Zr		118	181	41		160	80	–
Hf		2.18	4.12	2.09		3.87	2.27	1.85
Th		0.07	0.71	0.07		0.8	0.15	–
Ta		0.08	0.7	0.06		0.69	0.1	–
U		0.46	–	0.21		0.24	0.14	1.6
Mg#	62.1	62.1	64.1	63.6	60.9	64	65.1	64
$(La/Sm)_N$		0.45	1.2	0.46		1.13	0.4	0.43

TABLE IV (continued)

Sample	1388/2006	1388/2127	1389/1613	1389/1620	1389/1647	1389/1810	1389/1854B	1389/2041
Depth(m)	2220	2220	1874	1874	1797	1760	1755	1748
Sample type	Pa	PT	Pa	Hy	P	P	P	P
SiO_2	50.36	48.34	50.55	49.72	50.78	49.84	50.66	51.77
TiO_2	1.17	1.88	2.19	1.16	2.48	2.35	2.47	3.00
Al_2O_3	15.11	17.72	17.14	16.68	17.42	17.79	17.67	16.97
FeO*	9.62	8.55	8.20	8.51	8.03	8.12	7.89	8.92
MgO	8.17	7.46	5.15	8.43	4.59	6.10	4.55	3.00
CaO	12.96	10.90	9.13	12.12	8.45	8.23	8.19	7.22
Na_2O	2.36	3.46	4.40	2.73	4.67	4.50	4.78	5.31
K_2O	0.04	0.43	1.56	0.08	2.01	1.74	2.07	2.74
P_2O_5	0.11	0.26	0.66	0.14	0.83	0.74	0.53	1.04
Total	99.90	99.00	98.98	99.57	99.26	99.41	98.81	99.97
INNA-FeO*	9.34	8.17	7.79		7.5	7.79		7.65
INNA-Na_2O	2.38	3.41	4.32		4.33	4.31		4.30
La	1.69	9.75	28.77		37.00	32.74		36.64
Ce	5.38	25.21	58.60		72.20	65.80		72.40
Sm	2.56	4.47	6.25		6.98	6.68		6.97
Eu	0.97	1.55	2.03		2.19	2.21		2.20
Tb	0.64	0.81	0.92		6.96	0.97		0.93
Yb	2.72	3.17	2.98		2.97	2.80		3.04
Lu	0.39	0.47	0.43		0.44	0.41		0.44
Sc	43	31	28		24	20		24
Cr	337	191	116		86	162		90
Co	45	38	29		26	31		28
Ni	143	138	34		35	123		–
Rb	–	6	32		37	32		–
Cs	0.14	0.09	0.34		0.42	0.3		0.41
Sr	130	277	391		472	553		469
Ba	32	43	304		394	336		376
Zr	30	214	253		318	249		258
Hf	1.68	3.94	5.89		6.74	6.22		6.8
Th	0.13	0.55	3.87		4.79	3.84		4.71
Ta	<0.15	0.72	2.86		3.53	3.07		3.33
U	0.19	0.17	1.19		1.42	1.2		1.42
Mg #	64.5	65.1	57.3	67.9	55	61.6		41.8
$(La/Sm)_N$	0.36	1.19	2.52		2.9	2.68		2.88

TABLE IV (continued)

Sample	1389/2115A	1389/2115B	1390/1915	1390/1922	1390/1954	1390/2112	1391/1730	1391/2033
Depth(m)	1695	1695	2996	2969	2983	2975	2208	2156
Sample type	Pa	Pa	P	P	P	PT	M	Pa
SiO_2	50.47	50.64	48.99	48.97	50.43	50.72	50.20	48.33
TiO_2	2.46	2.44	0.91	0.90	1.64	1.38	1.28	1.81
Al_2O_3	17.72	17.75	17.96	17.56	15.12	15.71	15.83	17.43
FeO*	7.85	7.86	7.96	8.19	9.75	9.12	9.30	8.71
MgO	4.70	4.68	9.42	9.16	6.93	7.75	8.13	7.44
CaO	8.28	8.26	12.23	12.44	11.86	12.14	12.32	10.98
Na_2O	4.73	4.73	2.38	2.41	3.13	2.91	2.75	3.43
K_2O	2.00	2.02	0.03	0.02	0.28	0.10	0.06	0.47
P_2O_5	0.82	0.83	0.12	0.09	0.20	0.15	0.13	0.24
Total	99.03	99.21	100.00	99.74	99.34	99.98	100.00	98.84
INNA-FeO*	7.68		7.59		9.08	8.52	8.59	8.58
INNA-Na_2O*	4.72		2.41		2.98	2.81	2.82	3.54
La	38.60		0.70		6.32	2.92	2.42	9.91
Ce	75.80		3.11		15.66	9.52	8.21	26.20
Sm	7.19		2.03		3.64	3.02	2.90	4.68
Eu	2.29		0.88		1.33	1.18	1.13	1.62
Tb	0.94		0.54		0.75	0.67	0.69	0.90
Yb	3.09		1.97		2.94	2.67	2.75	3.34
Lu	0.44		0.28		0.42	0.38	0.41	0.48
Sc	24		29		41	39	38	32
Cr	83		476		296	358	375	197
Co	26		46		40	42	37	39
Ni	21		172		47	78	–	139
Rb	39		5		8	3	–	8
Cs	0.48		0.09		0.15	0.06	–	0.11
Sr	460		–		171	124	128	271
Ba	392		29		73	36	40	44
Zr	275		31		125	78	–	166
Hf	6.86		1.33		2.87	2.33	2.11	4.01
Th	5.18		–		0.51	0.08	0.06	0.78
Ta	3.82		<0.09		0.5	0.14	–	0.73
U	1.57		0.14		0.44	0.18	0.33	0.16
Mg#	56.1	56	71.6	70.5	60.3	64.5	65.1	64.6
$(La/Sm)_N$	2.94		0.19		0.95	0.53	0.45	1.16

FeO* = total iron oxide
T = Talus
P = pillow, in place
Pa = pahoehoe, in place
M = massive flow
Hy = hyaloclastite.

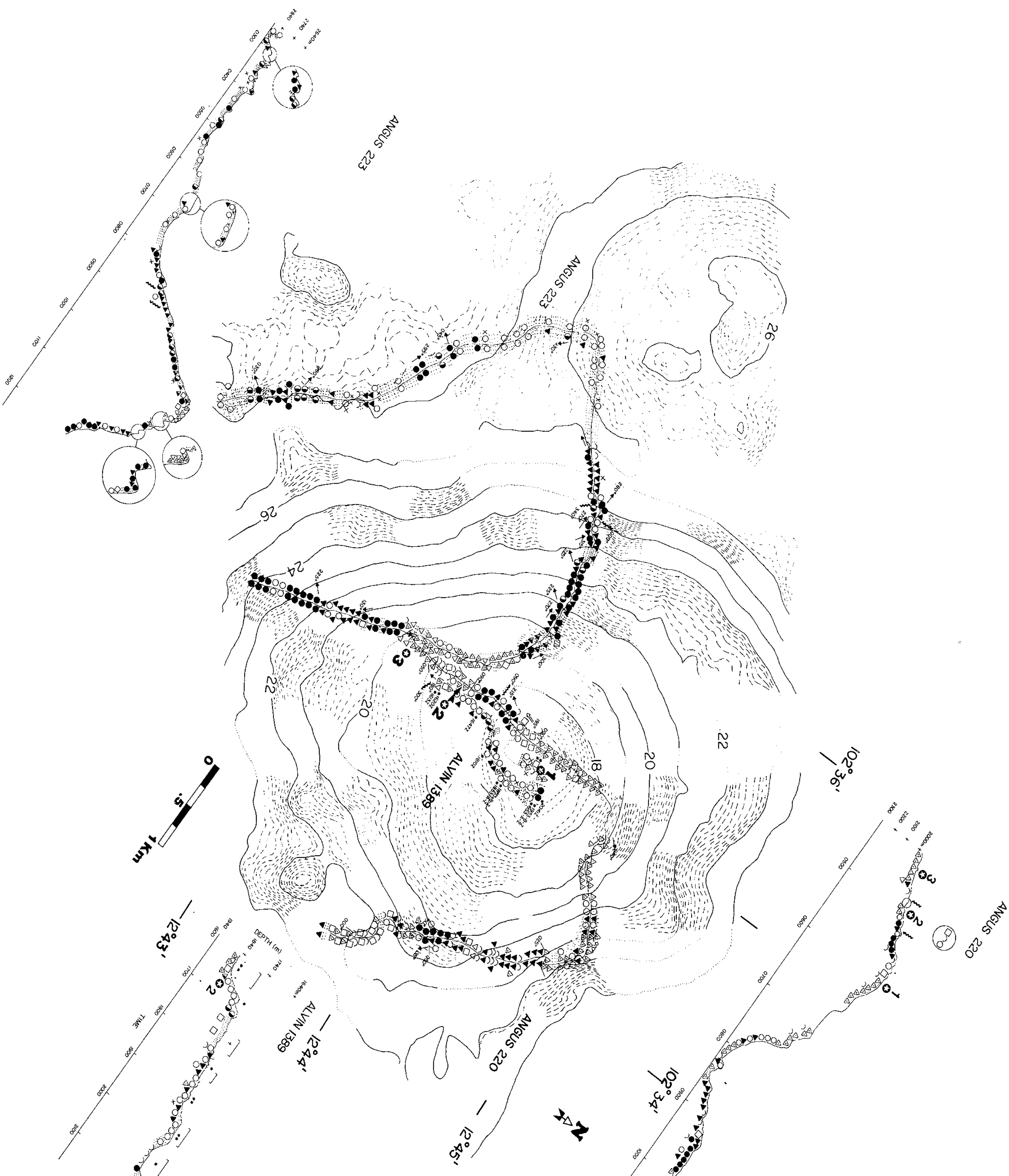

Fig. 15. Geology of seamount 6C along ANGUS and ALVIN tracks plus profile along the tracks (V.E. 4×).

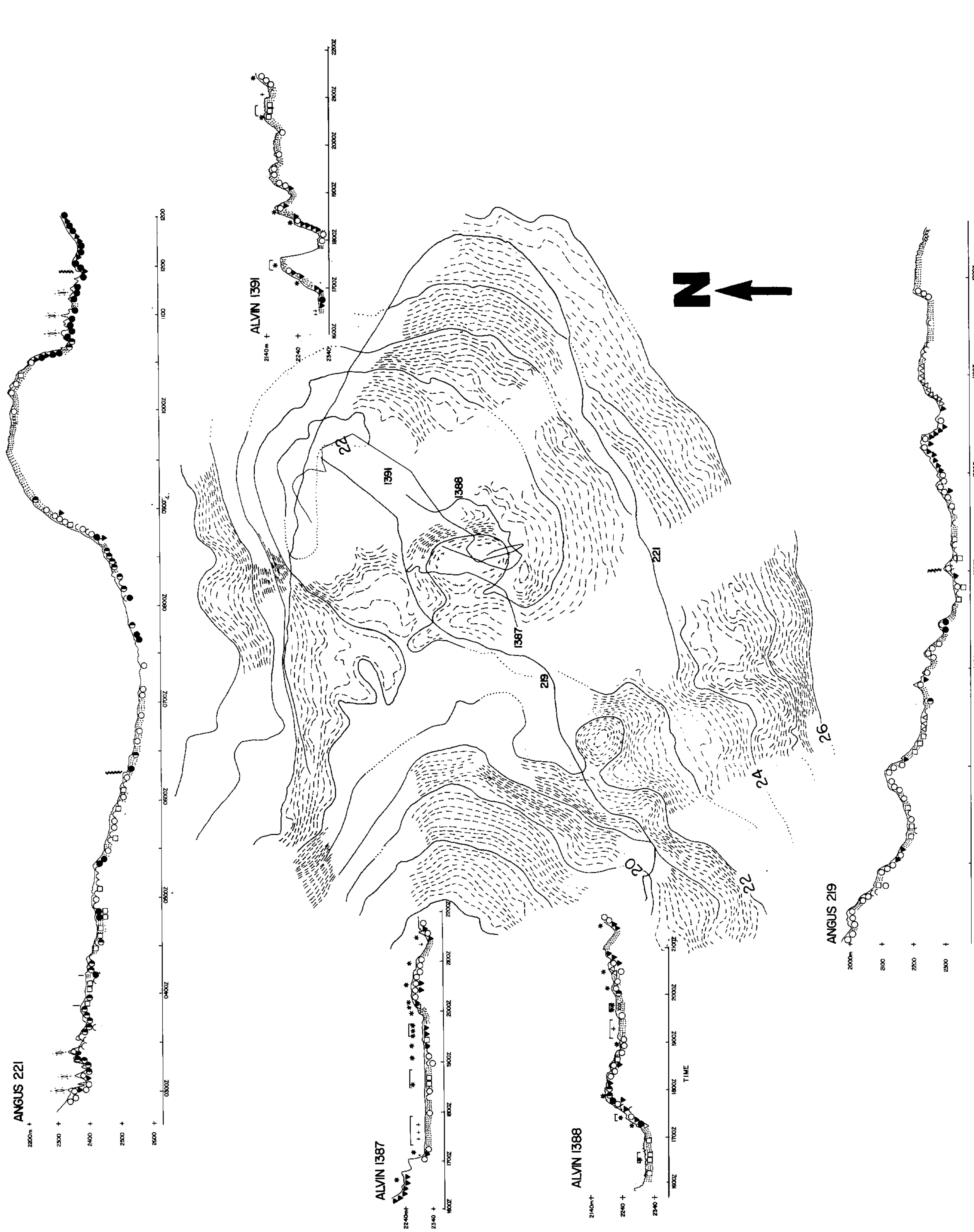

Fig. 16. Bathymetry of seamount 6E showing locations of ANGUS and ALVIN tracks and profiles (V.E. 4×) of geology with the same symbols as Figure 15.

Fig. 17. Geology along the ANGUS and ALVIN tracks of seamount 6E with same symbols as Figure 15.

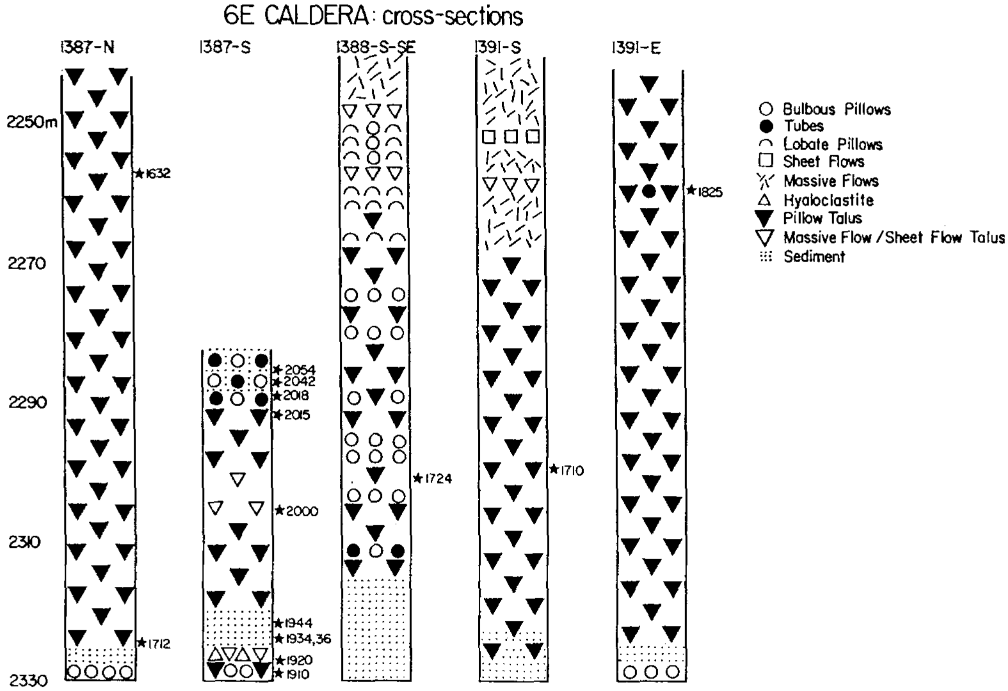

Fig. 18. Geologic cross section in the caldera of 6E, from ALVIN observations.

VII, VIII and IX for olivine, plagioclase spinel and clinopyroxene, respectively) extend slightly the observed range of mineral chemistry, but relations of mineral composition to texture and chemical composition are essentially those described previously by Batiza and Vanko (1984). As shown by previous model studies using major elements, trace elements and isotopic data, seamount 6 lavas are related by variable extents of melting and mixing of a heterogeneous mantle with superimposed low pressure fractional crystallization. The new data (Figures 20, 21; Tables IV-IX) are consistent with this interpretation.

SEAMOUNT 7

Seamount 7 is a large (680 km^3, 2300 m high), steep-sided volcano with a gently-sloping summit area. If it once had a caldera, it is now filled. Like Seamount 6, its lower, gentler-sloping flanks have many small volcanic cones up to 200 m high. The seamount is located along the East O'Gorman fracture zone north of Seamount 6 on crust about 3 Ma old (Figure 1). Figure 22 shows the locations of four ALVIN dives and three ANGUS runs on Seamount 7. Figures 23 and 24 show the geology of these traverses in map view and Figures 25 and 26 show the geology in cross sections.

The lava and cone fields (Plate 12) as well as the shallower summit and slopes (Plates 13–15) of Seamount 7 are well sedimented. Overall, most (80–85%) of the surface consists of sediment, and sediment transport is downslope. Most of the rock outcrops, including outcrops at the summit, consist of loose rock resembling talus. On steep slopes, these deposits probably represent talus deposits, but we suggest that near the summit on gentle slopes, these deposits are rubbly lava flows. At the summit, these rubbly deposits grade into flows consisting of small pillows. Pillows are also abundant on the deeper (as deep as 2000 m) portions of the flattish summit region (Plate 14) where pahoehoe (Plate 13) and lobate pillows also occur. The deeper flanks and lava fields consist of sediment-covered tubular and bulbous pillows and talus (Plate 12, Figures 24–26). Rock samples from the deep flanks have up to 3 cm of manganese coating and appear to be of similar age to samples from comparable settings on Seamount 6. As with Seamount 6, the thickness of manganese coatings decreases upslope. At the summit, rocks on Seamount 7 have only 1–3 mm thick coatings of manganese and appear quite fresh. We thus suggest that volcanism on Seamount 7 spanned a considerable period of time possibly including episodes of

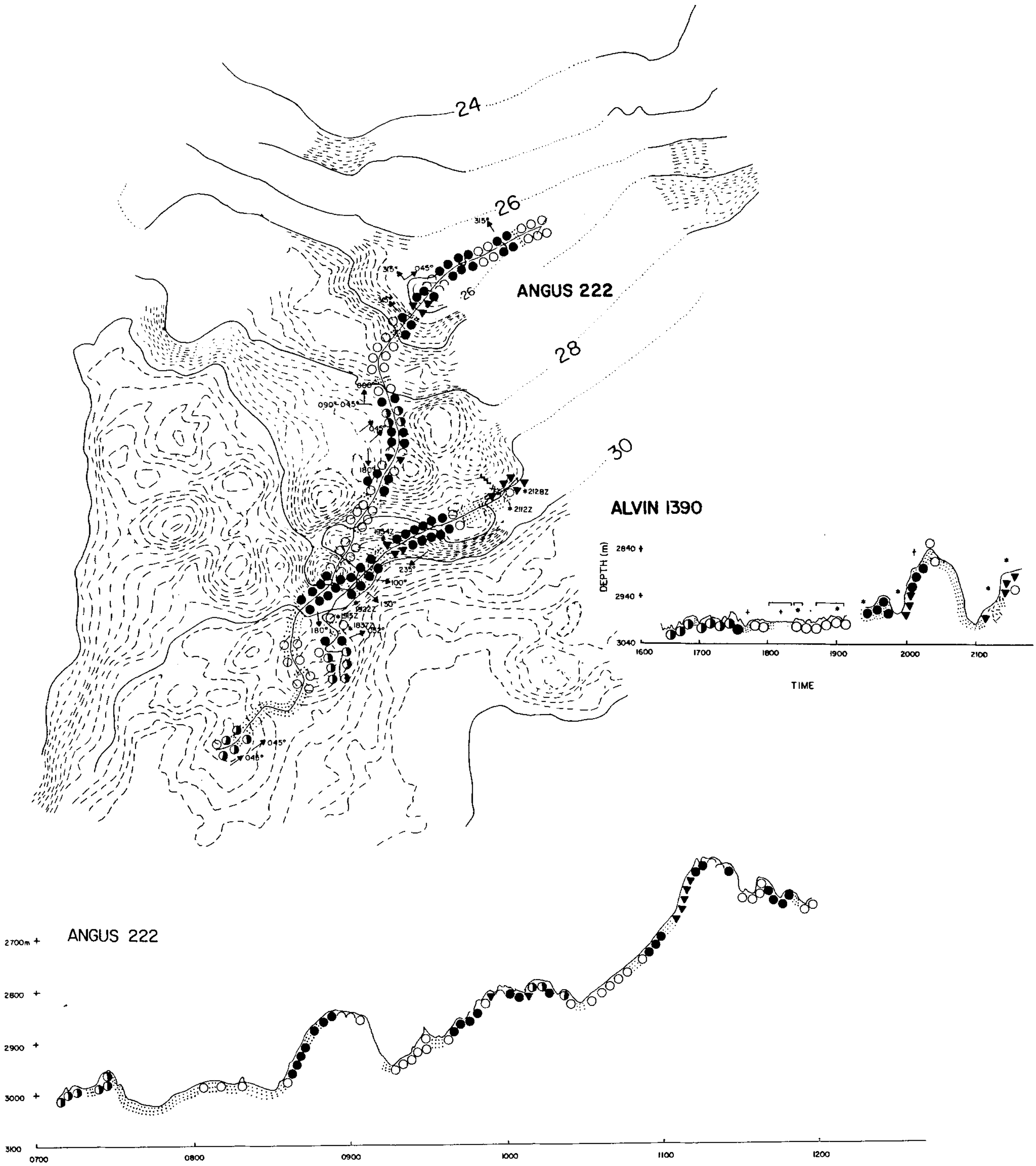

Fig. 19. Bathymetry of the cone/lava field on the flanks of seamount 6 showing geology along the ALVIN and ANGUS tracks, with profiles (V.E. 4×). Same symbols as Figure 15.

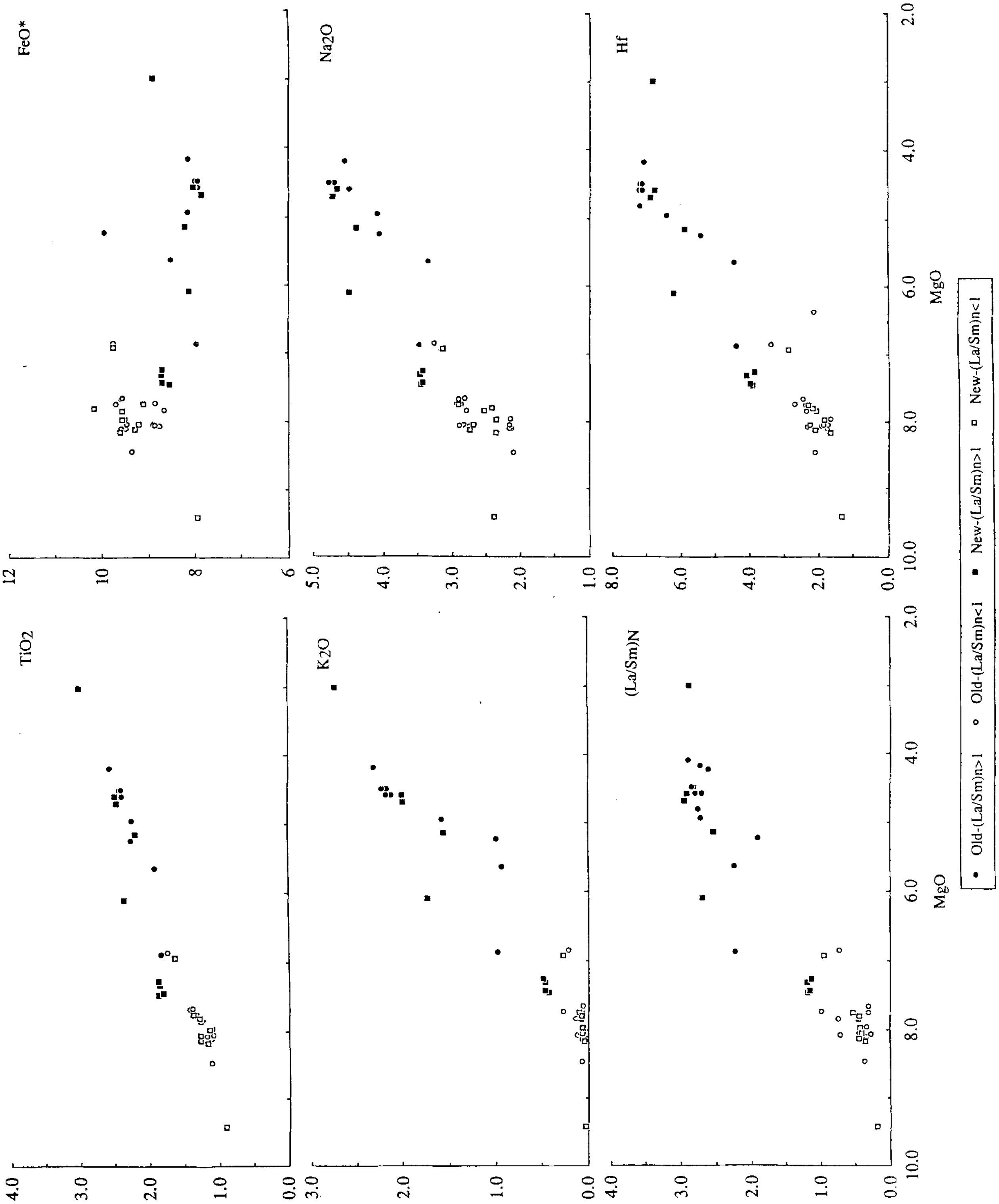

Fig. 20. MgO variation diagrams for lavas of seamount 6.

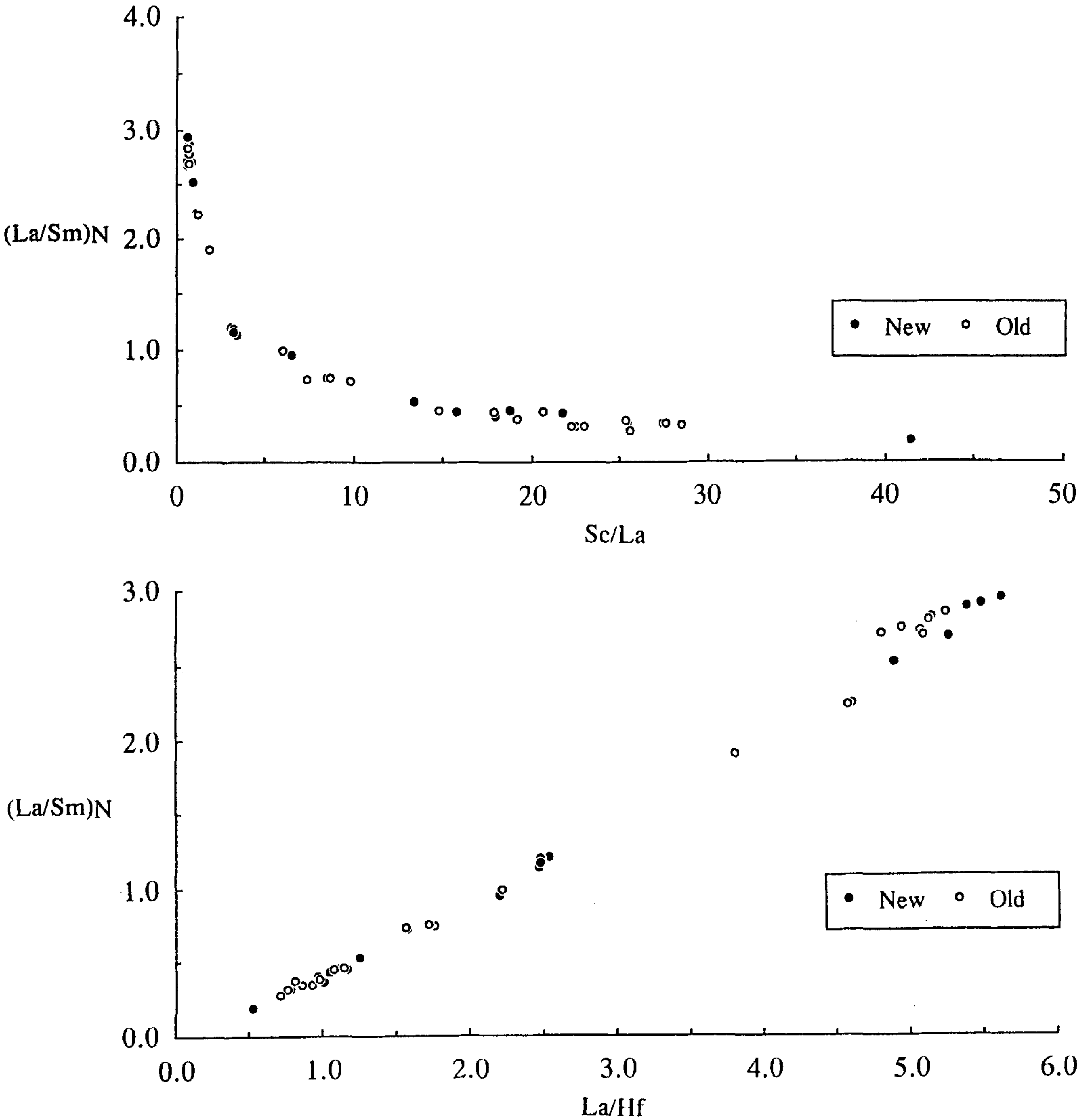

Fig. 21. Ratio-Ratio plots (Langmuir *et al.*, 1978) supporting mantle source area mixing for the diverse lavas of seamount 6.

caldera formation and filling. Unlike Seamount 6, however, Seamount 7 does not appear to have had a widespread episode of voluminous pahoehoe and hyaloclastite eruption at the summit. It is possible, of course, that evidence for such an episode could be buried beneath the pillows and rubbly flows which cap the summit.

Seamount 7, like seamount 6 was previously well-studied petrologically. New samples from seamount 7 recovered by ALVIN (Table X; Figures 27 and 28) slightly extend the previously known range of lava chemistry and the chemistry of mineral phases (Tables VI-IX). Seamount 7 contains depleted N-MORB and basalts that are transitional to undepleted alkali basalt. Unlike seamount 6, seamount 7 does not contain true alkali basalts or their differentiates. Even so, the chemical variation patterns of lavas from seamount 7 suggests a very similar

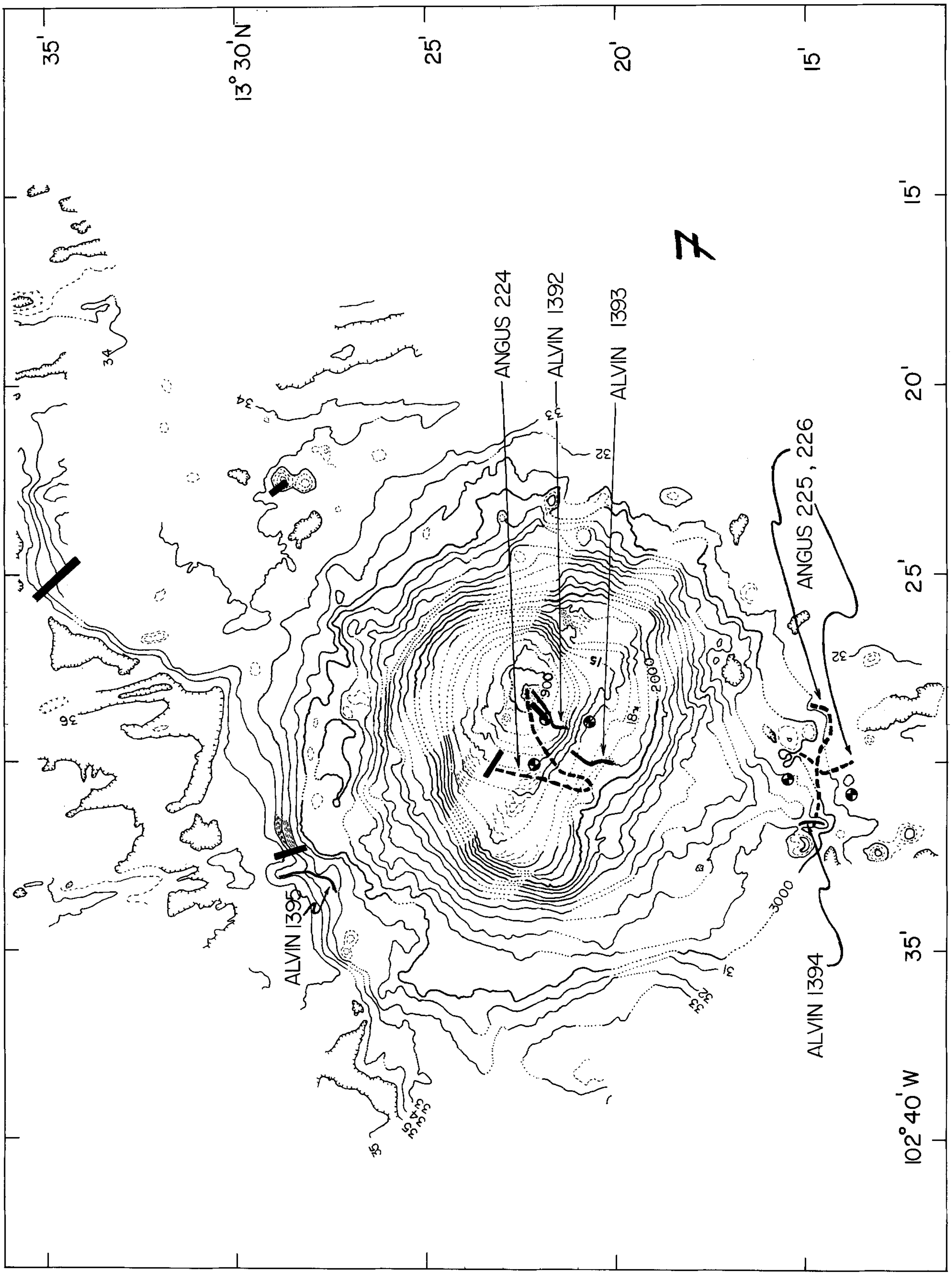

Fig. 22. Bathymetric map of seamount 7 showing the locations of acoustic transponders (Beachball symbol) ANGUS camera tracks (dashed) and ALVIN dives (solid line).

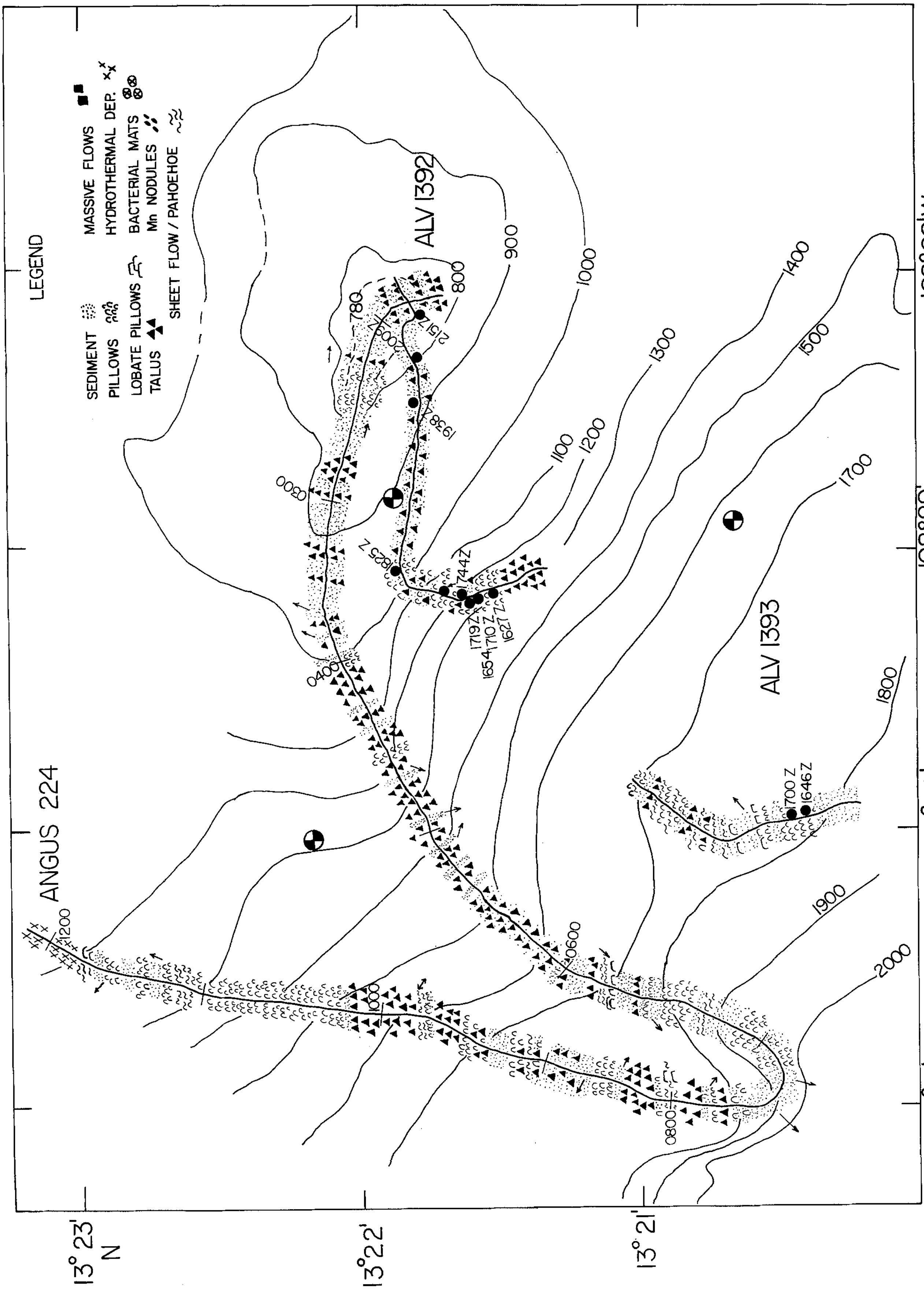

Fig. 23. Bathymetric map of the summit of seamount 7 showing the geology along ALVIN and ANGUS tracks.

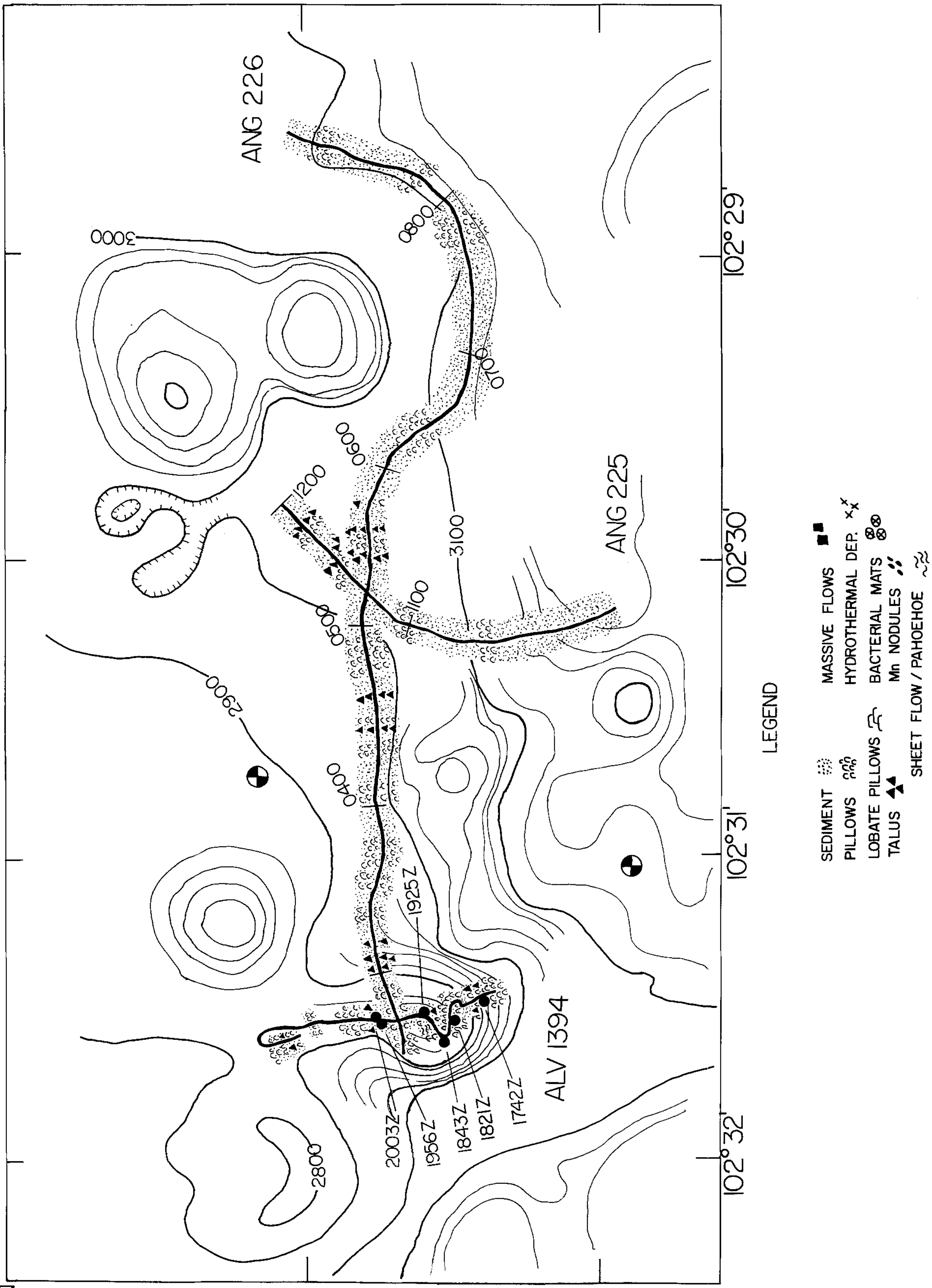

Fig. 24. Bathymetric map of the cone/lava field on the flanks of seamount 7 with geology along the ALVIN and ANGUS tracks.

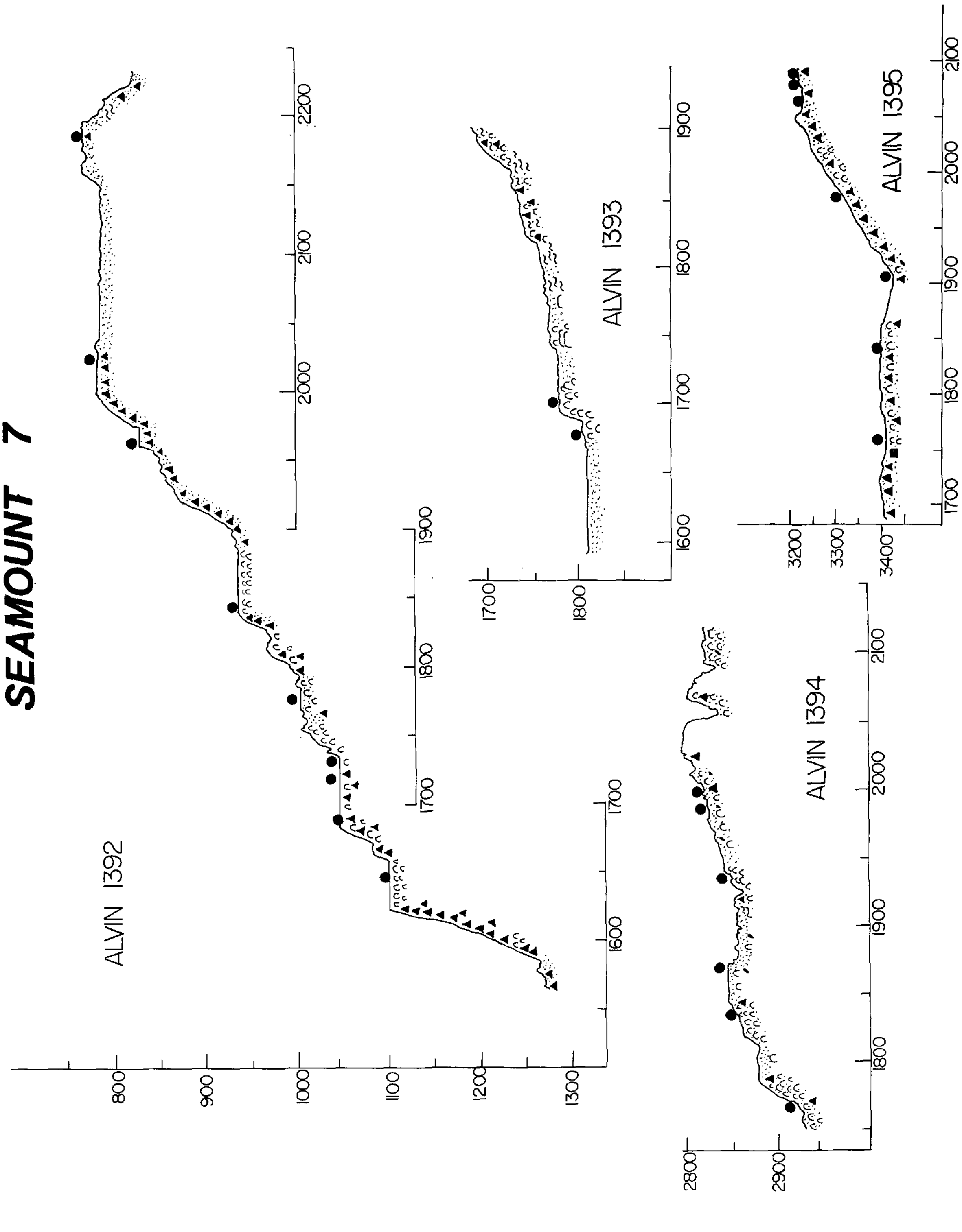

Fig. 25. Geology along ALVIN tracks on seamount 7. Vertical exaggeration is 4×; same symbols as Figure 24.

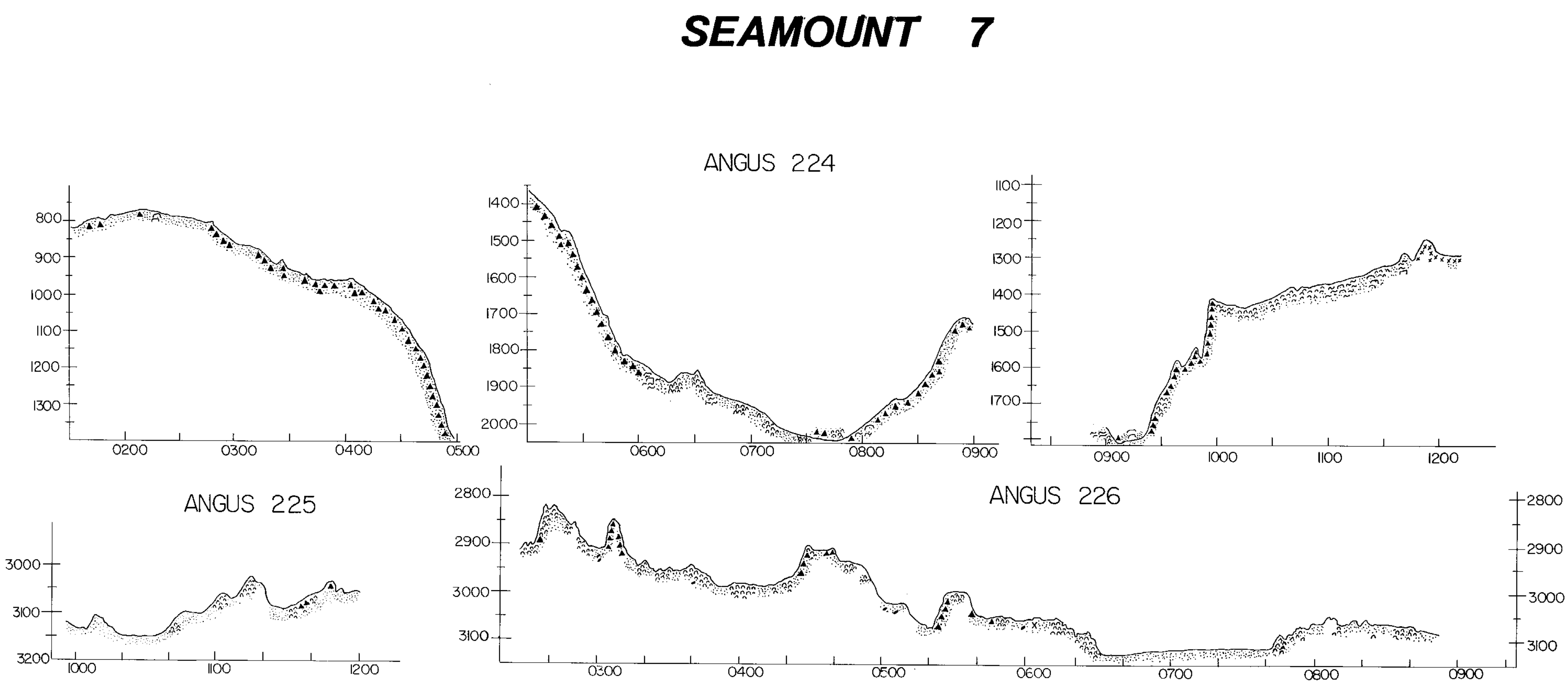

Fig. 26. Geology along ANGUS tracks on seamount 7. Vertical exaggeration is 4 ×; same symbols as Figure 24.

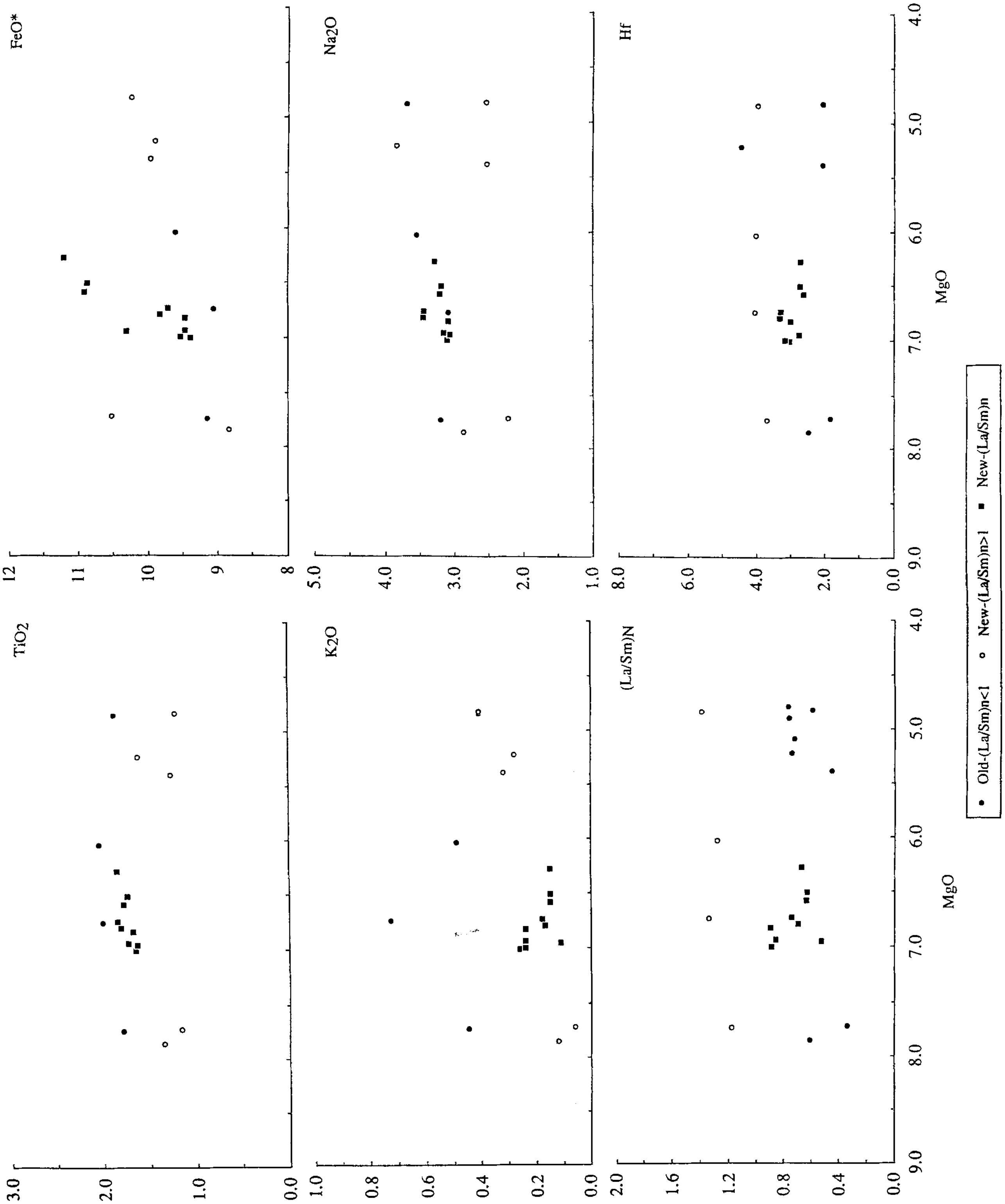

Fig. 27. MgO variation diagrams from lavas of seamount 7.

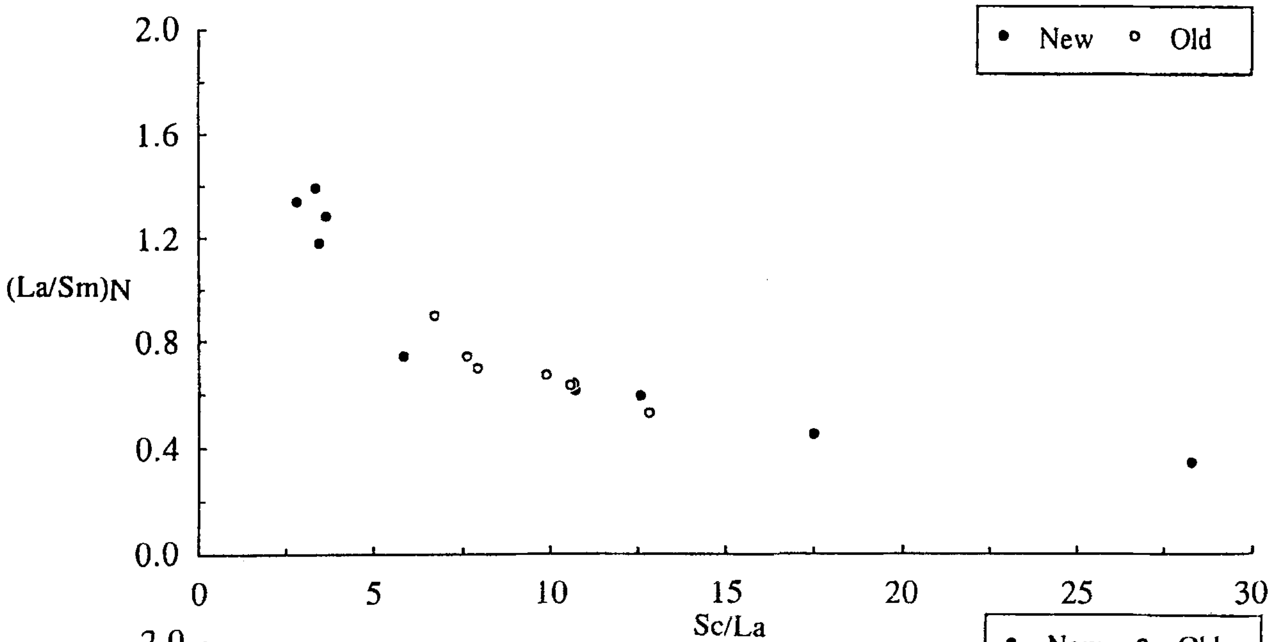

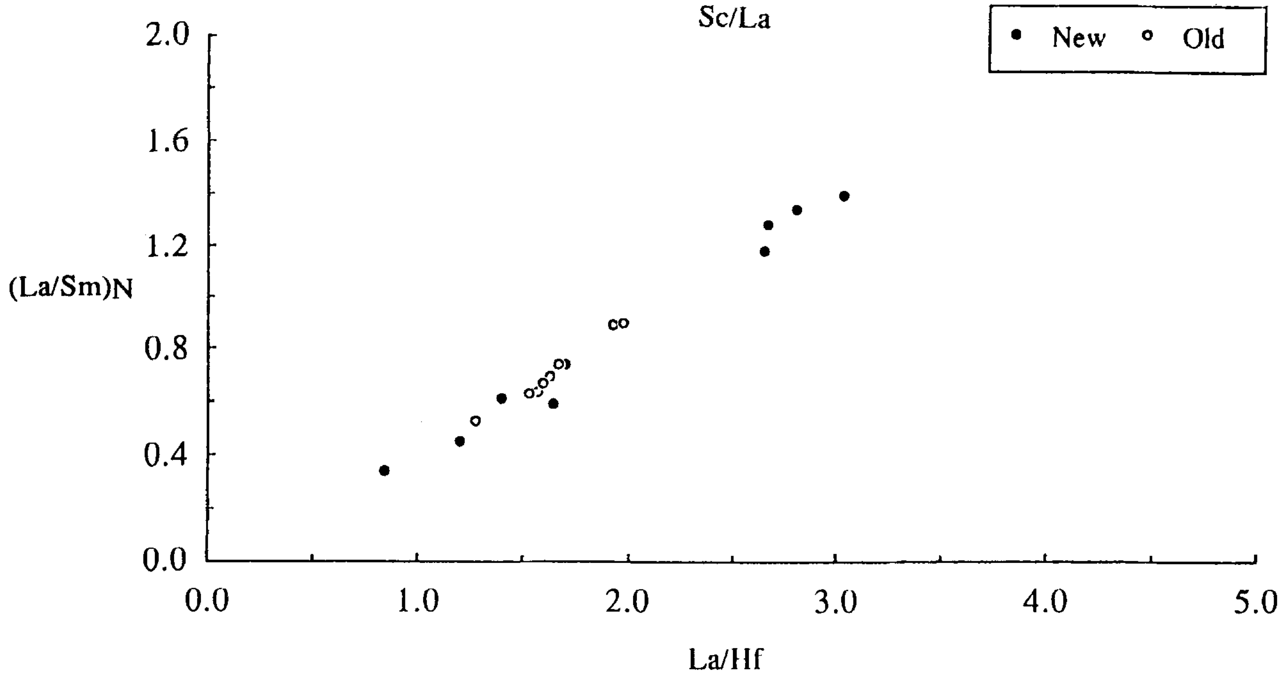

Fig. 28. Ratio-Ratio plots for the lavas of seamount 7.

petrogenetic history as that inferred for seamount 6: variable melting and mixing of a heterogeneous mantle source with variable amounts of crystal-liquid fractionation.

Discussion

Lava flows

ALVIN and ANGUS studies of seamounts 5, 6, 7 and D reveal a great variety in the morphology of lava flows. Such variation is doubtless controlled by a variety of factors such as magma chemistry, temperature, effusion rate, exit velocity, topography, water depth, and duration of eruption and are thus of great interest. Since most of the lava flows we examined are composed of MORB with only a small range of chemical variation, we do not ascribe major differences in flow morphology to differences in chemistry/eruption temperature which can affect both magma viscosity and yield strength (Bonatti and Harrison, 1988; Walker, 1973; Pieri and Baloga, 1986).

TABLE V

Mineral assemblages in lavas of seamounts 6 and 7

Sample	Plagioclase	Olivine	Clinopyroxene	Spinel
1387–1714	X	X	X	
1387–1920	X	X		X
1388–2127	X	X		X
1389–1613	X	X		X
1389–1810		X		X
1389–2041	X	X	X	X
1390–1915	X	X		X
1391–2033	X	X		X
1392–1627	X		X	
1392–1654	X			
1392–1710	X		X	
1393–1646	X	X	X	
1393–1700	X		X	
1394–2003	X		X	

ol-spl	pl-ol-spl	pl-ol-cpx-spl	pl-ol-cpx	pl	pl-cpx
1	1	1	1	1	1
	1		1		1
	1				1
	1				1
	1				

The seamounts we studied contain almost the entire spectrum of submarine lava flow types known (Bonatti and Harrison, 1988; Ballard and Moore, 1977; Ballard *et al.*, 1979; Fornari *et al.*, 1979). These include normal pillow lava, with a variety of sizes, shapes and budding characteristics (Plates 5–9, 14) and lobate pillows (Plate 2) lacking surface striations and commonly hollow, with thin horizontal ledges in their interiors. Lobate pillows are usually associated with submarine pahoehoe and sheet flows (Ballard *et al.*, 1979) and this is also the case on the seamounts of this study (e.g. Plate 2). Wrinkled and whorled pahoehoe (Lonsdale, 1977) and smooth, striated sheet flows are common at the summits of seamounts (Plates 1–4; 10, 13). Such flows probably form under conditions of rapid extrusion rate and/or ponding (Ballard *et al.*, 1979).

In general, the greatest differences in flow morphology are probably due to large differences in effusion rate and topography (Ballard *et al.*, 1979; Ballard and Moore, 1977). Low eruption rates are thought to result in the formation of pillow lava and progressively increasing eruption rates are thought to produce lobate pillows, sheet flows and submarine pahoehoe and hyaloclastites (Smith and Batiza, 1988). Spatter deposits and honeycomb-textured glassy lava probably result from high magmatic exit velocity and may be independent of effusion rate.

The most common flow forms on seamounts 5, 6, 7 and D are pillows. In general, pillows form haystacks and steep-sided pillow walls (Fornari *et al.*, 1979) but may also occur on gentle slopes. On steep slopes, pillows are invariably tubular and oriented mostly downslope whereas on gentler slopes, the pillows are usually more equant. Elongate tubular pillows comprise the outer flanks of seamounts and are also common on seamount summits, especially on arcuate summit benches. Pillow flows on seamounts differ greatly in size (0.2–3 m), shape, occurrence and abundance of pillow buds. They invariably show parallel extrusion marks and segmentation caused by episodic growth. Collapsed pillows are common, especially on steep slopes where pillows may locally exhibit transition to ropey, taffy-like forms resembling submarine pahoehoe.

Lotate pillows differ from ordinary pillows in that they are usually larger (3–6 m), more amoeboid and flattened in shape, lack surface markings from extrusion and typically are either mostly or partly hollow.

TABLE VI

Representative olivine compositions for seamounts 6 and 7

Sample	1389-1613-3	1389-1613-4	1389-1613-8	1389-1613-9	1389-1810-10	1389-1810-6	1389-1810-7	1389-2041-4	1389-2041-12	1389-2014-13	1393-1646-1	1393-1646-3
Smt	6	6	6	6	6	6	6	6	6	6	7	7
Type	A	A	A	A	A	A	A	A	A	A	Th	Th
Grain	MP-E	MP-C	P-E	P-C	GM	P-E	P-C	GM	P-C	P-E	P-E	P-C
SiO_2	39.28	39.23	38.06	39.45	39.68	39.41	39.77	39.12	39.47	37.92	38.52	39.44
TiO_2	0.03	0.03	0.02	0.02	0.01	0.02	0.03	0.03	0.02	0.06	0.02	Nd
Al_2O_3	0.04	0.03	0.03	0.03	0.03	0.05	0.03	0.04	0.03	0.03	0.05	0.03
Cr_2O_3	0.03	0.03	0.04	0.01	0.02	0.02	0.01	Nd	0.01	0.01	0.04	0.02
FeO*	16.31	16.66	15.71	15.91	14.29	13.59	14.00	17.21	16.50	17.65	15.22	15.03
MnO	0.34	0.25	0.33	0.24	0.26	0.27	0.26	0.35	0.23	0.29	0.30	0.30
NiO	0.14	0.08	0.07	0.07	0.29	0.27	0.24	0.09	0.09	0.12	0.16	0.16
MgO	43.94	43.79	43.94	44.14	45.68	45.62	45.52	43.55	43.87	42.60	45.28	45.36
CaO	0.28	0.29	0.33	0.28	0.23	0.24	0.23	0.29	0.26	0.27	0.31	0.31
Total	100.39	100.39	98.53	100.15	100.49	99.49	100.09	100.68	100.48	98.95	99.90	100.65
Fo%	82.77	82.41	83.30	83.18	85.07	85.68	85.29	81.86	82.58	81.14	84.13	84.32
Mg#	57.3	57.3	57.3	57.3	61.6	61.6	61.6	41.8	41.8	41.8	59.6	59.6

Sample	1393-1700-2	1387-1714-1	1387-1714-2	1391-2033-2	1391-2033-3	1391-2033-4	1388-2127-10	1388-2127-11	1388-2127-12	1387-1920-1	1387-1920-2	1387-1920-10
Smt	7	6	6	6	6	6	6	6	6	6	6	6
Type	Th	Th	Th	TR	TR	TR	TR	TR	TR	TR	TR	TR
Grain	GM	MP-C	MP-E	MP-C	P-E	P-C	MP-E	MP-C	GM	P-C	P-E	GM
SiO_2	39.47	39.01	38.76	38.53	39.12	40.02	39.58	39.53	39.95	39.34	39.41	40.40
TiO_2	0.03	0.02	0.04	–	0.04	–	0.01	Nd	0.04	0.01	0.03	–
Al_2O_3	0.05	0.04	0.03	0.03	0.04	0.04	0.05	0.05	0.04	0.05	0.03	–
Cr_2O_3	0.04	0.05	0.02	0.07	0.01	–	0.03	0.06	0.03	0.04	0.01	0.05
FeO*	15.57	14.86	14.53	15.91	12.72	13.31	12.99	13.06	13.74	13.11	12.83	12.94
MnO	0.28	0.26	0.28	0.25	0.28	0.28	0.29	0.21	0.29	0.20	0.26	0.27
NiO	0.08	0.10	0.08	0.19	0.24	0.27	0.30	0.22	0.25	0.32	0.30	0.33
MgO	44.84	45.43	45.29	44.26	46.77	46.78	46.79	46.58	45.47	46.47	46.77	46.75
CaO	0.36	0.32	0.34	0.27	0.29	0.28	0.28	0.26	0.34	0.27	0.28	0.31
Total	100.72	100.09	99.37	99.51	99.51	100.98	100.61	99.97	100.15	100.08	99.94	101.1
Fo%	83.7	84.49	84.75	83.22	86.77	86.24	86.52	86.41	85.51	86.33	86.67	86.57
Mg# of host	59.7	62.1	62.1	64.6	64.6	64.6	65.1	65.1	65.1	64.1	64.1	64.1

A = Alkalic; Th = Tholeiitic; P = Phenocryst; MP = Microphenocryst; GM = groundmass; E = Edge; C = Core.

Collapsed lobate pillows typically have multiple sets of thin, horizontal sheets in their interior which are separated from each other by gaps. These features are thought to be caused by episodic draining of magma. Large lobate pillows do not grow by extrusion budding, bifurcation and tube formation like ordinary pillows. Instead, they may grow by inflation of a thin quenched carapace but probably form initially by rapid extrusion of large volumes of melt as sheet-like, lobate projections.

Lobate pillows are usually closely associated with striated, smooth sheet flows or ropey submarine pahoehoe. These deposits are most common on flat or gently sloping areas of seamount summits. Many varieties of smooth, striated, buckled, wrinkled and ropey flow surfaces like those seen at the axis of the EPR are present on seamount summits. In many cases, lobate projections from sheet flows lead to the formation of lobate pillows on the edges of pahoehoe flow channels (Plate 2).

TABLE VII

Representative plagioclase compositions for seamounts 6 and 7

Sample	1389-2041-12	1389-2041-7	1389-2041-8	1389-2041-4	1389-2041-6	1389-1613-20	1389-1613-22	1389-1613-26	1389-1613-27	1391-2033-4	1391-2033-5	1391-2033-8	1391-2033-9
Smt.	6	6	6	6	6	6	6	6	6	6	6	6	6
Type	A	A	A	A	A	A	A	A	A	TR	TR	TR	TR
Grain	GM-C-S	P-R	P-C	MP-C	MP-R	P-C	P-R	P-R	P-C	MP-C	MP-R	MP-R	MP-C
SiO_2	54.87	53.21	48.25	49.98	52.17	51.91	52.69	49.61	50.49	48.80	51.01	46.68	46.83
TiO_2	0.16	0.12	0.07	0.11	0.11	0.10	0.08	0.09	0.10	0.05	0.08	0.03	0.05
Al_2O_3	27.93	29.15	32.73	32.17	30.18	30.80	30.45	32.07	31.10	33.44	31.81	34.22	34.12
FeO	1.02	0.65	0.39	0.37	0.59	0.52	0.49	0.40	0.41	0.42	0.53	0.44	0.35
MgO	0.19	0.20	0.13	0.10	0.12	0.16	0.17	0.11	0.13	0.15	0.15	0.14	0.16
CaO	10.44	11.56	15.37	14.16	12.19	13.07	12.68	14.44	13.95	15.58	13.83	16.88	16.28
Na_2O	5.30	4.95	2.69	3.37	4.50	3.93	3.98	3.12	3.40	2.80	3.79	2.01	2.22
K_2O	0.48	0.37	0.15	0.20	0.28	0.28	0.26	0.18	0.22	0.06	0.10	0.04	0.04
Total	100.39	100.21	99.78	100.46	100.14	100.77	100.80	100.02	99.80	101.30	101.30	100.44	100.05
An%	50.66	55.14	75.30	69.06	58.99	63.68	62.80	71.16	68.52	75.19	66.47	82.13	80.02
Or%	2.80	1.63	0.87	1.16	1.63	1.63	1.51	1.06	1.29	0.38	0.59	0.21	0.25

Sample	1393-1646-12	1393-1646-3	1393-1646-4	1394-2003-18	1394-2003-19	1393-1700-5	1393-1700-7	1393-1700-26	1390-1915-18	1390-1915-19	1390-1915-16	1390-1915-7	1390-1915-8
Smt.	7	7	7	7	7	7	7	7	7	7	6	6	6
Type	Th	Th	Th	Th	Th	Th	Th	Th	Th	Th	Th	Th	Th
Grain	P-C	MP-R	MP-C	P-C	P-R	MP-C	MP-R	GM	MP-C	MP-R	GM	MP-C	MP-R
SiO_2	49.87	48.77	48.83	46.94	51.62	49.44	48.27	51.36	48.28	47.16	49.52	46.05	47.90
TiO_2	0.08	0.04	0.05	0.06	–	0.08	0.07	0.08	0.06	0.05	0.01	0.03	0.03
Al_2O_3	32.16	32.79	31.57	34.74	31.02	31.52	32.78	30.62	33.02	33.42	32.71	34.55	32.54
FeO	0.46	0.44	0.52	0.27	0.47	0.57	0.39	0.76	0.37	0.45	0.40	0.29	0.28
MgO	0.15	0.16	0.18	0.18	0.21	0.20	0.19	0.25	0.19	0.17	0.24	0.19	0.22
CaO	14.76	15.87	15.44	17.59	14.06	14.16	15.13	13.40	15.64	16.31	15.51	17.75	16.33
Na_2O	3.06	2.51	2.89	1.59	3.60	3.62	2.96	4.04	2.76	2.46	2.64	1.39	2.22
K_2O	–	0.04	0.01	–	0.03	0.04	0.04	0.02	0.01	0.02	0.01	–	0.02
Total	100.54	100.62	99.49	101.37	101.01	99.63	99.83	100.53	100.51	100.04	101.05	100.25	99.54
An%	72.65	77.56	74.67	85.88	68.21	68.20	73.71	64.53	75.72	78.49	76.42	87.57	80.14
Or%	0.07	0.02	0.06	0.08	0.15	0.22	0.21	0.13	0.08	0.10	0.08	–	0.12

Sample	1388-2127-22	1388-2127-15	1388-2127-21	1388-1920-18	1387-1920-19	1387-1920-20	1387-1920-26	1387-1920-27	1392-1654-1	1392-1627-3	1392-1710-4a	1393-1710-5	1393-1646-11
Smt	6	6	6	6	6	6	6	6	7	7	7	7	7
Type	TR	TR	TR	TR	TR	TR	TR	TR	Th	Th	Th	Th	Th
Grain	GM	P-C	P-R	MP-C	MP-R	GM	P-R	P-C	GM	GM	P-C	P-R	P-R
SiO_2	51.07	50.19	50.92	47.62	49.60	50.58	45.88	47.02	50.74	50.94	48.61	52.46	52.54
TiO_2	0.10	0.07	0.07	0.05	0.06	0.20	0.07	0.08	0.08	0.09	0.04	0.10	0.05
Al_2O_3	30.96	31.90	31.54	33.87	32.30	31.06	33.74	33.83	31.28	30.92	33.42	30.36	29.58
FeO	0.84	0.36	0.52	0.39	0.54	0.86	0.46	0.27	0.59	0.57	0.40	0.65	0.64
MgO	0.28	0.17	0.22	0.16	0.19	0.28	0.16	0.14	0.24	0.22	0.13	0.28	0.24
CaO	13.70	14.09	13.81	16.69	15.10	13.83	16.24	16.41	13.91	13.52	16.83	13.82	12.74
Na_2O	3.71	3.27	3.50	2.09	3.04	3.73	2.13	2.19	3.62	3.94	1.98	3.69	4.46
K_2O	0.11	0.08	0.10	0.06	0.06	0.08	0.04	0.06	0.06	0.05	0.03	0.08	0.05
Total	100.77	100.13	100.64	100.93	100.89	100.62	98.72	100.00	100.52	100.25	101.44	101.44	100.30
An%	66.70	70.13	68.17	81.21	73.06	66.89	80.61	80.28	67.76	65.27	82.34	67.07	61.06
Or%	0.61	0.47	0.57	0.35	0.37	0.48	0.24	0.33	0.33	0.29	0.15	0.47	0.28

TABLE VII (continued)

Sample	1390-1915-9	1390-1915-10	1387-1714-4	1387-1714-16	1387-1714-19
Smt	6	6	6	6	6
Type	Th	Th	Th	Th	Th
Grain	P-C	P-R	GM	P-C	P-R
SiO_2	46.79	45.07	52.90	48.27	49.65
TiO_2	0.02	0.01	0.09	0.04	0.04
Al_2O_3	33.85	34.54	29.77	32.35	31.12
FeO	0.30	0.30	0.61	0.52	0.48
MgO	0.19	0.19	0.14	0.21	0.24
CaO	17.18	17.98	12.42	15.78	14.79
Na_2O	1.69	1.31	4.32	2.40	3.19
K_2O	0.02	0.02	0.11	0.01	0.02
Total	100.04	94.42	100.36	99.58	99.53
An%	84.84	88.22	61.00	78.43	71.84
Or%	0.09	0.14	0.61	0.03	0.12

Seamounts also contain fairly common outcrops of spattery lava forming 1–2 m high spatter cones (Lonsdale and Batiza, 1980; Fornari *et al.*, 1988b). These may superfically resemble wrinkled or ropey pahoehoe, but in some cases contain honeycomb-textured glass and spatter drips elongated downslope. In some cases, these spatter cones are associated with hyaloclastite flows, also common on seamount summits (Smith and Batiza, 1989). Seamount summits may also contain rubbly flows similar to subaerial aa flows. The evidence for this comes mainly from the presence, on Seamount 7, of large outcrop areas of loose rock on very gentle slopes, near the summit. While such deposits could form by in-situ fragmentation of pillow lava or other flow forms, it seems more likely that the deposits of angular basalt fragments represent primary volcanic products of rubbly flows. Unfortunately, the size, shape and total extent of these deposits could not be determined because of poor exposure (sediment burial).

Overall, the lava flow forms found on seamounts are broadly similar to those found at the axes of active mid-ocean ridges (Bonatti and Harrison, 1988), with the exception of hyaloclastites and spattery lava forms. Pillow flows form the flanks of most edifices, whereas lobate pillows, and sheet flows are abundant on the flat and gently sloping summit regions. Deposits of elongate pillow tubes on the flanks of seamounts appear to originate from radial feeders to form broad constructional radial ridges and isolated pillow cones on the flanks. In contrast, deposits at the summits appear to originate mostly from circumferential, arcuate feeders (Simkin, 1972, 1984) leading to the formation of flat expanses of sheet flow and lobate pillows or arcuate summit benches covered by pillow flows.

Hydrothermal activity

Previous submersible and camera studies of seamounts near the EPR have commonly revealed the presence of active hydrothermal venting or hydrothermal precipitates. Lonsdale *et al.* (1982) reported deposits of high-temperature sulfide minerals (Alt, 1988b; Alt *et al.*, 1987) and venting of warm hydrothermal fluids from volcanoes of the Larson seamounts. Hekinian and Fouquet (1985) reported abundant hydrothermal activity on a seamount near the EPR at 13° N. For volcanoes with calderas, hydrothermal activity is usually localized along circumferential faults associated with the calderas. However, calderas are not necessary for hydrothermal activity, as at the 13° N volcano (Hekinian and Fouquet, 1985) and a volcano at 14°09′ N (Batiza *et al.*, 1988). Some volcanoes with well-developed calderas, such as those of the Lamont seamount chain (Fornari *et al.*, 1988a, b) apparently have no or little hydrothermal activity or hydrothermal precipitates associated with them. On the other hand, because of the localized nature of such activity and

TABLE VIII

Representative spinel analysis for seamounts 6 and 7

Sample	1390-1915 SP-2	1390-1915 SP-3	1387-1920 SP-1	1387-1920 SP-2	1388-2127 SP-2	1388-2127 SP-4	1388-2127 SP-7	1391-2033 SP-2	1391-2033 SP-5	1389-1613 SP-2	1389-2041 SP-3	1389-2041 SP-4	1389-2041 SP-7	1389-1810 SP-1	1389-1810 SP-2	1389-1810 SP-3	1389-1810 SP-4	1389-1810 SP-5	1389-1810 SP-8	1389-1810 SP-9	1389-1810 SP-10
Rock type	Th	Th	Tr	Tr	Tr	Tr	Tr	Tr	Tr	A	A	A	A	A	A	A	A	A	A	A	A
Occurrence	P/E	P/C	AP	GM	AO	O	GM	O	AO	AP	P	GM	P	GM/C	GM/E	AP	P	AO	GM	GM	GM
Size (μ m)	75	75	30	40	25	27	25	56	30	25	15	20	25	30	30	20	15	15	25	25	15
SiO_2	0.08	0.09	0.07	0.05	0.09	0.06	0.09	0.09	0.08	0.05	0.07	0.07	0.06	0.07	0.08	0.09	0.05	0.07	0.05	0.07	0.09
TiO_2	0.22	0.25	0.86	0.95	0.88	0.87	0.84	0.86	0.93	3.32	3.14	3.71	3.32	1.81	2.00	2.03	1.92	1.97	1.86	1.76	2.21
Al_2O_3	46.59	46.42	38.81	37.38	38.64	38.26	37.54	38.00	37.21	22.32	24.97	23.43	24.15	31.62	32.80	30.45	30.17	30.25	23.24	24.76	31.55
FeO	8.75	9.97	14.48	13.98	13.66	13.81	13.60	14.23	12.24	22.14	21.43	22.65	22.49	17.47	16.84	17.31	17.24	17.22	17.85	18.01	16.88
Fe_2O_3	4.10	2.78	4.84	5.96	5.44	5.27	5.47	5.34	7.96	8.82	9.97	10.11	9.44	5.94	7.42	7.31	7.48	7.22	6.90	6.80	8.01
MgO	20.65	20.22	17.51	17.08	17.49	17.26	17.28	17.13	17.18	12.68	12.65	12.38	12.29	15.59	15.59	15.17	15.16	15.26	13.80	14.16	15.60
MnO	0.04	0.15	0.19	0.19	0.16	0.20	0.16	0.17	0.17	0.29	0.25	0.36	0.29	0.24	0.26	0.22	0.19	0.21	0.22	0.20	0.14
Cr_2O_3	20.39	21.02	24.21	25.18	24.12	24.55	24.99	25.01	24.72	29.80	26.77	27.35	27.56	27.59	26.05	21.31	27.99	28.14	36.25	35.49	25.86
NiO	0.17	0.19	0.26	0.21	0.005	0.19	0.18	0.30	0.26	0.08	0.21	0.13	0.10	0.31	0.23	0.22	0.21	0.19	0.13	0.18	0.31
CaO	0.12	0.25	0.12	0.09	0.001	0.03	0.08	0.02	0.04	0.16	0.27	0.09	0.15	0.07	0.08	0.05	0.05	0.10	0.048	0.07	0.13
Total	101.11	101.11	101.35	101.07	100.75	100.52	100.22	101.15	100.79	99.67	99.73	100.28	99.86	100.71	101.34	100.15	100.46	100.64	100.56	101.50	100.78
Si	0.002	0.002	0.002	0.001	0.002	0.002	0.002	0.003	0.002	0.002	0.002	0.002	0.002	0.002	0.002	0.002	0.002	0.002	0.002	0.002	0.002
Ti	0.004	0.005	0.018	0.020	0.019	0.019	0.018	0.018	0.020	0.078	0.072	0.086	0.077	0.040	0.044	0.045	0.042	0.043	0.043	0.041	0.048
Al	1.460	1.459	1.271	1.238	1.273	1.266	1.248	1.253	1.236	0.814	0.901	0.849	0.876	1.081	1.113	1.054	1.043	1.043	0.834	0.873	1.080
Fe^{2+}	0.195	0.222	0.337	0.328	0.320	0.324	0.321	0.333	0.289	0.573	0.549	0.583	0.578	0.424	0.406	0.425	0.424	0.422	0.407	0.450	0.410
Fe^{3+}	0.082	0.055	0.101	0.126	0.114	0.111	0.116	0.112	0.169	0.206	0.229	0.234	0.219	0.130	0.161	0.161	0.165	0.159	0.205	0.154	0.175
Mg	0.819	0.804	0.725	0.716	0.729	0.723	0.726	0.714	0.722	0.585	0.578	0.567	0.563	0.675	0.668	0.664	0.663	0.666	0.626	0.631	0.676
Mn	0.001	0.003	0.004	0.004	0.004	0.005	0.004	0.004	0.004	0.008	0.006	0.010	0.008	0.006	0.006	0.005	0.004	0.005	0.006	0.005	0.003
Cr^{3+}	0.429	0.443	0.532	0.559	0.533	0.545	0.557	0.553	0.551	0.729	0.648	0.664	0.670	0.633	0.592	0.635	0.649	0.651	0.873	0.873	0.594
Ni	0.004	0.004	0.006	0.005	0.005	0.004	0.004	0.007	0.006	0.002	0.005	0.003	0.002	0.008	0.005	0.005	0.005	0.004	0.003	0.004	0.007
Ca	0.003	0.001	0.003	0.003	0.001	0.001	0.002	-	0.001	0.005	0.009	0.003	0.005	0.002	0.002	0.001	0.001	0.003	0.002	0.002	0.004
Mg	0.808	0.783	0.683	0.685	0.695	0.690	0.694	0.682	0.714	0.505	0.513	0.494	0.493	0.614	0.623	0.610	0.611	0.612	0.606	0.584	0.622
Cr	0.227	0.233	0.295	0.311	0.295	0.301	0.309	0.306	0.308	0.473	0.418	0.439	0.434	0.369	0.348	0.376	0.384	0.384	0.511	0.490	0.355
Fe^{3+}	0.042	0.028	0.053	0.066	0.059	0.058	0.060	0.058	0.086	0.131	0.129	0.134	0.124	0.070	0.086	0.087	0.089	0.086	0.107	0.082	0.095
Type	Cr	Cr	Ti-Cr	Ti-Cr	Ti-Cr	Ti-Cr	Ti-Cr	Ti-Cr	Ti-Cr	?	Ti-Cr	?	?	Ti-Cr	Ti-Cr	Ti-Cr	Ti-Cr	Ti-Cr	Ti-Mg-Cr	Ti-Cr	Ti-Cr
Host gl Al_2O_3	17.96	17.96	17.38	17.38	17.72	17.72	17.72	17.43	17.43	17.14	16.97	16.97	16.97	17.79	17.79	17.79	17.79	17.79	17.79	17.79	17.79
Host gl Mg	71.60	71.60	64.10	64.10	65.10	65.10	65.10	64.60	64.60	57.3	41.8	41.8	41.8	61.60	61.60	61.60	61.60	61.60	61.60	61.60	61.60
Host gl	476	476	199	199	191	191	191	197	197	116	90	90	162	162	162	162	162	162	162	162	162

P = phenocrysts
GM = groundmass
O = within olivine
A = adhered to
P = plagioclase
E = edge
C = center

the relatively sparse coverage provided by even a detailed dive and camera program ($\ll 1\%$ of the surface), hydrothermal activity may exist but is yet to be discovered on seamounts of the Lamont chain.

Of the four seamounts in this study, only the youngest, seamount 5, showed evidence of hydrothermal activity. Very extensive areas of the summit, mostly concentrated near the caldera, are covered with hydrothermal crusts and/or soft brown hydrothermal mud. The latter apparently consists mostly of bacterial filaments with amorphoous Fe-rich, Mn-poor precipitates (Vanko, pers. comm.; Alt, 1988a). Patchy areas of 1 to 10^2 m^2 are covered by yellow and white bacterial mats and are probably areas of active, though diffuse, venting. Measurements with the ALVIN temperature probe in these areas showed only small temperature anomalies (<2 °C). We found no deposits of metal sulfides or obvious, localized low-temperature fluid venting, as on the Larson seamounts (Lonsdale *et al.*, 1982).

Seamount D, 6 and 7 show no evidence of active or ancient hydrothermal activity except for manganese coatings on surface lavas. In many cases, these coatings are quite thick (up to 7–8 cm) and are doubtless of low temperature hydrothermal origin. Because hydrothermal mineral precipitates appear to be so common on young seamounts near the EPR, it is likely that older seamounts, such as D, 6 and 7 may have buried hydrothermal deposits.

Mass wasting processes

The products and features created by mass-wasting processes, such as talus ramps, are ubiquitous on the steep volcanic slopes of all the seamounts we studied. Previous submersible studies also have shown that steep slopes are commonly characterized by loose rock, in many cases mixed with sediment or cemented by manganese (Fornari *et al.*, 1979; Lonsdale and Batiza, 1980; Lonsdale and Spiess, 1979; Batiza *et al.*, 1984; Fornari *et al.*, 1988b; Hekinian and Fouquet, 1985; Hekinian *et al.*, 1988). Young fault scarps such as caldera walls, as well as steep slump scarps on the outer volcanic flanks, are clearly degraded rapidly by mass wasting. As suggested by Taylor *et al.* (1975) and Stanley and Taylor (1977), these processes probably reflect a complex combination of down-slope sediment and debris movement resulting from current activity and seismic activity acting on steep gravitationally-unstable slopes. While some loose debris results from pillow extrusion on steep slopes, most rock debris is probably the result of rock falls and debris slides.

On seamount 5, young caldera faults are either vertical walls (up to 20–30 m high) or stepped vertical walls 3–5 m high interrupted by talus ramps. Some faults are partly covered by younger pillow-tube eruptives with tubes dipping 60–80°. In these cases, loose pillow buds and fragments of tubes litter the base of the slope. Older faults, such as the caldera walls of seamount 6E show progressive upward and outward growth of fan-like talus ramps as well as progressive mixing of loose rock with fine-grained sediment.

Mature talus deposits consist mostly of fine-grained sediment mixed with a variable but small proportion of rock fragments. Commonly, the angular rock fragments appear to be well-sorted. Such talus ramps are typically dissected by narrow (1–3 m wide) sediment chutes containing sediment mixed with pebble or granule-sized rock fragments. Crossings of mature talus ramps usually show that the ramp consists of a patchwork of distinct deposits. These deposits are distinguished by variable amounts of sediment, average size of rock debris and extents of sorting. The contacts between these different facies are sharp. Probably each deposit represents a distinct episode of down-slope movement, though the processes by which this movement occurs is not obvious. We did not observe any obvious slump scars on the talus ramps we studied.

Talus ramp commonly overlap each other the way subaerial talus aprons do or are separated by rocky outcrops. On caldera walls, these outcrop areas usually form buttresses on the caldera wall. Our examination of the steep outer flanks of seamounts 5, 6, 7 and D are limited, however outer volcanic slopes usually steepen upward toward the summit like Galapagos volcanoes (Simkin, 1984). In some cases, they consist of in situ pillow tubes and bulbous pillows mixed with loose rock debris. Mostly, however, the slopes consist of loose rock debris alone. These talus deposits may be the result of simple rock falls and rock slides, but in some cases probably result from slumping (Lonsdale and Batiza, 1980).

Sedimentation and sediment transport

All four seamounts we studied have sedimentary deposits of various kinds. Sediment samples collected

TABLE IX

Representative clinopyroxene analyses for seamounts 6 and 7

Sample	1389-2041-5	1389-2041-4	1389-2041-6	1389-2041-9	1387-1714-1	1387-1714-2	1387-1714-4	1387-1714-10	1392-1627-1	1392-1627-2	1393-1700-1
Smt	6	6	6	6	6	6	6	6	7	7	7
Type	A	A	A	A	Th	Th	Th	Th	Th	Th	Th
Grain	GM	GM	GM	GM	P-E	P-C	MP-C	P	GM	GM	P-C
SiO_2	43.16	43.03	43.02	43.80	46.78	43.66	43.53	45.69	48.48	46.69	49.19
TiU_2	4.53	4.92	4.25	4.40	2.56	4.28	4.22	2.91	1.39	2.23	1.40
Al_2O_3	7.98	8.08	8.68	6.81	3.95	6.56	5.74	4.28	6.80	7.80	5.35
Cr_2O_3	0.103	0.11	0.061	0.24	0.22	0.158	0.318	0.01	0.24	0.17	1.06
FeO*	8.19	8.08	8.51	8.28	11.54	10.36	11.38	11.46	6.54	7.37	5.64
FeO	4.12	4.69	4.27	4.35	7.20	5.83	6.57	6.46	4.10	4.80	4.02
Fe_2O_3	4.53	3.77	4.71	4.36	4.82	5.03	5.34	5.55	2.71	2.86	1.80
MnO	0.17	0.17	0.15	0.16	0.323	0.181	0.236	0.25	0.16	0.19	0.15
NiO	0.01	0.0001	0.014	0.03	0.056	0.022	–	0.01	0.04	0.05	–
MgO	11.79	11.77	11.36	11.79	11.46	10.78	10.49	11.49	15.92	13.36	15.84
CaO	21.78	21.49	21.83	22.17	21.64	21.99	21.47	21.53	19.70	21.39	20.42
Na_2O	0.544	0.533	0.54	0.51	0.539	0.562	0.604	0.53	0.28	0.34	0.29
K_2O	0.01	0.01	0.033	–	0.0002	0.008	0.009	–	–	–	0.01
Total	98.83	98.57	98.75	98.63	99.35	99.06	98.53	98.71	99.72	99.88	99.63
Wo	52.16	51.98	52.35	52.49	48.48	50.99	49.54	48.40	46.73	50.78	48.86
EN	28.23	28.47	27.24	27.91	25.67	24.99	24.20	25.83	37.76	31.72	37.71
Fs	19.61	19.55	20.41	19.60	25.85	24.02	26.26	25.76	15.51	17.50	13.43
Fe_2O_3:											
FeO	1.01	0.80	1.10	1.00	0.67	0.86	0.81	0.86	0.66	0.60	0.45
Ha	0.040	0.039	0.040	0.037	0.040	0.041	0.045	0.040	0.020	0.024	0.021
Hg	0.669	0.670	0.644	0.672	0.653	0.617	0.606	0.659	0.873	0.741	0.871
Al	0.358	0.364	0.389	0.306	0.178	0.297	0.262	0.194	0.294	0.342	0.233
Si	1.642	1.641	1.637	1.674	1.788	1.674	1.686	1.758	1.783	1.736	1.815
K	–	–	0.002	–	–	–	–	–	–	–	–
Ca	0.888	0.878	0.890	0.907	0.886	0.903	0.891	0.888	0.777	0.852	0.811
Ti	0.132	0.142	0.122	0.127	0.074	0.123	0.123	0.084	0.050	0.062	0.039
Cr	0.003	0.003	0.002	0.007	0.001	0.005	0.009	–	0.007	0.005	0.031
Mn	0.005	0.005	0.005	0.005	0.010	0.006	0.007	0.008	0.005	0.006	0.005
Fe^{2+}	0.131	0.150	0.136	0.139	0.230	0.187	0.213	0.208	0.126	0.149	0.124
Fe^{3+}	0.129	0.108	0.135	0.126	0.139	0.145	0.155	0.160	0.075	0.080	0.049
Ni	–	–	–	0.001	0.002	0.001	–	–	0.001	0.001	–
$Mg/(Mg+Fe^{2+})$	0.836	0.817	0.826	0.828	0.739	0.767	0.740	0.760	0.874	0.832	0.875

by ALVIN were studied by Levin and Nittrouer (1987). In general, the sediment present on seamount summits is white pelagic sand and is commonly rippled. While some exceptions do occur, for example, dark green, fine-grained sediment on some portion of the summit of seamount 7, it is clear that in general, finer grained sediment is winnowed by currents at seamount summits. This fine-grained sediment is deposited further downslope where it mixes with talus debris or simply coats rock outcrops. As discussed by Levin and Nittrouer (1987) and Stanley and Taylor (1977), sedimentation on seamounts is affected by a large number of variables, which include biologic productivity, currents, extent of bioturbation, hydrothermal activity (which can lithify sediment in situ to form crusts), and others.

Because of these complex effects and the general downslope movement (by winnowing and gravity) of sediment, the thickness of sediments on seamounts is, alone, a poor indicator of relative age within a single edifice or among various seamounts. Even so, based on sediment thickness, seamount 5 appears to be the youngest of the four seamounts studied. Seamount 6 and 7 appear to be younger than seamount D based on sediment thickness, but both are much taller edifices than D. This difference in

TABLE IX (continued)

Sample	1393-1700-2	1393-1700-5	1393-1646-1	1393-1646-4	1393-1646-5	1393-1646-6	1394-2003-4	1394-2003-7	1394-2003-11	1393-1646-2	1393-1646-3
Smt	7	7	7	7	7	7	7	7	7	7	7
Type	Th	Th	Th	Th	Th	Th	Th	Th	Th	Th	Th
Grain	P-E	GM	P	P	GM	GM	GM	GM	MP	P	P
SiO_2	48.91	49.94	52.34	49.55	47.65	49.06	50.52	50.69	50.99	49.83	49.55
TiO_2	1.54	0.96	0.63	1.29	2.53	1.25	0.91	0.80	0.76	0.64	1.26
Al_2O_3	5.37	3.56	2.31	4.41	4.57	5.20	4.13	3.56	3.65	2.20	4.49
Cr_2O_3	0.60	0.17	0.59	0.98	–	1.32	0.38	0.40	0.400	0.50	0.68
FeO*	6.14	5.84	6.17	5.55	10.71	5.96	6.67	5.72	6.73	6.05	5.83
FeO	4.20	2.93	4.76	3.05	7.22	3.03	4.74	3.48	5.33	4.61	3.84
Fe_2O_3	2.16	3.23	1.57	2.78	3.88	3.26	2.15	2.42	1.56	1.60	2.21
MnO	0.12	0.20	0.16	0.14	0.32	0.15	0.17	0.18	0.202	0.21	0.14
NiO	–	0.03	0.01	0.01	0.04	0.03	0.03	0.02	0.014	0.04	0.05
MgO	15.52	16.87	19.09	15.71	13.91	16.24	17.77	16.60	18.01	18.40	15.80
CaO	20.71	20.48	18.23	21.65	19.53	20.44	18.34	21.06	17.83	19.13	21.21
Na_2O	0.29	0.23	0.18	0.31	0.40	0.31	0.24	0.23	0.25	0.21	0.29
K_2O	0.001	0.01	–	0.01	0.001	–	–	0.003	–	0.01	–
Total	99.44	98.62	99.87	99.89	100.05	100.29	99.38	99.44	99.00	99.00	99.00
Wo	48.88	47.42	41.92	50.45	44.23	47.94	42.87	48.55	41.88	43.96	49.51
EN	36.63	39.06	43.90	36.61	31.51	38.09	41.54	38.27	42.31	42.22	36.88
Fs	14.49	13.52	14.19	12.93	24.26	13.98	15.59	13.19	15.81	13.88	13.61
Fe_2O_3:											
FeO	0.51	1.10	0.34	0.91	0.54	1.08	0.45	0.72	0.29	0.35	0.58
Na	0.021	0.016	0.012	0.022	0.030	0.022	0.017	0.016	0.018	0.015	0.021
Hg	0.856	0.935	1.038	0.864	0.778	0.888	0.975	0.912	0.991	1.003	0.0869
Al	0.235	0.156	0.099	0.192	0.202	0.225	0.179	0.155	0.159	0.095	0.195
Si	1.811	1.856	1.910	1.826	1.787	1.800	1.858	1.869	1.881	1.914	1.837
K	–	–	–	–	–	–	–	–	–	–	–
Ca	0.822	0.815	0.712	0.855	0.785	0.804	0.723	0.832	0.705	0.749	0.838
Ti	0.043	0.027	0.017	0.036	0.071	0.035	0.025	0.022	0.021	0.017	0.035
Cr	0.017	0.005	0.017	0.028	–	0.038	0.011	0.012	0.011	0.014	0.020
Mn	0.004	0.006	0.005	0.004	0.010	0.005	0.005	0.006	0.006	0.006	0.004
Fe^{2+}	0.130	0.091	0.145	0.094	0.226	0.093	0.146	0.107	0.164	0.141	0.118
Fe^{3+}	0.060	0.090	0.043	0.077	0.109	0.090	0.060	0.069	0.043	0.044	0.062
Ni	–	0.001	–	0.000	0.001	0.001	0.001	0.001	–	0.001	0.001
$Mg/(Mg+Fe^{2+})$	0.868	0.911	0.877	0.902	0.775	0.905	0.870	0.895	0.858	0.677	0.880

Same codes as Table VI.

elevation, vis a vis, significant differences in the current regime (Roden, 1987) might account for differences in the amount of sediment present on the summits of 6 and 7 versus D.

Tectonics and structure

Nakamura (1977) showed that the shapes of volcanoes commonly reflect patterns of regional tectonic stress. It is also well known that the distribution of volcanic eruptions is controlled by patterns of fractures which can act as volcanic conduits. Batiza and Vanko (1983) showed that the shapes of many seamounts can be used to infer the geometry of linear volcanic conduits. For very small seamounts near the EPR, Fornari *et al.* (1987b) showed that volcano shape is commonly a reflection of the distribution of volcanic conduits. In addition to tectonic stress and the conduit geometry, volcano shapes are also strongly influenced by gravitational stress, particularly for large volcanoes (Fiske and Jackson, 1972; Simkin, 1984). Gravitational stresses are thought to be responsible for linear flank rift zones and the flat-topped nature of most oceanic volcanoes.

As discussed by Batiza and Vanko (1983) and Fornari *et al.* (1987b), the shapes of seamounts 5, 6, 7 and D are probably affected by both regional tectonic stress patterns, inherited deep faults within

TABLE X

Major and trace element data for Seamount 7

Sample	1392/1627	1392/1654	1392/1710	1392/1744	1392/1938	1392/2151	1393/1646	1393/1700
Depth(m)	1115	1045	1041	1001	827	768	1786	1760
Sample type	PT	P	P	P	PT	PT	P	P
SiO_2	50.33	50.33	50.16	50.48	50.33	50.52	50.75	50.67
TiO_2	1.74	1.67	1.66	1.69	1.72	1.7	1.82	1.85
Al_2O_3	15.5	15.45	15.22	15.17	15.09	15.20	15.08	15.15
FeO*	9.47	9.40	9.54	9.47	9.52	9.50	9.84	9.72
MgO	6.94	7.01	7.00	6.83	6.856	6.95	6.80	6.74
CaO	11.80	11.80	11.79	11.88	11.82	11.89	11.76	11.79
Na_2O	3.16	3.10	3.11	3.09	3.31	3.34	3.46	3.45
K_2O	0.24	0.26	0.24	0.24	0.20	0.19	0.17	0.18
P_2O_5	0.20	0.18	0.18	0.18	0.12	0.21	0.21	0.21
Total	99.38	99.28	99.90	99.03	99.02	99.51	99.89	99.76
INNA-FeO*	9.02	8.91	9.14	9.01			9.14	8.99
INNA-Na_2O	3.08	3.02	3.09	2.95			3.34	3.29
La	6.07	6.09	6.13	5.95			5.41	5.49
Ce	15.54	16.9	16.62	16.21			15.1	16.2
Sm	3.83	3.73	3.76	3.62			4.18	4.05
Eu	1.402	1.377	1.407	1.378			1.59	1.517
Tb	0.94	0.76	0.78	0.72			0.92	0.78
Yb	2.7	2.69	2.8	2.77			3.03	3
Lu	0.39	0.38	0.4	0.39			0.41	0.43
Sc	41	41	41	40			43	42
Cr	265	262	268	259			285	281
Co	41	40	41	39			40	42
Ni	38	85	–	75			62	65
Rb	10	5	–	8			10	4
Cs	0.14	0.09	0.14	0.09			0.03	0.08
Sr	250	238	222	227			100	195
Ba	40	41	–	34			120	47
Zr	125	174	–	143			123	116
Hf	315	3.04	3.19	3.02			3.34	3.31
Th	0.66	0.3	0.38	0.32			0.46	0.22
Ta	0.36	0.39	0.38	0.39			0.31	0.32
U	0.21	0.23	–	0.3			0.21	0.31
Mg#	61.0	61.4	61.0	60.6	60.6	60.9	59.6	59.7
$(La/Sm)_N$	0.86	0.89	0.89	0.90			0.70	0.74

the ocean crust, and gravitational stresses within the edifice as it grows larger. All the volcanoes of this study, even seamount 7, are grossly flat-topped, probably reflecting a cone-sheet geometry of conduits that developed as the volcanoes grew (Simkin, 1972). In contrast, most linear elements, such as the N-S flank rift zone on seamount 6, the N-S summit bench on seamount D and the breach directions of calderas on 6E and 5 probably all reflect the orientations of abyssal hills and EPR-perpendicular and oblique faults which have acted as volcanic conduits at various stages of growth.

In contrast with large shield volcanoes like Hawaii and the star-shaped volcanoes of the western Pacific (e.g. Vogt and Smooth, 1984), the small lateral rifts of volcanoes near the EPR probably reflect crustal fault patterns rather than gravitational stress. Apparent lateral rifts may in some cases be partly buried

TABLE X (continued)

Sample	1394/1742	1394/1821	1394/1843A	1394/1925	1394/2003	1395/1825	1395/1948
Depth(m)	2923	2858	2839	2844	2813	3393	3317
Sample type	P	P	P	P	PT	P	M
SiO_2	50.70	50.66	50.55	50.98	51.05	50.56	50.90
TiO_2	1.71	1.79	1.72	1.75	1.85	1.64	1.67
Al_2O_3	14.61	14.54	14.41	14.48	14.34	14.79	14.46
FeO*	10.61	10.91	10.69	10.87	11.21	10.32	10.66
MgO	6.65	6.59	6.56	6.51	6.28	6.95	6.83
CaO	11.55	11.61	11.72	11.54	11.31	12.11	11.8
Na_2O	3.21	3.21	3.20	3.19	3.29	3.07	2.98
K_2O	0.14	0.15	0.14	0.15	0.15	0.11	0.14
P_2O_5	0.18	0.16	0.18	0.18	0.2	0.17	0.2
Total	99.36	99.62	99.17	99.65	99.68	99.72	99.64
INNA-FeO*		9.74		9.73	9.76	8.66	
INNA-Na_2O		2.99		3.02	2.97	3.08	
La		4.12		4.17	4.36	3.51	
Ce		12.43		12.2	12.9	11.21	
Sm		3.52		3.59	3.57	3.57	
Eu		1.349		1.39	1.299	1.339	
Tb		0.78		0.81	0.75	0.76	
Yb		3.05		3.04	3.1	3	
Lu		0.45		0.42	0.45	0.45	
Sc		44		44	43	45	
Cr		152		157	152	262	
Co		43		42	42	43	
Ni		66		57	–	–	
Rb		7		12	–	–	
Cs		0.14		0.13	0.09	0.07	
Sr		153		74	136	141	
Ba		74		64	41	46	
Zr		110		198	–	–	
Hf		2.63		2.74	2.74	2.77	
Th		0.15		0.18	–	–	
Ta		0.23		0.17	0.21	0.17	
U		0.3		255	0.21	0.31	
Mg#	57.3	56.3	56.7	56.1	54.5	59.0	57.8
$(La/Sm)_N$		0.64		0.63	0.67	0.53	

FeO* = total iron oxide
T = Talus
P = pillow, in place
M = massive flow

volcanic ridges from the early stages of volcanic growth (Fornari *et al.*, 1987b) rather than later features. Likewise, cone and lava fields on the deep flanks of near EPR volcanoes may be old relicts from the early stages of growth rather than the young products of flank eruptions. This is probably the case for the lava and cone fields near volcanoes 6 and 7 based on apparent age as well as chemical composition. Lavas from such cone fields appear older and more altered than summit lavas and systematically less evolved (higher MgO) than most of the edifice, contrary to what would be expected for flank rift zone eruptions (Wright and Fiske, 1971). These cone/lava fields probably formed early in the evolution of seamounts 6 and 7 when eruptions were widely distributed by patterns of sea-floor faults. Very small nascent seamounts near the EPR (Fornari *et al.*, 1987b; Batiza and Vanko, 1983) and lava fields that cover seafloor faults near the Siqueiros and Clipperton fracture zones (Batiza *et al.*, 1988) and elsewhere (Fornari *et al.*, 1985) are morphologically identical to the deep flank cone/lava fields near seamounts 6 and 7. In later stages of growth, eruptions on seamount 6 and 7 probably became more centrally focused along the widest, best-heated conduits, thereby stranding certain distal cone and lava fields. Similar constructs probably underly most seamounts and unburied relicts are commonly found in the vicinity of large edifices (e.g. the Lamont seamount chain, Fornari *et al.*, 1988a, b). The thermal maturation of eruptive conduits probably also explains the increasingly primitive nature of N-MORB lavas on seamounts 5 and D with time.

Other prominent structures on near-EPR seamounts include calders and inferred buried calderas that are manifested as flat terraces at or near the summits of mature volcanoes. Calderas probably do not form only at a particular late stage of evolution. Furthermore, caldera formation is probably not a singular event. Instead, calderas probably form and partially fill continually during a seamount's growth and calderas may deepen, expand and become nested or breached (Fornari *et al.*, 1984). The evidence for this is not only progressive caldera development as exhibited by the Lamont seamount chain (Fornari *et al.*, 1984), but also the fact that even the tiniest seamounts (100–200 m high) commonly have calderas or craters (Batiza and Vanko, 1983). Furthermore, calderas are very common and are not restricted to volcanoes of a particular size class. Volcanoes with present-day caldera tend to be tholeiitic (N-MORB) or transitional, whereas volcanoes with abundant alkali basalts lavas tend to have either flat summits, flattish but bumpy summits, or even approach conical form. These forms are most likely the result of caldera filling by late-stage lavas.

Most commonly, calderas are thought to result from summit collapse after lateral or summit eruptions drain a shallow magma reservoir (Ryan, 1988). It is also possible, however, that draining of deeper reservoirs or conduits may cause collapse to form calderas as suggested recently by Fornari *et al.* (1988a, b). It may be possible to distinguish between these modes of formation by the presence or absence of fractionated basalts and flank eruption or by the location, shape and size of collapse features. There is no direct evidence for the depth of magma withdrawal that led to formation of caldera on seamounts 6, D and 5.

VOLCANIC EVOLUTION

The four seamounts of this study show very clear trends of evolution in eruptive style (pillow lavas vs. sheet flow vs. hyaloclastite), morphology and petrologic evolution. Seamounts 6C and 7 have summit caps of transitional and alkalic lavas overlying a tholeiitic edifice. Neither volcano has a caldera presently, and their cappings form a bumpy surface on a gently sloping summit. It seems reasonable that both 6C and 7 represent a N-MORB-only edifice, such as seamounts 5 or D, to which an alkalic or transitional cap has been added. This cap would first fill any summit depressions and then build up further to form a gently-sloping bumpy summit region. Seamount 6E appears to have experienced a transitional phase, with an old caldera and transitional basalts in addition to N-MORB.

Seamounts 5 and D are composed of mostly pillow lava on the flanks with lobate pillows and submarine pahoehoe on their flat summits. Post-caldera pillow lava on both volcanoes forms haystacks and pillow walls which may coalesce to form arcuate summit benches. The summit bench of seamount D, however, also contains products of more rapid eruption rates, so eruption rate probably varies over a large range during seamount growth. High eruption rate products appear to be confined to the flat top, whereas low eruption rate pillows commonly coat the flanks. These relationships are consistent with the overall morphology of the seamount: high eruption rate lavas build the central cylindrical mass of the volcano, with lower eruption rate, less voluminous lavas building the steeply sloping flanks.

Eruption rates on seamounts 5, D and 7 appear to have waned with time, with the extrusion of post-caldera pillows over pre-caldera sheet flows and lobate pillows. In contrast, eruption rates on 6C appear to have increased, with hyaloclastite and pahoehoe overlying pillows. Volcano 6E is more like 5, D and 7, with abundant pillows on the surface. On 6E, many of these, as on 7, are transitional E-MORB whereas on 5 and D, they are N-MORB. On 6C, the hyaloclastites are N-MORB and are found together (interstratified?) with alkalic differential lavas comprising both pillow and sheet flows.

These relationships suggest that eruption rates, even in the waning stages of either an N-MORB or alkalic-capped edifice may fluctuate, though perhaps in general they decrease. Drilling would be needed in order to determine whether eruption rates fluctuate during construction of the main edifice mass, are more or less constant, or decreases with time. Since this study includes seamounts with a range of sizes, our results may provide some guidance. If so, they indicate that the main mass of the edifice consists of ponded caldera-filling lava, sheet flows and minor pillow flows whereas the flanks consist mainly of pillows. Petrologically, it appears that volcanoes need not go on to evolve alkalic and E-MORB caps but may cease evolving at the N-MORB stage. It appears that location on EPR-perpendicular structures may enhance the possibility of evolution beyond the N-MORB stage, since most near-EPR volcanoes with alkalic lavas are so-located (Batiza and Vanko, 1984). However, there are still only limited data available and alkalic basalts may yet be found on seamounts that are not located on EPR-perpendicular structures.

AGE CONSTRAINTS

Several approaches may be used to constrain the age of volcanism of seamounts 5, 6, 7 and D and the time period over which they evolved. These include: thickness of manganese coatings, sediment thickness, extent of freshness/weathering of rock samples, magnetic studies and isotopic dating results. Assuming constant accumulation rate, manganese thickness and sediment cover indicate that seamount 5 is the youngest volcano, the summits of seamounts 6 and 7 next, then seamount D and the lower flanks of seamounts 6 and 7 appear to be the oldest. These criteria are qualitative and subject to large errors for reasons discussed previously.

Measurements of the total magnetic field constrained by modelling studies and ALVIN gradiometer measurements (McNutt, 1986) provide useful age constraints. Both seamounts 5 and 7 are mainly normally polarized but have reversely polarized lavas on their summits. Seamount 5 is located on normally polarized crust whereas seamount 7 is built on reversely polarized crust. The bulk of seamount 7 was thus erupted off-ridge whereas the bulk of seamount 5 could have erupted very near the axis of the EPR. The reversed polarity lavas and least squares models (McNutt, 1986) indicate that both volcanoes probably grew rapidly but that their evolution was protracted over ~ 1 Ma or more. In contrast, magnetic results show uniform normal polarity for seamount 6 and suggest a simpler evolution.

Isotopic ages for materials from the four seamounts are limited and difficult to interpret. Baked foraminifera separated from a hyaloclastite sampled on seamount 5 give a ^{14}C AMS age of $11{,}020 \pm 95$ years (G. Jones, pers. comm.) which may represent the age of youngest volcanism on seamount 5. If so, this would indicate that seamount 5 has remained active for ~ 1Ma, consistent with the abundant hydrothermal activity.

$^{40}Ar/^{39}Ar$ data for samples from seamounts 6 and 7 (Honda *et al.*, 1987) are scattered and give an age of <3 Ma for seamount 7 and <2 Ma for seamount 6. The latter age is in rough agreement with an $^{40}Ar/^{39}Ar$ age determination on sample 1389–1810Z of 2.62 ± 0.45 Ma (R. Duncan, pers. comm.). In contrast with these results, $^{3}He/^{4}He$ disequilibrium ages for seamount 6 (Graham *et al.*, 1987) are all younger than 1 Ma and range from only ~ 50–10 Ka to ~ 900 Ka. The $^{40}Ar/^{39}Ar$ and $^{3}He/^{4}He$ ages are thus discordant. For example, sample 1389–1810Z gives $^{3}He/^{4}He$ ages of 270 ± 17 and 255 ± 16 Ka versus 2.6 Ma by $^{40}Ar/^{39}Ar$. This discordance is difficult to explain but is not unexpected given the difficulty of dating young MORB.

The $^{3}He/^{4}He$ ages agree with the Mn-thickness and outcrop freshness observations in that the youngest ages are for samples from the summit of 6C. However, the ages span a large range (0.9 Ma – ~ 5 Ka). The youngest ages from 6C are younger than the ages from 6E (~ 100–120 Ka) in agreement with field observations.

While available age constraints are relatively weak, they permit several tentative conclusions: (1) Seamount 5, closest to the EPR, is clearly the youngest of the four and may still be an an active volcano. (2) Seamount D appears to be inactive, but the age of the youngest volcanism is highly uncertain. It is possible that seamount D grew quickly near the EPR and became inactive even before seamount 5 appeared. (3) The summits of seamounts

6 and 7 appear young, but some of the rocks show incipient clay alteration (in contrast to rocks from seamounts 5 and D). The youthful appearance of outcrops favors ages <1 Ma, in agreement with the $^{3}He/^{4}He$ results. However, the incipient alteration and magnetic studies weakly favor older ages, in agreement with the $^{40}Ar/^{39}Ar$ results.

Petrogenesis and petrologic evolution

The new petrologic and geochemical data for the four seamounts are consistent with the earlier interpretations of Batiza and Vanko (1984) and Zindler *et al.* (1984). Near-EPR seamounts tap the same mantle material as the EPR axis but they do so in a different manner. Seamount N-MORB is more primitive and diverse than EPR lavas indicating that rising batches of melt reach off-axis seamount eruption sites more rapidly and with less modification (e.g. cooling, mixing) than EPR axis magmas. Furthermore, the diversity of seamount lavas indicates either that seamount magma batches are smaller or that EPR magmas are subjected to more mixing prior to eruption (or both).

The range of N-MORB, transitional and alkalic lavas found on near-EPR seamounts is satisfactorily explained by mixing of different mantle source materials prior to melting (Batiza and Vanko, 1984; Zindler *et al.*, 1984; Graham *et al.*, 1988; Aggrey *et al.*, 1988). The observed stratigraphic succession of N-MORB, transitional basalt (E-MORB) and alkalic basalts both interstratified with N-MORB, is consistent with gradual deepening of the mantle source region and waning amounts of thermal energy available for melting (Batiza and Vanko, 1984). This succession of melt types does not occur on all near-EPR seamounts, however, and special conditions may be required for the entire sequence to be completed. Apparently, location on structures that are parallel to relative plate motion enhances the possibility of evolving past the early N-MORB-only stage, but not all volcanoes on these structures necessarily evolve beyond this early stage.

With the exception of an early alkalic stage, the evolution of near-EPR seamounts parallels the evolution of Hawaiian volcanoes (Clague, 1987). Though much smaller, near-EPR volcanoes can evolve toward more alkalic compositions, paralleling the petrologic (and morphologic) evolution of Hawaiian volcanoes.

Summary

Submersible and camera study of four near-EPR volcanoes, together with laboratory study of their lavas, shows that these volcanoes typically evolve from small, cratered N-MORB edifices near the EPR to more alkalic volcanoes with filled calderas and flattish bumpy summit areas. These volcanoes probably begin with aerially dispersed eruptions from many intersecting linear conduits, forming lava and cone fields near the EPR. With continued growth, eruptions are focused at the largest, hottest conduits to form a flat-topped, Galapagos-type shield volcano. These focused eruptions are fed mainly by circumferential feeders, though radial feeders can build volcanic ridges emanating from the eruptive center. At this stage, characterized by N-MORB and, in some cases, transitional E-MORB lavas, the volcano may grow by repeated collapse and infilling of a central caldera. Alternately, collapse may be off-center (breached calderas) and/or the volcano can become inactive. Lavas comprising the central part of the volcano are mainly lobate pillows, sheet flows and ponded flows, whereas lavas on the steep flanks are mainly pillow tubes. Hydrothermal activity is probably common at this stage of evolution.

Many volcanoes become inactive at this early stage, but some continue to evolve, erupting mainly transitional and alkalic lavas from summit circumferential vents. Achieving the alkalic stage of development seems to be favored for volcanoes located on features oriented parallel to relative plate motion.

Acknowledgements

We gratefully acknowledge funding support from the NSF (OCE 83–08980 and OCE 84–15270) and the ONR. Great thanks go to the Captain and crew of the ATLANTIS II and to the pilots of the DSV ALVIN, without whose expert help this study could not have been done. We are grateful to W. Melson and T. O'Hearn for providing the major element glass analyses. We thank Dan Kremser for help with the probe analyses and L. Haskin, R. Korotev and M. Lindstrom for help with INAA. Members of the scientific party on AII-112-18 were instrumental in the success of the cruise and we extend our heartfeld thanks to each of them. We are also grateful to R. Duncan and G. Jones for providing unpublished results of their geochronologic studies. The review comments of D. Fornari and M. Perfit were very helpful. This is Hawaii Institute of Geophysics Contribution No. 2166.

References

Aggrey, K. E., Muenow, D. W., and Batiza, R., 1988, Volatile Abundances in Basaltic Glasses from Seamounts Flanking the East Pacific Rise and 21° N and 12°–14° N, *Geochim. Cosmochim. Acta* **52**, 211–2119.

Allan, J. F., Batiza, R., and Lonsdale, P., 1987, Petrology of Lavas from Seamounts Flanking the East Pacific Rise, 21° N: Implications Concerning the Mantle Source Composition for Both Seamount and Adjacent EPR Lavas, in B. Keating, P. Fryer, R. Batiza and T. J. Boehler (eds.), *Seamounts, Islands and Atolls, AGU Monogr. Series 43* pp. 255–282.

Alt, J. C., 1988a, Hydrothermal Oxide and Nontronite Deposits on Seamounts in the Eastern Pacific, *Mar. Geol.* **81**, 227–239.

Alt, J. C., 1988b, The Chemistry and Sulphur Isotope Compositions of Massive Sulfide and Associated Deposits on Green Seamount, Eastern Pacific, *Econ. Geol.* **83** (in press).

Alt, J. C., Lonsdale, P., Haymon, R., and Muehlenbachs, K., 1987, Hydrothermal Sulfide and Oxide Deposits in Seamounts near 21° N, East Pacific Rise, *Geol. Soc. Am. Bull.* **98**, 157–168.

Ballard, R. D. and Moore, J. G., 1977, *Photographic Atlas of the Mid-Atlantic Ridge Rift Valley*, Springer-Verlag, New York, 114 pp.

Ballard, R. D., Holcomb, R. T., and Van Andel, T. H., 1979, The Galapagos Rift at 86° W, 3. Sheet Flows, Collapse Pits and Lava Lakes of the Rift Valley, *J. Geophys. Res.* **84**, 5407–5422.

Barr, S. M., 1974, Seamount Chains Formed near the Crest of the Juan de Fuca Ridge, Northeast Pacific Ocean, *Mar. Geol.* **17**, 1–19.

Batiza, R., 1980, The Origin and Petrology of Young Oceanic Central Volcanoes: Are Most Tholeiitic Rather than Alkalic? *Geology* **8**, 447–482.

Batiza, R. and O'Hearn, T., 1982, Major Element Chemistry of Basalt Glasses Dredged from Young Isolated Volcanoes and the East Pacific Rise, 10°–14°, *Proc. Intl. Symp. Activity of Oceanic Volcanoes*, No. III, Azores Arquipelage, San Miguel, pp. 201–230.

Batiza, R. and Vanko, D., 1983, Volcanic Development of Small Oceanic Central Volcanoes on the Flanks of the East Pacific Rise Inferred from Narrow Beam Echo Sounder Surveys, *Mar. Geol.* **54**, 53–90.

Batiza, R. and Vanko, D. A., 1984, Petrology of Young Pacific Seamounts, *J. Geophys. Res.* **89**, 11235–11260.

Batiza, R., Fornari, D. J., Vanko, D. A., and Lonsdale, P., 1984, Craters, Calderas and Hyaloclastites on Young Pacific Seamounts, *J. Geophys. Res.* **89**, 8371–8390.

Batiza, R. and Brodholt, J., 1988, Petrogenesis of Young Seamounts near Transforms and OSC's of the EPR 5°–15° N, *Eos Trans. AGU* **69**, 1475.

Bonatti, E. and Harrison, C. G. A. 1988, Eruption Styles of Basalt in Oceanic Spreading Ridges and Seamounts: Effect of Magma Temperature and Viscosity, *J. Geophys. Res.* **93**, 2957–2980.

Clague, D. A., 1987, Hawaiian Alkaline Volcanism, in J. G. Fitton and B. G. J. Upton (eds.), *Alkaline Igneous Rocks, Geol. Soc. Spec. Pub.* **30**, pp. 227–252.

Davis, E. E. and Karsten, J. L., 1986, On the Cause of Asymmetric Distribution of Seamounts about the Juan de Fuca Ridge: Ridge Crest Migration near a Heterogeneous Aesthenosphere, *Earth Planet. Sci. Lett.* **79**, 385–396.

Fiske, R. S. and Jackson, E. D., 1972, Orientation and Growth of Hawaiian Volcanic Rifts: The Effect of Regional Structure and Gravitational Stresses, *Proc. Roy. Soc. London* **329A**, 299–326.

Fornari, D. J., Malahoff, A., and Heezen, B. C., 1979, Visual Observations of the Volcanic Micromorphology of Tortuga, Lorraine and Tutu Seamounts: and Petrology and Chemistry of Ridge and Seamount Features in and around the Panama Basin, *Mar. Geol.* **31**, 1–30.

Fornari, D. J., Ryan, W. B. F., and Fox, P. J., 1984, The Evolution of Craters and Calderas on Young Seamounts: Insights from SeaMARC I and Seabeam Sonar Surveys of a Small Seamount Group near the Axis of the East Pacific Rise, *J. Geophys. Res.* **89**, 11 069–11 084.

Fornari, D. J., Ryan, W. B. F., and Fox, P. J., 1985, Seafloor Lava Fields on the East Pacific Rise, *Geology* **13**, 413–416.

Fornari, D. J., Batiza, R., and Luckman, M. A., 1987a, Seamount Abundances and Distribution near the East Pacific Rise 0°–24 °N Based on Seabeam Data, in B. Keating, P. Fryer, R. Batiza and T. J. Boehler (eds.), *Seamounts, Islands and Atolls, AGU Monogr. Series 43* pp. 13–21.

Fornari, D. J., Batiza, R., and Allan, J. F., 1987b, Irregularly Shaped Seamounts near the East Pacific Rise: Implications for Seamount Origin and Rise Axis Processes, in B. Keating, P. Fryer, R. Batiza and F. Boehlert (eds.), *Seamounts, Islands and Atolls, AGU Monogr. Series 43* pp. 35–47.

Fornari, D. J., Perfit, M. R., Allan, J., and Batiza, R., 1988a, Small Scale Heterogeneities in Depleted Mantle Sources: Near-ridge Seamount Lava Geochemistry and Implications for Mid-Ocean Ridge Magmatic Processes, *Nature* **331**, 511–513.

Fornari, D. J., Perfit, M. R., Allan, J. F., Batiza, R., Barone, A., Haymon, R., Ryan, W. B. F., Smith, T., Simkin, T., and Luckman, M. A., 1988b, Geochemical and Structural Studies of the Lamont Seamounts: Seamounts as Indicators of Mantle Processes, *Earth Planet. Sci. Lett.* **89**, 63–83.

Graham, D. W., Jenkins, W. J., Kurz, M. D., and Batiza, R., 1987, Helium Isotopic Disequilibrium Geochronology of Glassy Submarine Basalts, *Nature* **326**, 384–386.

Graham, D. W., Zindler, A., Kurz, M. D., Jenkins, W. J., Batiza, R., and Staudigel, H., 1988, Helium, Lead, Strontium, Neodymium Isotope Constraints on Magma Genesis and Mantle Heterogeneity beneath Young Pacific Seamounts, *Contrib. Mineral. Petrol.* **99**, 446–463.

Hekinian, R. and Fouquet, Y., 1985, Volcanism and Mettalogenesis of Axial and Off-axis Structures on the East Pacific Rise near 13° N, *Econ. Geol.* **80**, 221–249.

Hekinian, R., Thompson, G., and Bideau, D., 1988, Petrology and Morphology of the Volcanics from the East Pacific Rise near 12°43′ N and 11°30′ N, *J. Geophys. Res.* (in press).

Honda, M., Bernatowicz, T., Podosek, F. A., Batiza, R., and Taylor, P. T., 1987, Age Determination of East Pacific Seamounts (Henderson, 6 and 7)—Implications for Near-Ridge and Intraplate Volcanism, *Mar. Geol.* **74**, 79–84.

Klitgord, K. D. and Mammerickx, J., 1982, Northern East Pacific Rise: Magnetic Anomaly and Bathymetric Framework, *J. Geophys. Res.* **87**, 6725–6750.

Langmuir, C. H., Vocke, R. D., Hanson, G. N., and Hart, S. R., 1978, A General Mixing Equation with Applications to Icelandic Basalts, *Earth Planet. Sci. Lett.* **37**, 380–392.

Levin, L. A. and Nittrouer, C. A., 1987, Textural Characteristics of Sediments on Deep Seamounts in the Eastern Pacific Ocean between 10° N and 30° N, in B. Keating, P. Fryer, R. Batiza and G. Boehlert (eds.), *Seamounts, Islands and Atolls, AGU Monogr. Series 43* pp. 187–203.

Lonsdale, P., 1977, Abyssal Pahoehoe with Lava Coils at the Galapagos Rift, *Geology* **5**, 147–152.

Lonsdale, P., 1985, Non-transform Offsets of the Pacific-Cocos Plate Boundary and their Traces on the Rise Flank, *Geol. Soc. Am. Bull.* **96**, 313–327.

Lonsdale, P., 1989a, Structural Patterns of the Pacific Floor Offshore of Peninsular California, in J. P. Dauphin, G. Ness and B. R. T. Simoneit (eds.), *The Gulf and Peninsula Province of the Californias, AAPG Mem* (in press).

Lonsdale, P., 1989b, The Rise Flank Trails Left by Migrating Offsets of the Equatorial East Pacific Rise Axis, *J. Geophys. Res.* **94**, 713–743.

Lonsdale, P. and Batiza, R., 1980, Submersible Study of Hyaloclastite and Lava Flows on Young Seamounts at the Mouth of the Gulf of California, *Geol. Soc. Am. Bull.* **91**, 545–554.

Lonsdale, P. and Spiess, F. N., 1979, A Pair of Young Cratered Volcanoes on the East Pacific Rise, *J. Geol.* **87**, 157–173.

Lonsdale, P., Batiza, R., and Simkin, T., 1982, Metallogenesis at Seamounts on the East Pacific Rise, *Mar. Tech. Soc. J.* **16**, 54–61.

Macdonald, K. C., Fox, P. J., Perram, L. J., Perram, M. F., Eisen, M. F., Haymon, R. M., Miller, S. P., Carbotte, S. M., Cormier, M.-H., and Shor, A. N., 1988, A New View of the Mid-ocean Ridge from the Behavior of Ridge-axis Discontinuities, *Nature* **335**, 217–225.

McLain J. *et al.*, 1989, The East O'Gorman Fracture Zone, *Mar. Geophys. Res.* (in press).

McNutt, M., 1986, Non-uniform Magnetization of Seamounts: A Least Squares Approach. *J. Geophys. Res.* **91**, 3686–3700.

Nakamura, K., 1977, Volcanoes as Possible Indicators of Tectonic Stress Orientation—Principle and Proposal, *J. Volc. Geotherm. Res.* **2**, 1–16.

Pieri, D. C. and Baloga, S. M., 1986, Effusion Rate, Area and Length Relationships for Some Hawaiian Lava Flows, *J. Volc. Geotherm. Res.* **30**, 29–45.

Roden, G. I., 1987, Effects of Seamounts and Seamount Chains on Ocean Circulation and Thermohaline Structure, in B. Keating, P. Fryer, R. Batiza and F. Boehlert (eds.), *Seamounts, Islands and Atolls, AGU Monogr. Series 43* pp. 335–354.

Ryan, M. P., 1988, The Mechanics and Three-Dimensional Internal Structure of Active Magmatic Systems: Kilauea Volcano, Hawaii, *J. Geophys. Res.* **93**, 4213–4248.

Schouten, H., Dick, H. J. B., and Klitgord, K. D., 1987, Migration of Mid-ocean Ridge Volcanic Segments, *Nature* **326**, 835–839.

Simkin, T., 1972, Origin of Some Flat-topped Volcanoes and Guyots, *Geol. Soc. Am. Mem.* **132**, 183–193.

Simkin, T., 1984, The Geology of the Galapagos, in R. Perry (ed.), *The Galapagos*, Pergamon Press, Oxford, pp. 15–41.

Smith, T. L., 1987, Geology and Volcanic Development of a Near-Ridge Seamount and New Evidence for the Diversity of Origin of Seamount Hyaloclastites: Results from Integrated Alvin/ANGUS and Laboratory Study, M.A. thesis, Washington University, St. Louis, Mo.

Smith T. and Batiza, R., 1989, New Field and Laboratory Evidence for the Origin of Hyaloclastite Flows on Seamount Summits, *Bull. Volc.* **51**, 96–114.

Stanley, D. J. and Taylor, P. T., 1977, Sediment Transport Down a Seamount Flank by a Combined Current and Gravity Process, *Mar. Geol.* **23**, 77–88.

Taylor, P. T., Stanley, D. J., Simkin, T., and John, W., 1975, Gilless Seamount: Detailed Bathymetry and Modification by Bottom Current, *Mar. Geol.* **19**, 139–157.

Vogt, P. R., 1971, Asthenosphere Motion Recorded by the Ocean Floor South of Iceland, *Earth Planet. Sci. Lett.* **13**, 153–160.

Walker, G. P. L., 1973, Length of Lava Flows, *Phil. Trans. Roy. Soc. London* **A. 274**, 107–118.

Wright, T. L. and Fiske, R. S., 1971, Origin of the Differentiated and Hybrid Lavas of Kilauea Volcano, Hawaii, *J. Petrol.* **12**, 1–65.

Zindler, A., Staudigel, H., and Batiza, R., 1984, Isotope and Trace Element Geochemistry of Young Pacific Seamounts: Implications for the Scale of Upper Mantle Heterogeneity, *Earth Planet. Sci. Lett.* **70**, 175–195.

Plate 1. Oblique view from ALVIN (Dive 1401, 1710Z) of wrinkled, ropey submarine pahoehoe. The site is on the gently summit of seamount 5 west of the caldera (depth = 1260 m). The foreground is ~2–3 m across and the area is about 5–6 m. from foreground to back.

Plate 2. ANGUS photo showing normal incidence view of wrinkled pahoehoe and lobate pillows. Area is about 5 m × 5 m in size. Many pahoehoe and sheet flows have lobate pillows at their margins. ANGUS 227 0408Z, same general area of seamount 5 as Plate 1.

Plate 3. ANGUS view of smooth and wrinkled/coiled pahoehoe about 10 m away from Plate 3.

Plate 4. ANGUS photo of striated, smooth sheet flow about 5 m from Plates 2 and 3.

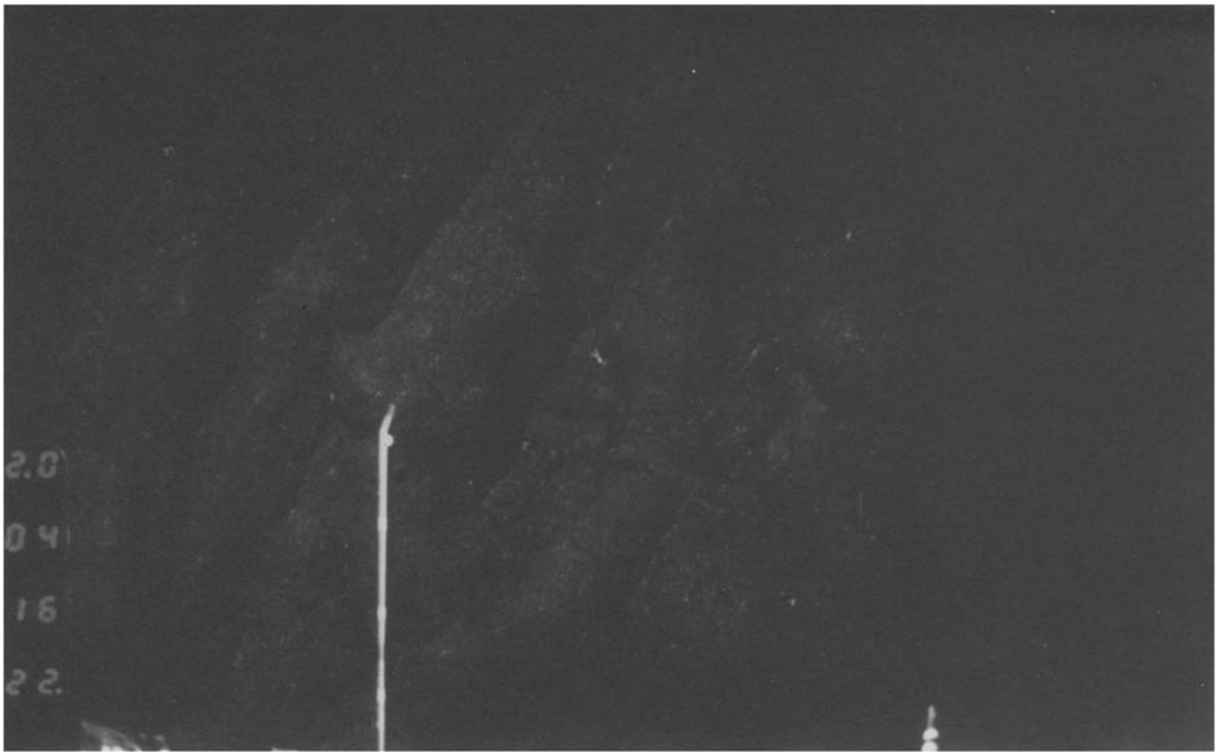

Plate 5. ALVIN view (Dive 1399, 1722Z) of a steep slope of elongate pillows in the vicinity of the summit bench on seamount 5. View is looking directly onto the steep (60–70°) slope.

Plate 6. ALVIN photo (Dive 1397, 1830Z) of bulbous and tubular pillows on the southern part of the summit bench of seamount 5.

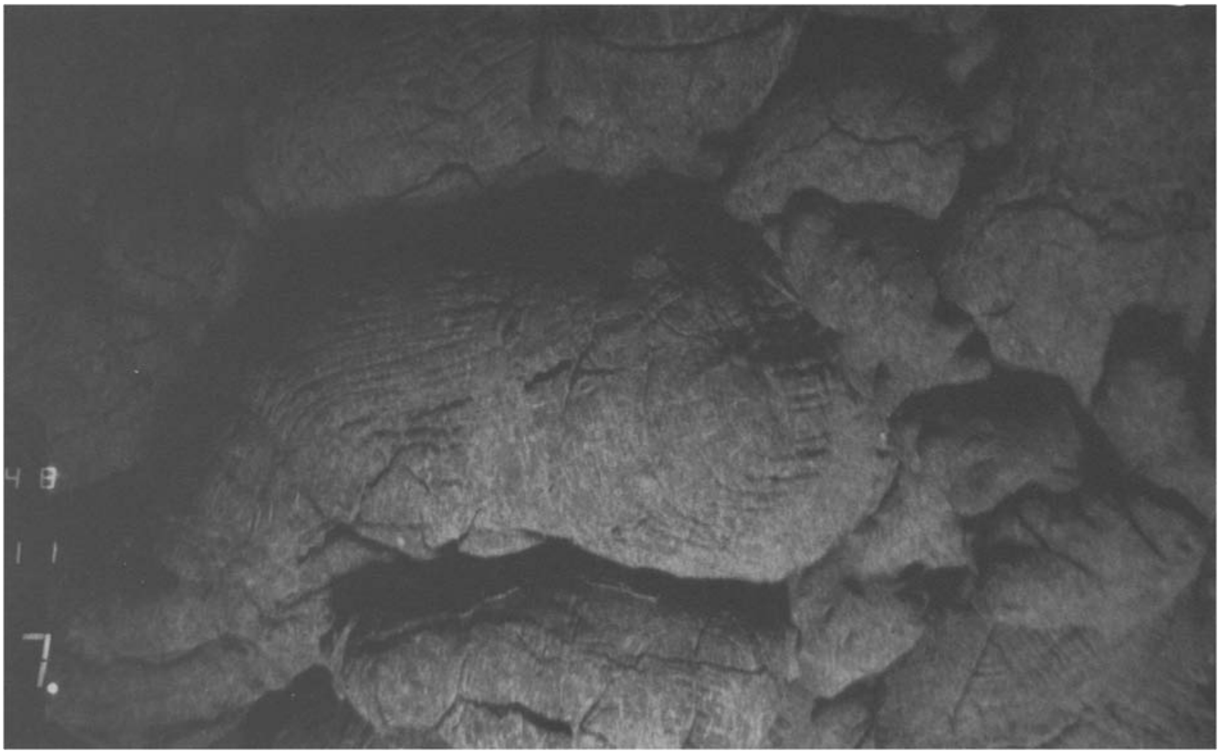

Plate 7. ANGUS photo (227, 0640Z) of normal bulbous pillows near the floor of the breached caldera on seamount 5.

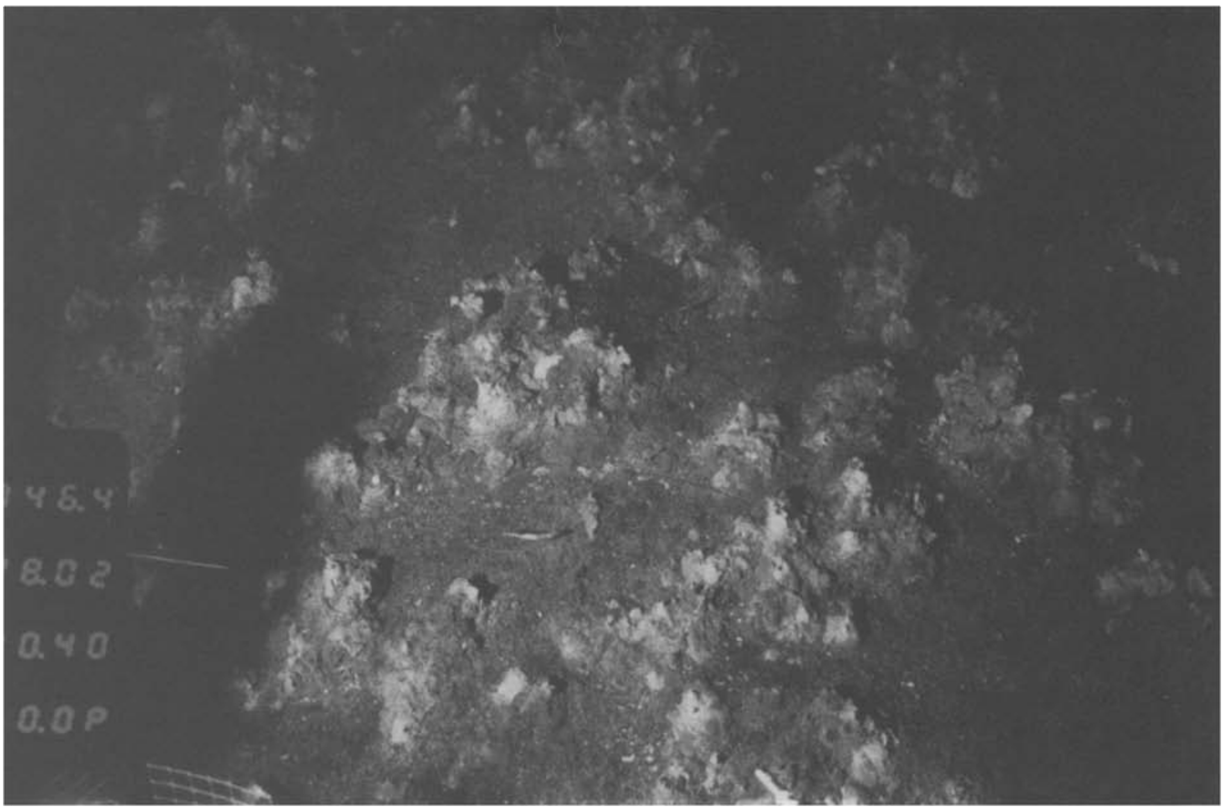

Plate 8. ALVIN photo (Dive 1400) of hydrothermal precipitates with yellow bacterial coatings in the breached caldera of seamount 5.

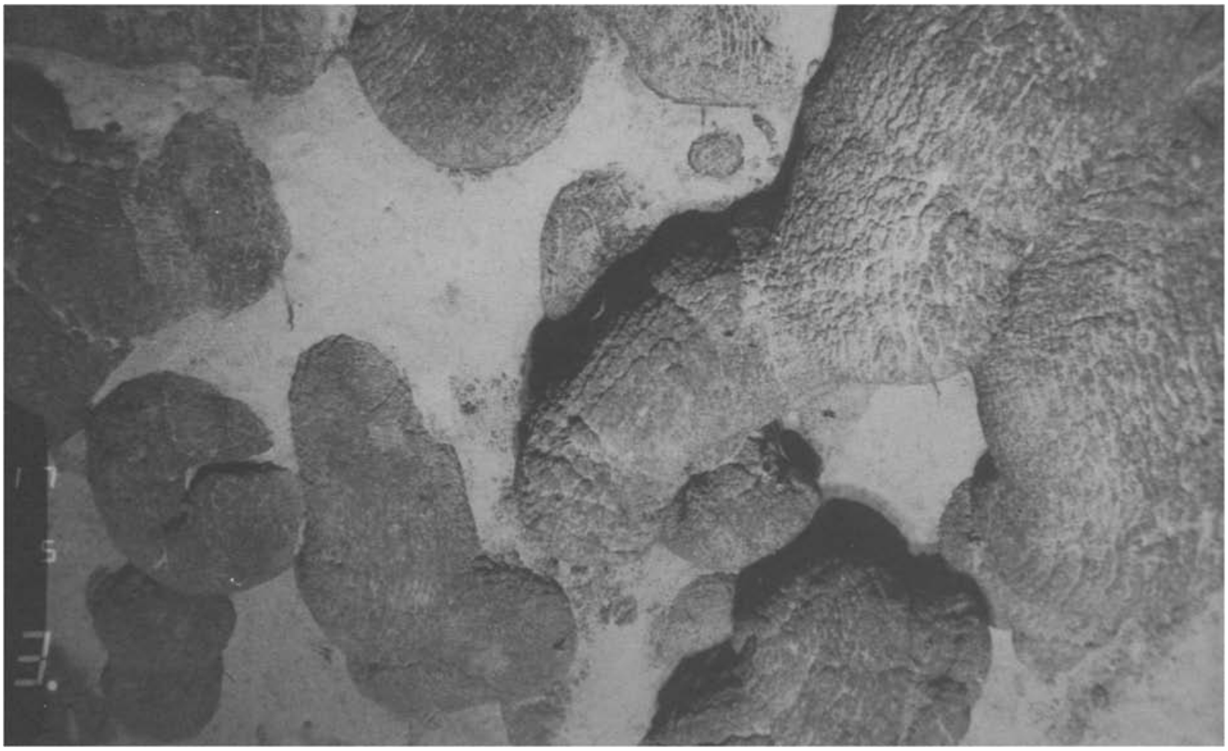

Plate 9. Elongate and bulbous pillows on the south flanks of seamount 6C. ANGUS 223, 0918Z.

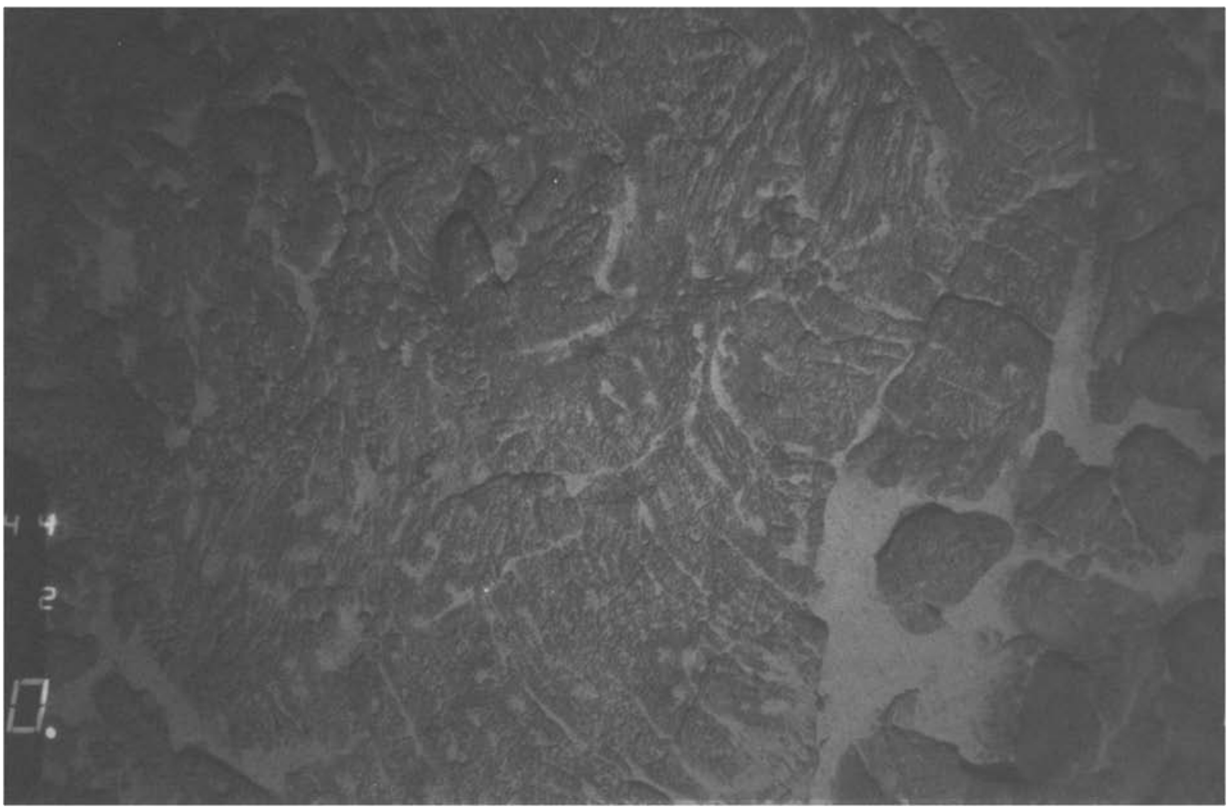

Plate 10. Ropey pahoehoe on the gentle slopes of 6C near the saddle with 6E. ANGUS 220, 1044Z.

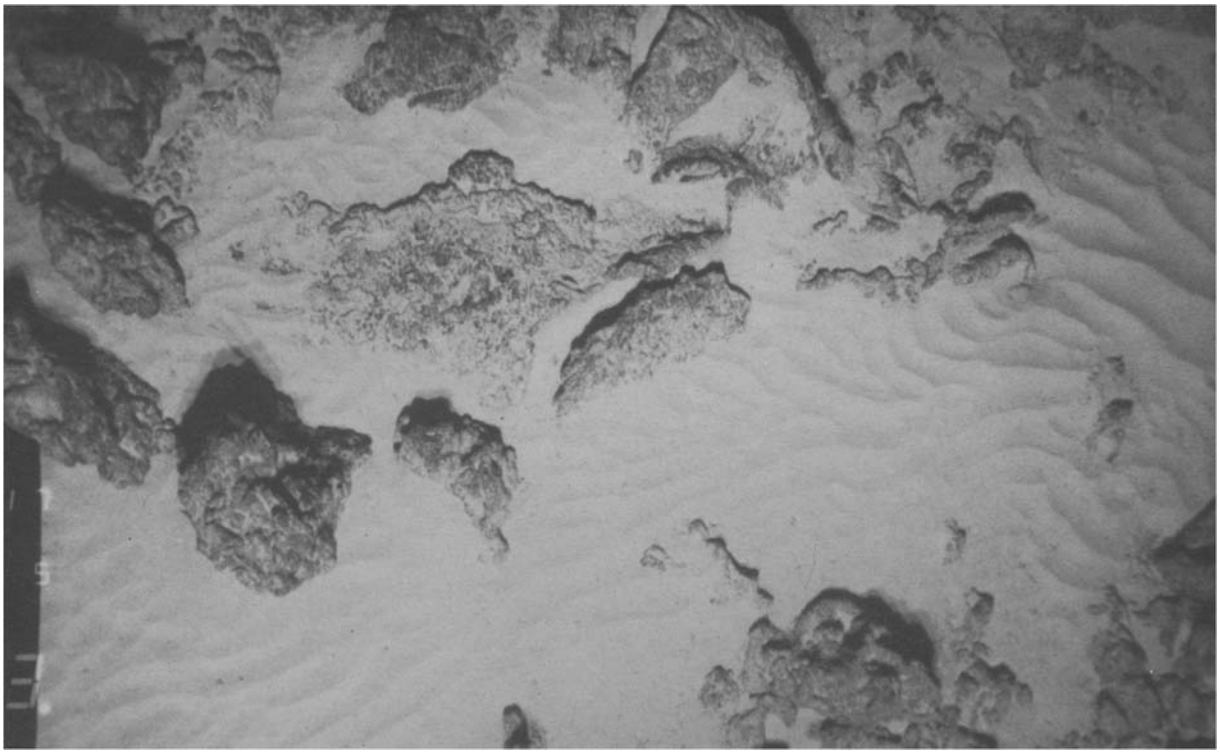

Plate 11. Tabular hyaloclastite and rubbly lava with rippled sediment on the summit terrace of seamount 6C. ANGUS 223, 1017Z.

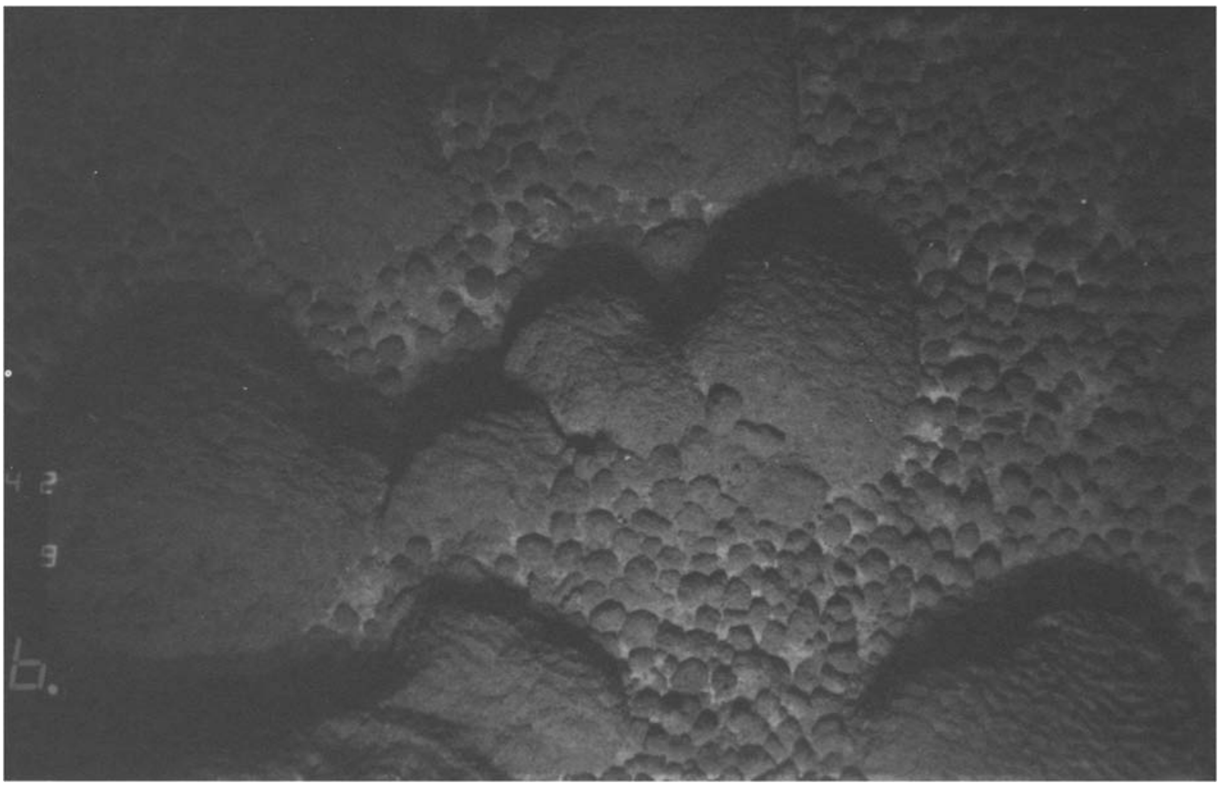

Plate 12. Sediment-covered pillows and manganese nodules in the cone/lava field on the south flanks of seamount 7. ANGUS run 226, 0242Z.

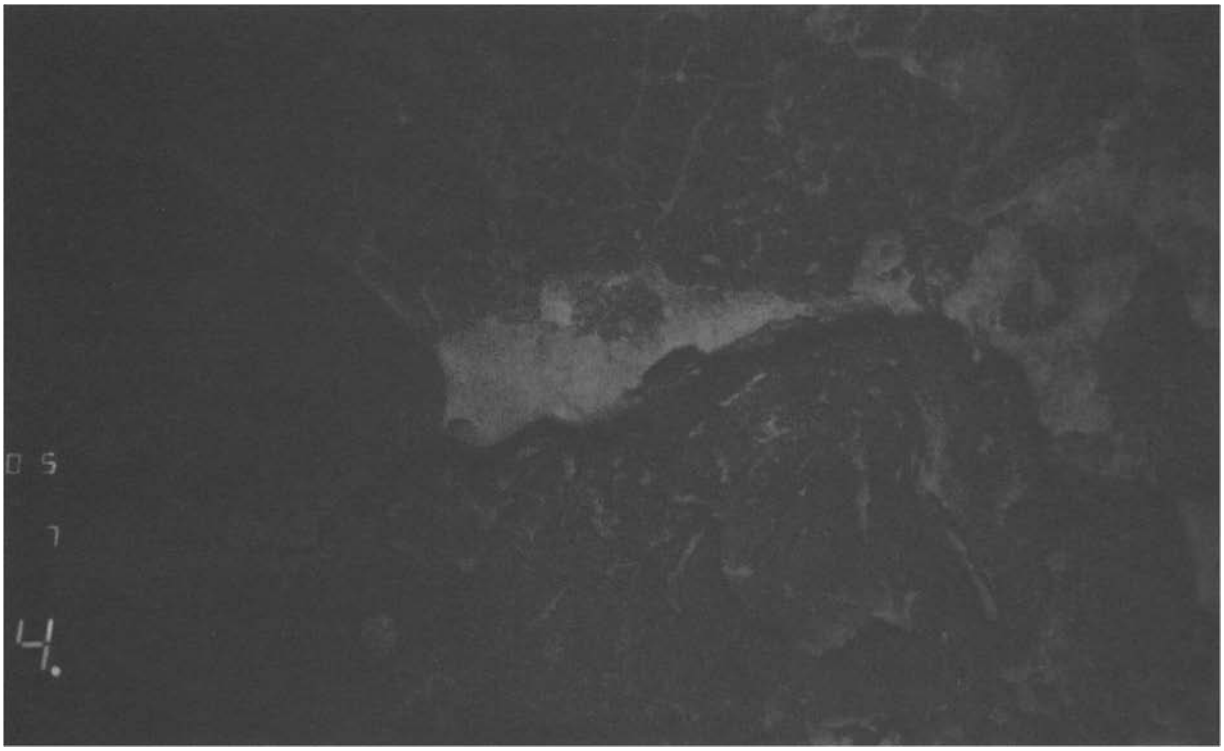

Plate 13. Manganese covered pahoehoe on the gentle upper slopes of seamount 7. ANGUS run 224, 0616Z.

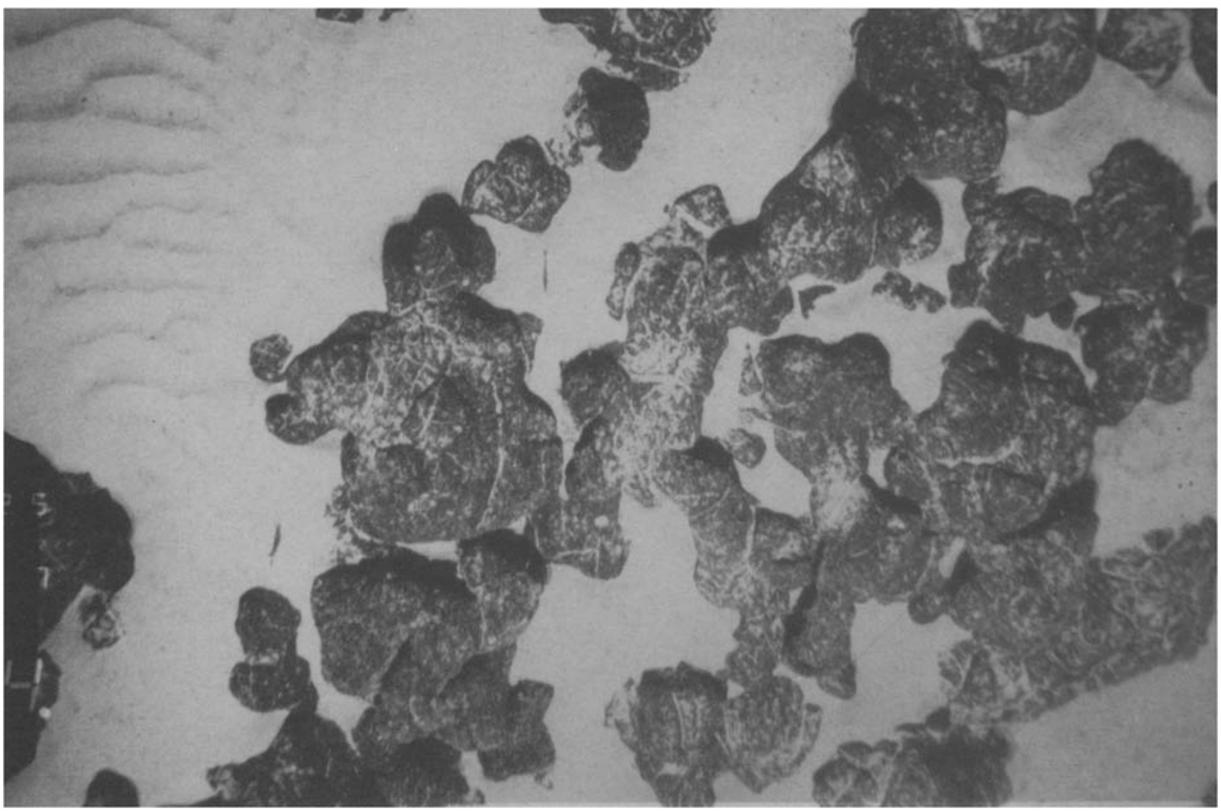

Plate 14. Small tubular pillows and ripple pelagic sediment west of the summit of seamount 7. ANGUS 224, 1120Z.

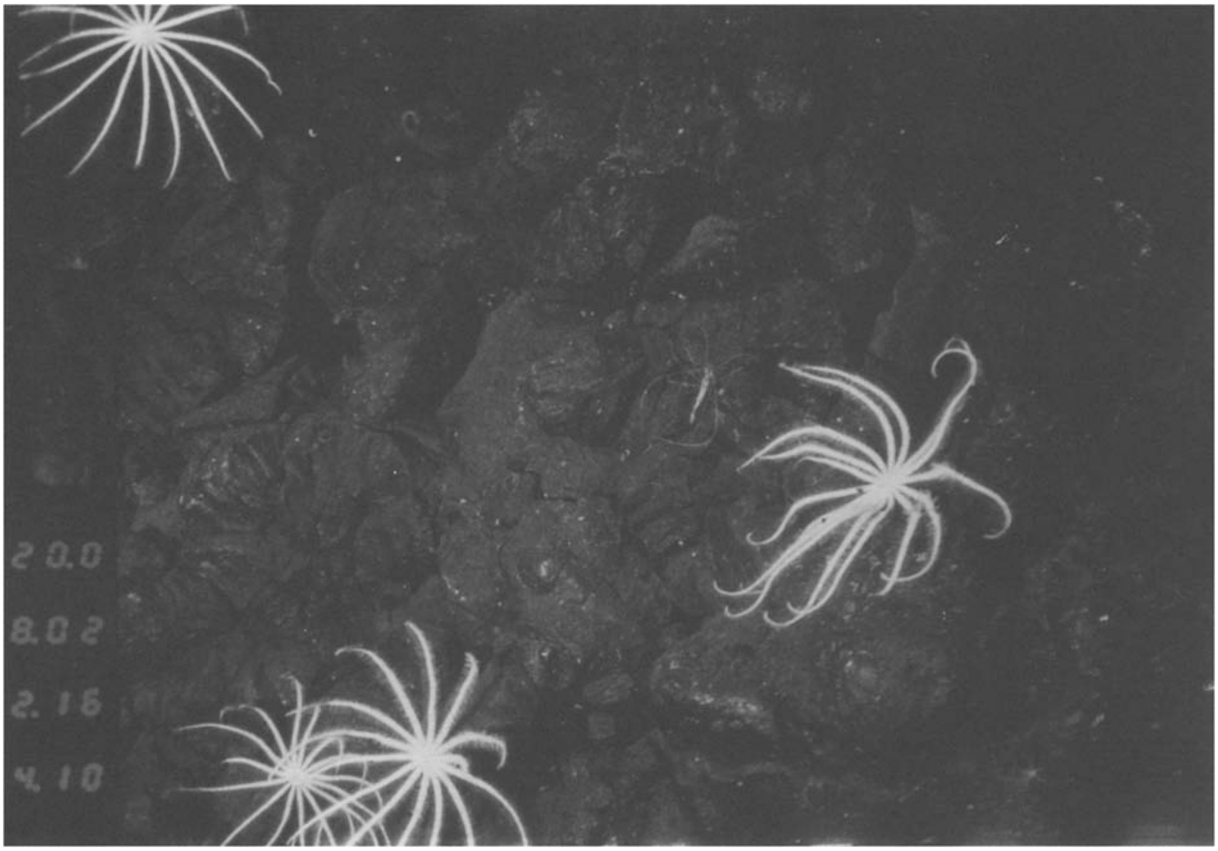

Plate 15. Pillow talus on the gentle flanks of seamount 7 near the summit. ALVIN 139Z, 1810Z.